Available online at www.sciencedirect.com
SCIENCE DIRECT®
Physics Reports 425 (2006) 195–264
PHYSICS REPORTS
www.elsevier.com/locate/physrep

Quantum control of bound and continuum state dynamics

Moshe Shapiro[a, b, *], Paul Brumer[c]

[a] *Department of Chemical Physics, The Weizmann Institute of Science, Rehovot, 76100, Israel*
[b] *Departments of Chemistry and Physics, The University of British Columbia, Vancouver, Canada V6T 1Z1*
[c] *Department of Chemistry, and Center for Quantum Information and Quantum Control, University of Toronto, Toronto, Canada M5S 3H6*

Accepted 12 December 2005
Available online 24 January 2006
editor: I. Procaccia

Abstract

We review theoretical work in the field of "coherent control" (CC) of bound- and continuum-state dynamics. We explain the principles of bichromatic and polychromatic control and show that CC is made possible through the execution of a *disentanglement transformation*. We discuss limitations to control and show that controllability in continuum states is linked to a generalized Schwarz inequality of vector spaces. We illustrate the success of these techniques in controlling photo-current directionality in semiconductors using one- vs. two-photon interferences. We next turn our attention to CC using adiabatic passage (AP) processes, enabling the achievement of *both* selectivity and complete population transfer. We demonstrate controllability in bound state dynamics by the explicit construction of guiding fields which solve the "non-degenerate quantum control" problem. The CC + AP methodology is then extended to the control of manifolds composed entirely of degenerate bound states. We use AP techniques in the control of *photoassociation* and especially in the controlled recombination of ultracold atoms to form ultracold molecules. We next discuss the optical manipulation of interferences between overlapping, decaying resonances as a way of suppressing spontaneous emission, intramolecular vibrational redistribution, and internal conversion in molecules. Finally we discuss decoherence and the way material and radiative phase-instabilities diminish controllability. We show how to combat decoherence and how to use CC to construct "decoherence-free subspaces".

PACS: 32.80.Qk; 33.80.Gj; 33.80.Ps; 33.50.Hv

Keywords: Quantum mechanics; Control; Coherence; Decoherence; Photodissociation; Photoassociation; Selectivity; Interference; Entanglement; Adiabatic passage

Contents

* Corresponding author.
E-mail address: mshapiro@chem.ubc.ca (M. Shapiro).

0370-1573/$ - see front matter © 2006 Elsevier B.V. All rights reserved.
doi:10.1016/j.physrep.2005.12.005

1. Introduction

Quantum mechanics, though a probabilistic theory, gives a "deterministic" answer to the question of how the present determines the future. In essence, in order to predict future probabilities, we need to (numerically) propagate the time dependent Schrödinger equation from the present to the future. The field of *Quantum Control* deals with an important modification of this task, namely, it asks—given a wave function in the present, what dynamics (e.g. the Hamiltonian) guarantees a desired outcome ("objective") in the future?

In practice one can modify the Hamiltonian by introducing external fields (e.g. laser light). It is then possible to reach the objective in a "trial-and-error" fashion, that is, one can guess a Hamiltonian, propagate the initial wave function to the future, compare the result with the desirable objective, and correct the guess for the Hamiltonian until satisfactory agreement with the objective is reached. A systematic way of executing this procedure is the sub-field called *optimal control* [1–27].

This trial-and-error method is very time consuming, requiring the repeated solution of the time dependent Schrödinger equation. When the explicit time-dependent terms in the Hamiltonian merely serve to prepare a state which then evolves in the absence of an external field, or when its explicit time dependence can be treated adiabatically, there exists a much more elegant method, called *coherent control* (CC) [2–57], which necessitates the solution of the (time-independent) Schrödinger equation only once. Moreover, in that case, the CC solution allows for the simultaneous exploration of other possible future outcomes (and not just a single "desirable" objective) resulting from different preparations of the initial wave function. The CC method is the subject of the present review.

2. The principles of coherent control

2.1. The generation of entanglement in multi-channel Photodissociation

In this section we show that much of the difficulty in controlling future events, in pure state dynamics, arises from the generation of entangled states, associated with many possible future outcomes. This is the situation in many natural

processes, such as the dissociation of a molecule by a photon ("photodissociation"), a process that will serve here as a generic example of a quantum-dynamical event. In Section 2.2 we show how to overcome this difficulty and disentangle material states, thus giving rise to just one, pre-chosen, future outcome.

Consider a photodissociation process of the type,

$$ABC \overset{\hbar\omega}{\to} ABC^* \to \begin{cases} A + BC, & q = 1, \\ B + AC, & q = 2, \\ C + AB, & q = 3. \end{cases} \tag{1}$$

Here ABC is a polyatomic molecule in a bound state, with A, B or C being atoms or groups of atoms. ABC^* represents the same molecule in an excited dissociative state, with a light source of carrier frequency $\hbar\omega$ inducing the transition between these states. The $q = 1, 2, 3$ quantum number designates the various ways ("arrangement channels") to which the molecule can break apart in the remote future. In addition to this quantum number there is a set of quantum numbers, designated collectively as $\mathbf{n}$ (or $\mathbf{m}$), which describe the individual states of the molecular fragments in a given q arrangement. For example, $\mathbf{n}$ can incorporate the v, j, m_j, and $\hat{\mathbf{k}}$ quantum numbers, designating respectively, the vibrational level, rotational level, angular momentum projection on the z axis, and direction of recoil of the fragments.

Consider a coherent light field of the form

$$\mathbf{E}(t) = \hat{\boldsymbol{\epsilon}}\varepsilon(t) = \hat{\boldsymbol{\epsilon}} \int \mathrm{d}\omega \epsilon(\omega) \exp(-\mathrm{i}\omega t) \tag{2}$$

acting on the ABC molecule. Here $\varepsilon(t)$ is the magnitude of the field, $\hat{\boldsymbol{\epsilon}}$ is its polarization direction and $\epsilon(\omega)$ is the field's Fourier component at frequency ω. The entire dynamics is determined by $\Psi(t)$, the time dependent material wave function, satisfying the time dependent Schrödinger equation,

$$\mathrm{i}\hbar\partial\Psi(t)/\partial t = H\Psi(t), \tag{3}$$

where H is the full matter + radiation Hamiltonian,

$$H = H_M + H_{\mathrm{MR}}(t), \tag{4}$$

where H_M is the purely material Hamiltonian and $H_{\mathrm{MR}}(t)$ is the radiation-matter interaction, given in the dipole approximation as

$$H_{\mathrm{MR}}(t) = -\varepsilon(t)\hat{\boldsymbol{\epsilon}} \cdot \vec{\mu}, \tag{5}$$

with $\vec{\mu}$ being the transition dipole operator.

We consider a common situation in which the system resides initially (at $t = 0$) in a *single* bound ("precursor") state $|E_1\rangle$. As a result of the interaction with the photon, some population is transferred to a dissociative manifold, spanned by the $|E, \mathbf{n}, q^-\rangle$ set of fully interacting scattering states. Both the initial and scattering states are eigenstates of the material Hamiltonian, i.e.,

$$\lim_{\epsilon\to+0} [E - \mathrm{i}\epsilon - H_M]|E, \mathbf{n}, q^-\rangle = 0; \quad [E_1 - H_M]|E_1\rangle = 0. \tag{6}$$

The $-\mathrm{i}\epsilon$ boundary condition makes the scattering state go over, as $t \to \infty$, to *individual* fragment states,

$$\lim_{t\to\infty,\epsilon\to+0} |E, \mathbf{n}, q^-\rangle \mathrm{e}^{-\mathrm{i}(E-\mathrm{i}\epsilon)t/\hbar} = |e_{\mathbf{n},q}\rangle|\mathbf{k}_{\mathbf{n},q}\rangle \mathrm{e}^{-\mathrm{i}Et/\hbar} \equiv |E, \mathbf{n}, q; 0\rangle \mathrm{e}^{-\mathrm{i}Et/\hbar}. \tag{7}$$

Here, $e_{\mathbf{n},q}$ denotes the internal energy of the fragments in the q arrangement and $\mathbf{n}$ internal state, while $\hbar\mathbf{k}_{\mathbf{n},q}$ is the linear momentum of the free motion of the fragments in the q-arrangement, the magnitude of which is given via energy conservation as

$$\hbar^2 k^2_{\mathbf{n},q}/(2m_q) = E - e_{\mathbf{n},q}, \tag{8}$$

where m_q is the reduced mass in the q-arrangement. For example, $m_{q=1} \equiv m(A)m(BC)/[m(A)+m(BC)]$, with $m(A)$ being the mass of the A fragment, etc.

Using the above states we can expand $|\Psi(t)\rangle$ as

$$|\Psi(t)\rangle = b_1(t)\mathrm{e}^{-\mathrm{i}E_1 t/\hbar}|E_1\rangle + \sum_{\mathbf{n},q}\int \mathrm{d}E b_{E,\mathbf{n},q}(t)\mathrm{e}^{-\mathrm{i}Et/\hbar}|E,\mathbf{n},q^-\rangle. \tag{9}$$

The photodissociation *amplitude* to observe a specific fragment state labeled by $(\mathbf{m}, q')$ at time t is given as

$$\begin{aligned} A_{\mathbf{m}}^{(q')}(t) &= \langle e_{\mathbf{m},q'}, \mathbf{k}_{\mathbf{m},q'}|\Psi(t)\rangle = b_1(t)\langle e_{\mathbf{m},q'}, \mathbf{k}_{\mathbf{m},q'}|E_1\rangle \mathrm{e}^{-\mathrm{i}E_1 t/\hbar} \\ &\quad + \sum_{\mathbf{n},q}\int \mathrm{d}E b_{E,\mathbf{n},q}(t)\langle e_{\mathbf{m},q'}, \mathbf{k}_{\mathbf{m},q'}|E,\mathbf{n},q^-\rangle \mathrm{e}^{-\mathrm{i}Et/\hbar}. \end{aligned} \tag{10}$$

Assuming that $\langle e_{\mathbf{m},q'}, \mathbf{k}_{\mathbf{m},q'}|E_1\rangle = 0$, (e.g., the two states belong to different electronic states), it follows from Eqs. (10), (7) and the orthogonality of the continuum states that $P_{\mathbf{m}}^{(q')}(E)$, the photodissociation *probability* to observe a particular fragment state in the remote future at total energy E is given by

$$P_{\mathbf{m}}^{(q')}(E) = |A_{\mathbf{m}}^{(q')}(E)|^2 = |b_{E,\mathbf{m},q'}(t\to\infty)|^2. \tag{11}$$

In order to obtain the b_1 and $b_{E,\mathbf{n},q}$ expansion coefficients we substitute Eq. (9) into the time-dependent Schrödinger equation and use the orthogonality of the basis functions to obtain the usual set of first-order differential equations,

$$\frac{\mathrm{d}}{\mathrm{d}t}b_1 = \mathrm{i}\int \mathrm{d}E \sum_{\mathbf{n}} \Omega_{1,E,\mathbf{n}}(t) b_{E,\mathbf{n},q}(t)\mathrm{e}^{-\mathrm{i}\Delta_E t} \tag{12a}$$

$$\frac{\mathrm{d}}{\mathrm{d}t}b_{E,\mathbf{n},q} = \mathrm{i}\Omega_{1,E,\mathbf{n}}^*(t)\mathrm{e}^{\mathrm{i}\Delta_E t} b_1(t) \quad \text{for each } E \text{ and } \mathbf{n} \tag{12b}$$

where we have retained only the "rotating waves" terms. The detuning, $\Delta_{E,i}$, is defined as

$$\Delta_{E,i} \equiv \omega_{E,i} - \omega_L \quad \text{with } \omega_{E,i} \equiv (E - E_i)/\hbar, \quad i = 1,\ldots, \tag{13}$$

and $\Omega_{1,E,\mathbf{n}}(t)$, the (time-varying) "Rabi-frequency", is defined as

$$\Omega_{1,E,\mathbf{n}}(t) \equiv \langle E_1|\hat{\epsilon}\cdot\vec{\mu}|E,\mathbf{n},q^-\rangle \varepsilon(t)/\hbar. \tag{14}$$

We proceed [58] by integrating the $b_{E,\mathbf{n},q}$ continuum coefficients of Eq. (12) over time, while imposing the boundary condition that only the $|E_1\rangle$ state is initially populated, i.e., that $b_{E,\mathbf{n},q}^{(1)}(t\to-\infty) = 0$. With this boundary condition, we have that,

$$b_{E,\mathbf{n},q}(t) = \mathrm{i}\int_{-\infty}^{t} \mathrm{d}t' \Omega_{1,E,\mathbf{n}}^*(t') b_1(t')\mathrm{e}^{\mathrm{i}\Delta_E t'}. \tag{15}$$

Hence,

$$\frac{P_{\mathbf{n}}^{(q)}(E)}{P_{\mathbf{m}}^{(q')}(E)} = \left|\frac{b_{E,\mathbf{n},q}(\infty)}{b_{E,\mathbf{m},q'}(\infty)}\right|^2 = \left|\frac{\langle E,\mathbf{n},q^-|\hat{\epsilon}\cdot\vec{\mu}|E_1\rangle}{\langle E,\mathbf{m},q'^-|\hat{\epsilon}\cdot\vec{\mu}|E_1\rangle}\right|^2. \tag{16}$$

Note that all laser pulse parameters and the time dependence have neatly canceled out in the expression for the branching ratio. We conclude that in traditional photodissociation the branching ratios at a fixed energy E are *independent of the laser power and pulse shape*. This result, though independent of the pulse strength, coincides with that of perturbation theory. It holds true whenever only *one* "precursor" state $|E_1\rangle$ exists.

This argument motivates the idea that the way to control photodissociation is to use more than one "precursor" state, or in greater generality, to use multiple excitation pathways to the same continuum state. Below we demonstrate that such a strategy allows us to actively influence and control which photodissociation product is formed. These ideas,

which introduce the notion of "coherent control", will be later shown to hold true for any dynamical process, not just for photodissociation.

2.2. The basic principle of coherent control

We introduce the basic principles of CC through a series of examples. In particular, we first extend the treatment of the previous section to the photodissociation of a non-stationary *superposition* of bound states,

$$|\chi(t)\rangle = \sum_i b_i(t)|E_i\rangle e^{-iE_i t/\hbar}. \tag{17}$$

Numerous experimental techniques can be used to create the $\chi(t)$ state (see e.g., Refs. [59–61]). Whatever the method of preparation, the amplitude and phase of $b_i(t)$ and matrix elements connecting $|E_i\rangle$ to the continuum are functions of the experimentally controllable preparation and excitation lasers parameters.

With $\chi(t)$ as the initial state Eq. (9) becomes

$$|\Psi(t)\rangle = \sum_i b_i(t)e^{-iE_i t/\hbar}|E_i\rangle + \sum_{\mathbf{n},q}\int dE\, b_{E,\mathbf{n},q}(t)e^{-iEt/\hbar}|E,\mathbf{n},q^-\rangle. \tag{18}$$

Assuming that the field does not directly couple the $|E_i\rangle$ bound states (because e.g., its Fourier components are far off resonance with respect to the $\omega_{i,j} \equiv (E_i - E_j)/\hbar$ transition frequencies), we obtain a set of equations analogous to Eq. (12):

$$\begin{aligned}
\frac{db_j(t)}{dt} &= \frac{i}{\hbar}\int dE \sum_{\mathbf{n},q} \varepsilon(t)e^{-i\omega_{E,j}t}\langle E_j|\hat{\epsilon}\cdot\vec{\mu}|E,\mathbf{n},q^-\rangle b_{E,\mathbf{n},q}(t),\\
\frac{db_{E,\mathbf{n},q}(t)}{dt} &= \frac{i}{\hbar}\sum_i \langle E,\mathbf{n},q^-|\hat{\epsilon}\cdot\vec{\mu}|E_i\rangle\varepsilon(t)e^{i\omega_{E,i}t}b_i(t), \quad \text{for all } E,\mathbf{n},q.
\end{aligned} \tag{19}$$

Solving Eq. (19) for the continuum coefficients we obtain

$$b_{E,\mathbf{n},q}(t) = \frac{i}{\hbar}\sum_i \langle E,\mathbf{n},q^-|\hat{\epsilon}\cdot\vec{\mu}|E_i\rangle\int_0^t dt'\varepsilon(t')e^{i\omega_{E,i}t'}b_i(t'). \tag{20}$$

As a result, the photodissociation probability is given by

$$P_{\mathbf{n}}^{(q)}(E) = |b_{E,\mathbf{n},q}(\infty)|^2 = \frac{1}{\hbar^2}\left|\sum_i \langle E,\mathbf{n},q^-|\hat{\epsilon}\cdot\vec{\mu}|E_i\rangle\int_0^\infty dt\,\varepsilon(t)e^{i\omega_{E,i}t}b_i(t)\right|^2. \tag{21}$$

Note that it is no longer possible to factor out the pulse parameters from the above expression. We say that the light fields have been "entangled" with the material system.

In the weak field limit we can assume that the initial coefficients do not get significantly depleted by the photodissociating pulse and equate $b_i(t) \approx b_i(0) \equiv b_i$ to obtain that

$$P_{\mathbf{n}}^{(q)}(E) = \left|\sum_i b_i\langle E,\mathbf{n},q^-|\hat{\epsilon}\cdot\vec{\mu}|E_i\rangle\int_0^\infty dt\,\varepsilon(t)e^{i\omega_{E,i}t}\right|^2 = \left(\frac{2\pi}{\hbar}\right)^2\left|\sum_i b_i\langle E,\mathbf{n},q^-|\hat{\epsilon}\cdot\vec{\mu}|E_i\rangle\epsilon(\omega_{E,i})\right|^2. \tag{22}$$

Thus, the probability to produce a fragment state $\mathbf{n},q$ at energy E involves *multiple interfering pathways*. In each pathway a different on-resonance $\epsilon(\omega_{E,i})$ Fourier component of the laser pulse connects a different precursor state $|E_i\rangle$ to the same continuum state $|E,\mathbf{n},q^-\rangle$. By changing the amplitude and phase of these Fourier components (i.e., by "shaping" the pulse) we can affect the nature and magnitude of the interference between all the pathways. Since this interference is affected also by the $\langle E,\mathbf{n},q^-|\hat{\epsilon}\cdot\vec{\mu}|E_i\rangle$ complex matrix elements, it is possible to induce destructive interference in one fragment channel and constructive interference in another, thereby achieving the desired channel *selectivity*.

Beyond the weak field limit one can no longer neglect the variation in the initial coefficients during the pulse. Rather, we can get a more accurate answer by substituting Eq. (20) into the first part of Eq. (19) to obtain

$$\frac{\mathrm{d}b_j(t)}{\mathrm{d}t} = -\frac{1}{\hbar^2}\sum_i \sum_{\mathbf{n},q} \varepsilon(t) \int_0^t \mathrm{d}t' \varepsilon(t') \mathrm{e}^{\mathrm{i}(E_j t - E_i t')/\hbar} \times \int \mathrm{d}E \mathrm{e}^{-\mathrm{i}E(t-t')/\hbar} \langle E_j|\hat{\boldsymbol{\epsilon}}\cdot\vec{\mu}|E,\mathbf{n},q^-\rangle\langle E,\mathbf{n},q^-|\hat{\boldsymbol{\epsilon}}\cdot\vec{\mu}|E_i\rangle b_i(t'). \tag{23}$$

Assuming that $\langle E_j|\hat{\boldsymbol{\epsilon}}\cdot\vec{\mu}|E,\mathbf{n},q^-\rangle$ varies slowly with E we can use the so-called slowly varying continuum approximation (SVCA) [62] to replace it by its value at some representative energy $\bar{E}$:

$$\langle E_j|\hat{\boldsymbol{\epsilon}}\cdot\vec{\mu}|E,\mathbf{n},q^-\rangle \approx \langle E_j|\hat{\boldsymbol{\epsilon}}\cdot\vec{\mu}|\bar{E},\mathbf{n},q^-\rangle. \tag{24}$$

With this approximation, the last integral of Eq. (23) becomes

$$\begin{aligned}&\int \mathrm{d}E \mathrm{e}^{-\mathrm{i}E(t-t')/\hbar} \langle E_j|\hat{\boldsymbol{\epsilon}}\cdot\vec{\mu}|E,\mathbf{n},q^-\rangle\langle E,\mathbf{n},q^-|\hat{\boldsymbol{\epsilon}}\cdot\vec{\mu}|E_i\rangle \\ &\quad\approx \langle E_j|\hat{\boldsymbol{\epsilon}}\cdot\vec{\mu}|\bar{E},\mathbf{n},q^-\rangle\langle\bar{E},\mathbf{n},q^-|\hat{\boldsymbol{\epsilon}}\cdot\vec{\mu}|E_i\rangle \int \mathrm{d}E \mathrm{e}^{-\mathrm{i}E(t-t')/\hbar} \\ &\quad= 2\pi\hbar\langle E_j|\hat{\boldsymbol{\epsilon}}\cdot\vec{\mu}|\bar{E},\mathbf{n},q^-\rangle\langle\bar{E},\mathbf{n},q^-|\hat{\boldsymbol{\epsilon}}\cdot\vec{\mu}|E_i\rangle\delta(t-t').\end{aligned} \tag{25}$$

Using Eq. (25), and the identity $\int_0^t \mathrm{d}t'\delta(t-t') = 1/2$, we obtain from Eq. (23) that,

$$\frac{\mathrm{d}}{\mathrm{d}t}b_j(t) = -\sum_i \varepsilon(t)^2 \mathrm{e}^{\mathrm{i}\omega_{j,i}t} \Gamma_{j,i}(\bar{E}) b_i(t), \tag{26}$$

where $\Gamma_{j,i}(\bar{E})$ are elements of the "width" matrix $\Gamma(\bar{E})$,

$$\Gamma_{j,i}(\bar{E}) \equiv \frac{\pi}{\hbar}\sum_q \langle E_j|\hat{\boldsymbol{\epsilon}}\cdot\vec{\mu}\left\{\sum_{\mathbf{n}} |\bar{E},\mathbf{n},q^-\rangle\langle\bar{E},\mathbf{n},q^-|\right\}\hat{\boldsymbol{\epsilon}}\cdot\vec{\mu}|E_i\rangle \equiv \sum_q \Gamma_{j,i}^{(q)}(\bar{E}), \tag{27}$$

where $\Gamma_{j,i}^{(q)}(\bar{E})$ defined via Eq. (27) are the *partial* width matrix elements associated with arrangement q,

$$\Gamma_{j,i}^{(q)}(\bar{E}) \equiv \frac{\pi}{\hbar}\sum_{\mathbf{n}} \langle E_j|\hat{\boldsymbol{\epsilon}}\cdot\vec{\mu}|\bar{E},\mathbf{n},q^-\rangle\langle\bar{E},\mathbf{n},q^-|\hat{\boldsymbol{\epsilon}}\cdot\vec{\mu}|E_i\rangle. \tag{28}$$

It is clear from Eq. (26) that the $\omega_{j,i}$ are the most important Fourier components of $|\varepsilon(t)|^2$. We now consider a pulse composed of discrete Fourier components of the form,

$$\epsilon(\omega) = \sum_i \varepsilon_i\delta(\omega-\omega_{E,i}) + \varepsilon_i^*\delta(\omega+\omega_{E,i}). \tag{29}$$

As a function of time this pulse is a discrete sum of continuous waves (cw)

$$\varepsilon(t) = \sum_i \varepsilon_i \exp(-\mathrm{i}\omega_i t) + \text{c.c.}, \tag{30}$$

whose intensity is given by

$$\varepsilon^2(t) = \sum_{i'i} [I_{i',i}\exp(-\mathrm{i}(\omega_{i'}-\omega_i)t) + J_{i',i}\exp[-\mathrm{i}(\omega_{i'}+\omega_i)t] + \text{c.c.}], \tag{31}$$

where

$$I_{i',i} = \varepsilon_{i'}\varepsilon_i^*, \quad J_{i',i} = \varepsilon_{i'}\varepsilon_i.$$

Setting $\omega_i = \omega_{E,i} = (E - E_i)/\hbar$ and neglecting the very fast Fourier components of $|\varepsilon(t)|^2$ associated with $J_{i',i}$, we have from Eq. (26) that

$$\frac{\mathrm{d}}{\mathrm{d}t}b_j(t) = -\sum_i \sum_{i',i''}[I_{i',i''}\exp[\mathrm{i}(\omega_{j,i} - (\omega_{i'} - \omega_{i''})t] + I^*_{i',i''}\exp[\mathrm{i}(\omega_{j,i} + (\omega_{i'} + \omega_{i''})t]]\Gamma_{j,i}(\bar{E})b_i(t). \tag{32}$$

Keeping just those terms for which $\omega_{j,i} - (\omega_{i'} + \omega_{i''}) = 0$ or $\omega_{j,i} + (\omega_{i'} + \omega_{i''}) = 0$, i.e., $i' = j$ and $i'' = i$, we have that

$$\frac{\mathrm{d}}{\mathrm{d}t}b_j(t) = -\sum_i I_{j,i}\Gamma_{j,i}(\bar{E})b_i(t). \tag{33}$$

By eliminating the continuum in Eqs. (26)–(33) we have obtained a discrete number of first order coupled differential equations which can be readily solved numerically. The results can then be inserted into Eqs. (20) and (21) to obtain the photodissociation probability. In addition to the diagonal $\Gamma_{i,i}$ terms, which describe the decay of each bound state to the continuum, the off diagonal $\Gamma_{j,i}$ terms allow for laser-induced population transfer between the bound states, in what amounts to a stimulated resonance Raman process via the continuum. Thus, a strong pulse whose power spectrum encompasses the $\omega_{j,i}$ component, would, even if operating on a single precursor $|E_i\rangle$ state, give rise in a short time to the formation of a superposition of $|E_j\rangle$ states (i.e., the $|\chi(t)\rangle$ state of Eq. (17)). Pulse shaping thus acts not only to modify the photo-excitation to the continuum, but also to modify the composition of the precursor $|\chi(t)\rangle$ state.

2.3. Pulse shaping control as a disentanglement transformation

As stressed above, the object of control in a photodissociation experiment is the preparation of a single $|E, \mathbf{n}, q^-\rangle$ state. If this is achieved we are guaranteed, by Eq. (7), complete control insofar as only *one* fragment target state $|E, \mathbf{n}, q; 0\rangle$ is populated as $t \to \infty$. With this in mind, we rewrite Eq. (9) in matrix notation as

$$|\Psi^{(1)}(t)\rangle = \int \mathrm{d}E\mathrm{e}^{-\mathrm{i}Et/\hbar}(b^{(1)}_{E,\mathbf{n}_1,q_1}(t), b^{(1)}_{E,\mathbf{n}_2,q_2}(t), ..) \cdot \begin{pmatrix} |E, \mathbf{n}_1, q_1^-\rangle \\ |E, \mathbf{n}_2, q_2^-\rangle \\ \vdots \end{pmatrix}, \tag{34}$$

where $|\Psi^{(1)}(t)\rangle$ is the excited portion of the wave packet that originated from state $|E_1\rangle$, namely

$$|\Psi^{(1)}(t)\rangle \equiv |\Psi(t)\rangle - b_1|E_1\rangle\mathrm{e}^{-\mathrm{i}E_1t/\hbar}. \tag{35}$$

In order to achieve the control target we consider preparing a whole array of wave packets, by, for example, starting with other initial states composed of the system bound states $|E_i\rangle$. That is,

$$\underline{|\Psi_t\rangle} = \int \mathrm{d}E\mathrm{e}^{-\mathrm{i}Et/\hbar}\underline{\underline{\mathrm{b}}} \cdot \underline{|E, \mathbf{n}\rangle}, \tag{36}$$

where

$$\underline{|\Psi_t\rangle} \equiv \begin{pmatrix} |\Psi^{(1)}(t)\rangle \\ |\Psi^{(2)}(t)\rangle \\ \vdots \end{pmatrix}, \tag{37}$$

$$\underline{\underline{\mathrm{b}}} \equiv \begin{pmatrix} b^{(1)}_{E,\mathbf{n}_1,q_1}, b^{(1)}_{E,\mathbf{n}_2,q_2}, .. \\ b^{(2)}_{E,\mathbf{n}_1,q_1}, b^{(2)}_{E,\mathbf{n}_2,q_2}, .. \\ \vdots \end{pmatrix} \tag{38}$$

and

$$\underline{|E, \mathbf{n}\rangle} \equiv \begin{pmatrix} |E, \mathbf{n}_1, q_1^-\rangle \\ |E, \mathbf{n}_2, q_2^-\rangle \\ \vdots \end{pmatrix}. \tag{39}$$

It is easy to see that the $\underline{\underline{\mathrm{b}}}$ matrix factorizes as

$$\underline{\underline{\mathrm{b}}} = \hat{\varepsilon}(E) \cdot \underline{\underline{M}}(E), \tag{40}$$

where

$$\underline{\underline{M}}(E) = \begin{pmatrix} \langle E_1|\mu|E, \mathbf{n}_1, q_1^-\rangle, \langle E_1|\mu|E, \mathbf{n}_2, q_2^-\rangle, .. \\ \langle E_2|\mu|E, \mathbf{n}_1, q_1^-\rangle, \langle E_2|\mu|E, \mathbf{n}_2, q_2^-\rangle, .. \\ \vdots \end{pmatrix} \tag{41}$$

with $\hat{\varepsilon}(E)$ being a diagonal matrix of the Fourier transform of the pulse amplitude times the bound states coefficients, at the transition frequencies $\omega_{E,i}$,

$$\hat{\varepsilon}(E) = \begin{pmatrix} \varepsilon_1(E), 0, 0, .. \\ 0, \varepsilon_2(E), 0, .. \\ \vdots \end{pmatrix} \tag{42}$$

with

$$\varepsilon_i(E) = \int_{-\infty}^{\infty} \mathrm{d}t \varepsilon^*(t) \mathrm{e}^{\mathrm{i}\Delta_{E,i}t} b_i(t). \tag{43}$$

Writing the array of possible wave function produced as

$$\underline{|\Psi_t\rangle} = \int \mathrm{d}E \mathrm{e}^{-\mathrm{i}Et/\hbar} \hat{\varepsilon}(E) \cdot \underline{\underline{M}}(E) \cdot \underline{|E, \mathbf{n}\rangle}, \tag{44}$$

allows us to examine the possibility of taking different linear combinations of the components of the $\underline{|\Psi_t\rangle}$ vector so as to satisfy the control objectives of producing a single $|E, \mathbf{n}_i, q_i^-\rangle$ state. In this way different pathways starting with different precursor states leading to the same $|E, \mathbf{n}_i, q_i^-\rangle$ state will be seen to interfere to achieve the desired goal.

As an example, we consider a superposition state composed of the sum over the components of $\underline{|\Psi_t\rangle}$,

$$\Psi'(t) = \sum_k \int \mathrm{d}E \mathrm{e}^{-\mathrm{i}Et/\hbar} \varepsilon_k(E) \sum_j \underline{\underline{M}}(E)_{k,j} |E, \mathbf{n}_j, q_j^-\rangle. \tag{45}$$

In the weak field limit, the population and the phase of the initial levels can be assumed constant with time,

$$b_k(t) \approx b_k \equiv b_k(-\infty), \tag{46}$$

in which case all the $\varepsilon_k(E)$ matrix elements factor as

$$\varepsilon_k(E) \approx b_k \int_{-\infty}^{\infty} \mathrm{d}t \varepsilon^*(t) \mathrm{e}^{\mathrm{i}\Delta_{E,k}t} = 2\pi b_k \bar{\varepsilon}(\Delta_{E,k}), \tag{47}$$

where

$$\bar{\varepsilon}(\omega) \equiv (1/2\pi) \int_{-\infty}^{\infty} \mathrm{d}t \varepsilon^*(t) \mathrm{e}^{\mathrm{i}\omega t}. \tag{48}$$

Our objective to populate exclusively the ith fragment state $|E, \mathbf{n}_i, q_i^-\rangle$ can be realized in the weak field domain by choosing the pulse shape which defines $\Psi'(t)$ [Eq. (45)] to satisfy the condition

$$b_k \bar{\varepsilon}_i(\Delta_{E,k}) = \left(\underline{\underline{M}}(E)^{-1}\right)_{i,k}. \tag{49}$$

This choice eliminates all but a *single* $|E, \mathbf{n}_i, q_i^-\rangle$ state in $\Psi'(t)$ given by Eq. (45). We have thus achieved a *disentanglement* of the entangled wave packet produced by the single-precursor-state photodissociation processes.

We see that the disentanglement of the material system to achieve a single ith product state, is realized by actively *entangling* the material system with the photons. Conceptually, the disentanglement is performed in two steps: We first create a superposition of bound states,

$$|\Phi(t)\rangle = \sum_k b_k |E_k\rangle e^{-iE_k t/\hbar} \tag{50}$$

and then act on the superposition with photons of different frequencies, whose weights determine the pulse shape according to Eq. (49). This allows for multiple-path interference between the various ways of generating the $|E, \mathbf{n}_i, q_i^-\rangle$ state. The weight of each pathway is chosen so as to cause destructive interference in the production of all the $|E, \mathbf{n}, q^-\rangle$ states but one, the $|E, \mathbf{n}_i, q_i^-\rangle$ state. Thus, pulse shaping leads to control only insofar as it allows for interference between different coherently related bound states comprising Φ, or more generally, between different pathways leading to the same product.

2.4. Controllability in the continuum

In this sub-section we discuss limitations in the use of polychromatic light to controlling events that occur in the continuum. As in previous sections we shall use photodissociation as a generic example of events occurring in the continuum.

One reason control is incomplete is that in practice the perfect disentanglement transformation, as embodied in the pulse-shaping of Eq. (49), cannot be constructed simultaneously for all energies. This can be seen by noting that the $(\underline{\underline{M}}(E)^{-1})_{i,k}$ matrix element, which (for a single i) is a general function of two variables, k and E, must be factorisable as a product of b_k, which only depends on k, and $\bar{\varepsilon}_i(\Delta_{E,k})$ which only depends on $\Delta_{E,k}$. This factorization is satisfied only when either $\underline{\underline{M}}(E)$ does not vary too rapidly with E, or, conversely, when the $\langle E_1|\mu|E, \mathbf{n}, q^-\rangle$ matrix elements, which determine $\underline{\underline{M}}(E)$ (and the absorption spectrum), span a very narrow range of energies (e.g., the spectrum is composed of narrow, well spaced, resonances).

Whereas in the weak field limit control is achievable in two separable steps, in the strong field domain the factorization of Eq. (47) does not hold and these two steps become one. In that case the control conditions become

$$\varepsilon_{i,k}(E) = (\underline{\underline{M}}(E)^{-1})_{i,k}. \tag{51}$$

In this strong field regime the $b_k(t)$ coefficients are embedded in $\varepsilon_k(E)$ (see Eq. (43)) and are themselves functions of $\varepsilon(t)$. Hence the problem is inherently non-linear, necessitating an iterative solution. Nevertheless, the same interference mechanism outlined in the weak field domain applies. The only difference is that the pulse-shaping conditions are given implicitly via Eq. (51), rather than explicitly via Eq. (49), as in the weak field domain.

There are also *size* limitations to control of continuum processes, having to do with the number of *open channels* (i.e., in photodissociation the number of internal quantum states of each fragment that are accessible at a given total energy E) relative to the number of interfering processes we employ in order to control the outcome.

In order to see how control is limited by the size of the space we wish to control, we focus attention on a system whose Hamiltonian eigenstates are partitioned into bases for three subspaces A_0, A_1 and A_2 of dimensionality M_0, M_1 and M_2, respectively. States in A_i ($i = 0, 1, 2$) are denoted $|i, n_k\rangle$, where $n_k = 1, \ldots, M_i$ labels the state and i labels the subspace. Dynamics initiated in A_0 can flow into A_1 and A_2 (and inelastically into A_0) under the influence of a collection of scattering matrices S. The aim of control in this case is to find a particular set of vectors residing initially in the A_0 space that would evolve solely into the $\mathsf{A}_0 \oplus \mathsf{A}_1$ spaces. Below we find limitations to control, i.e., that the possibilities to eliminate the parasitic $\mathsf{A}_0 \to \mathsf{A}_2$ transitions which naturally accompany the $\mathsf{A}_0 \to \mathsf{A}_1$ transitions, are limited by the size of A_0 relative to the size of A_2.

A trivial solution of the above problem is obtained for a particular S for which all the elements connecting space A_0 to space A_2 are zero. This special solution is of little interest because the control challenge is whether it is possible in the general case, in which S *has* matrix elements that connect vectors in all sub-spaces, including vectors in the A_0 and A_2 spaces, to eliminate "parasitic" transitions to A_2. We show below that under these conditions, it is possible to attain this goal only if $M_2 < M_0$. When this size limitation is not met, namely when $M_2 \geqslant M_0$, it is not possible to construct an initial superposition state in A_0 which would evolve under the action of a general S matrix exclusively into $\mathsf{A}_0 \oplus \mathsf{A}_1$ [63].

The long-time evolution of a general initial state $|i_0\rangle \in \mathsf{A}_0$, expanded as

$$|i_0\rangle = \sum_{n_i=1}^{M_0} c_{n_i} |0, n_i\rangle \tag{52}$$

is given (using the linearity of S) as

$$\mathsf{S}|0, n_i\rangle = \sum_{j=0}^{2} \sum_{n_k=1}^{M_j} S^{(0,j)}_{n_i,n_k} |j, n_k\rangle. \tag{53}$$

By construction, the matrix elements $S^{(0,j)}_{n_i,n_k}$ ($j \neq 0$) are non-zero. Hence,

$$\mathsf{S}|i_0\rangle = \sum_{n_i=1}^{M_0} c_{n_i} \sum_{j=0}^{2} \sum_{n_k=1}^{M_j} S^{(0,j)}_{n_i,n_k} |j, n_k\rangle. \tag{54}$$

Projecting this state onto $\langle 2, n_f|$, squaring and summing over n_f, gives the probability of finding the system in A_2:

$$P(\mathsf{A}_2) = \sum_{n_f} \left| \sum_{n_i=1}^{M_0} c_{n_i} S^{(0,2)}_{n_i,n_f} \right|^2. \tag{55}$$

Under what conditions can we prevent transfer of populations into A_2? To do so requires $P(\mathsf{A}_2) = 0$, i.e.

$$\sum_{n_i=1}^{M_0} c_{n_i} S^{(0,2)}_{n_i,n_f} = 0 \quad \text{for } n_f = 1, \ldots, M_2, \tag{56}$$

or in matrix notation

$$\mathsf{S}_{M_0,M_2} \cdot \mathsf{c}_{M_0} = 0, \tag{57}$$

where S_{M_0,M_2} is the $M_0 \times M_2$ portion of S and c_{M_0} is an M_0 dimensional vector.

Eq. (57) has non-trivial solutions [64] if and only if the rank of S_{M_0,M_2} is less than M_0. This is certainly the case [65] for $M_2 < M_0$. However, for $M_2 > M_0$ the rank of S_{M_0,M_2} can be greater than or equal to M_0, and unless all M_0 dimensional sub-matrices of S_{M_0,M_2} are singular no non-trivial solution will exist. In more detail, denoting the kth such sub-matrix by $\mathsf{S}^{(k)}_{M_0,M_0}$ ($k = 1, [M_2!/(M_2 - M_0)!M_0!]$), non-trivial solutions are only possible if

$$\det \mathsf{S}^{(k)}_{M_0,M_0} = 0 \tag{58}$$

for all k. Clearly this imposes very stringent conditions on the possibility of the desired control, making it virtually impossible under all physically realizable conditions.

The inability to direct dynamics from A_0 away from A_2 under physical conditions, if $M_2 \geqslant M_0$, is entirely a quantum limitation. To see this consider the analogous situation classically. Here one examines a phase space region A_0 of volume M_0 containing trajectories which flow into final phase space regions A_0, A_1 and A_2, of volume M_0, M_1 and M_2. If one wants, for example, to design an initial state in A_0 which goes solely into A_1 one can do so by (1) allowing all trajectories to evolve from A_0 and settle into A_0, A_1 or A_2; and (2) time reverse just those trajectories which went from A_0 into A_1, to give a distribution in A_0. The resultant distribution, when propagated forward in time, will evolve solely from A_0 to A_1.

The simplest way to understand the difference between the classical and quantum results is to note that in classical mechanics each classical state (i.e. each trajectory) goes from A_0 into a specific A_i. This is not the case quantum mechanically where each A_0 state has non-zero S matrix elements with states in both $\mathsf{A}_0 \oplus \mathsf{A}_1$ and A_2.

The quantum restriction we have obtained is completely general, applying to both systems which are controlled, in which case S defines a process which we design for control purposes, as well as to uncontrolled system evolution in which S is dictated by nature. The result establishes an important inequality between the dimension of the subspace (A_2)

which we desire not to populate and the initial subspace (A_0). Further, unlike quantum entropy arguments for example, the result imposes a fundamental restriction on the dynamical evolution of the wave function itself. No observer or measurement need be invoked.

3. Applications of coherent control: the one-photon vs. two-photon interference

As an application of the above formulation we briefly discuss here a CC scenario in which we interfere a one-photon process with a two-photon process in order to control the directionality of electronic currents in semiconductors and other environments [66], with related applications in material transport [67].

We can do so by irradiating the material system by two fields, $A_1 e^{-i\omega_1 t - i\phi_1}$, inducing a *one-photon* transition, and $A_2 e^{-i\omega_2 t - i\phi_2}$, where $\omega_2 = \omega_1/2$, induces a *two-photon* transition (Fig. 1).

Given an initial $|\mathbf{k}_v\rangle$ valence-band state, and that both processes are in resonance with transitions to $|\mathbf{k}_c\rangle$ conduction-band states, the probability-density in the conduction-band, $P(\mathbf{k}_c)$, is given as the square of the sum of one-photon and two-photon amplitudes. Explicitly, $P(\mathbf{k}_c) = |f(\mathbf{k}_c)|^2$ with

$$f(\mathbf{k}_c) \propto A_1 p_{c,v} e^{-i\phi_1} + A_2^2 d_{c,v} e^{-2i\phi_2}, \tag{59}$$

where

$$p_{c,v} \equiv \langle \mathbf{k}_c | \mathrm{p} | \mathbf{k}_v \rangle, \quad d_{c,v} \equiv \sum_i \frac{p_{c,i} p_{i,v}}{\hbar\omega_2 - E_i}.$$

In the above, $p_{i,v} \equiv \langle \mathbf{k}_i | \mathrm{p} | \mathbf{k}_v \rangle (p_{c,i} \equiv \langle \mathbf{k}_c | \mathrm{p} | \mathbf{k}_i \rangle)$ are the momentum matrix elements between the initial (final) state and all intermediate states $|\mathbf{k}_i\rangle$ of energy E_i.

Squaring Eq. (59) and separating out $P_{\mathrm{non}} \equiv |A_1 p_{cv}|^2 + |A_2^2 d_{cv}|^2$, the non-interfering sum of one-photon and two-photon probabilities, from the interference term, $2R_e\{A_1^* p_{cv}^* A_2^2 d_{cv} e^{i[\phi_1 - 2i\phi_2]}\}$, i.e., twice the real part of the product of the one-photon and two-photon amplitudes, we can write $P(\mathbf{k}_c)$ as

$$P(\mathbf{k}_c) \propto P_{\mathrm{non}} + P_{\mathrm{int}} \cos(\delta_{1,2} + \phi_1 - 2\phi_2), \tag{60}$$

where $P_{\mathrm{int}} \equiv |A_1 A_2^2 p_{c,v} d_{c,v}|$, with $\delta_{1,2}$ denoting the phase of the $p_{cv}^* d_{cv}$ product. We see that we can control the sign of the interference term and hence whether the interference be constructive or destructive, by varying $\phi_1 - 2\phi_2$.

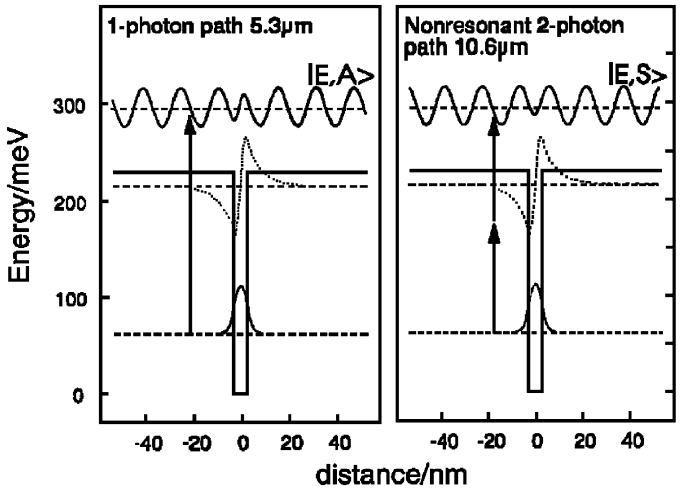

Fig. 1. A schematic illustration of an experiment in which the directionality of current formed in the conduction band of a semiconducting quantum well system was controlled by irradiating the sample with a combination of a fundamental frequency (that of the CO_2 laser) and its second harmonics. Taken from [68].

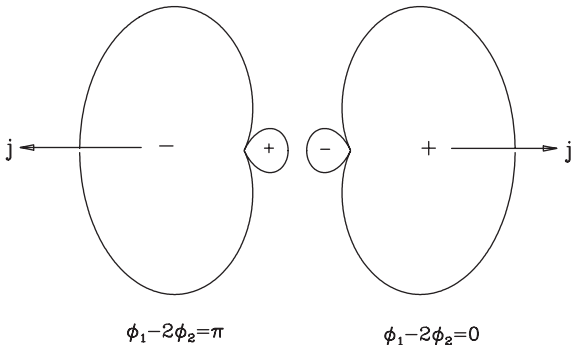

Fig. 2. Polar plots of the angular distribution of the symmetry-broken wave functions formed by exciting a 1*s* orbital by a combination of a fundamental frequency and its second harmonic at two relative phase values, $\phi_1 - 2\phi_2 = 0$ and $\phi_1 - 2\phi_2 = \pi$, determining **j**, the DC injection currents formed as a result of the process.

The type of symmetry-broken angular distributions formed as a result of the action of the two fields are shown in Fig. 2. We see that a phase difference that results in the interference being constructive in the forward direction leads to destructive interference in the backward direction, and vice versa.

Depending on the $\phi_1 - 2\phi_2$ *relative phase* the injection rates into the $|\pm k_c\rangle$ states can be different, resulting in the generation of a DC electric current, $j_c \propto \int \mathbf{k}_c P_{\mathbf{k}_c}\, \mathrm{d}\mathbf{k}_c \neq 0$ ($j_v \neq j_c$), in the conduction (valence) band of the semiconductor.

4. Coherent control and adiabatic passage

The "quantum control" (QC) problem can be phrased as finding ways of inducing complete transfer of population from an arbitrary "initial" wave packet of states to a desired "target" wave packet of states. In searching for useful control strategies we look for methods that can be *generally* applied to an entire class of systems. In addition to generality, the method should ideally also be *robust* and be based on some simple and *transparent* principle. Such method arises when we merge CC, by which one may attain *selectivity* in a multi-channel situation, and adiabatic passage, which enables the *complete* transfer of populations between a pair of quantum states (Fig. 3).

4.1. Adiabatic passage

With the introduction in the 1980s of new laser sources a number of powerful population transfer techniques, such as, overtone pumping (OTP) [69], off-resonance stimulated Raman scattering (ORSRS) [70,71] and stimulated emission pumping (SEP) [72], were developed. These methods resulted however in only *partial* population transfer between quantum states. The adoption in optics of the Adiabatic Passage (AP) technique [73–76] operating (in contrast to CC) along a *single* quantum pathway, has opened the way for affecting a *complete* population transfer between states.

Complete population transfer in AP was shown theoretically [74] and independently implemented experimentally a few years later in a method called Stimulated Raman adiabatic passage (STIRAP) [75,76]. In this method, which is a variant of the Stimulated Raman process, the two ("pump" and "dump") pulses are employed in the reverse ("counter-intuitive") order to that of the usual stimulated Raman process, namely, in STIRAP the "dump" pulse precedes the "pump" pulse. We now explain how the "counter-intuitive" pulse ordering leads to the desired complete population transfer.

Consider irradiating the ("Λ-type") three state system depicted in Fig. 4 by two laser pulses, a "pump" pulse (P) of center frequency ω_P and pulse envelope $\varepsilon_P(t)$ and a "dump" pulse (D) of center frequency ω_D and pulse envelope $\varepsilon_D(t)$. The Hamiltonian for this system is written as

$$H = H_M - 2\mu_{0,1}\varepsilon_P(t)\cos(\omega_P t) - 2\mu_{2,0}\varepsilon_D \cos(\omega_D t), \tag{61}$$

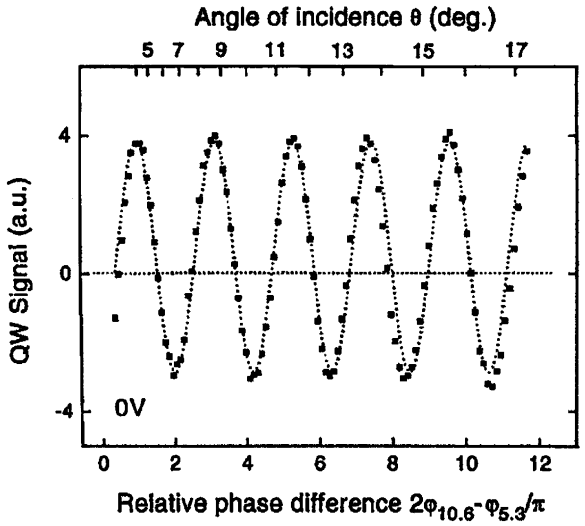

Fig. 3. Experimental control of current directionality. Shown is the DC current generated by the experimental setup of Fig. 1 as a function of the phase difference between the fundamental source (wavelength of 10.6 μm) and its second harmonic. Taken from [68].

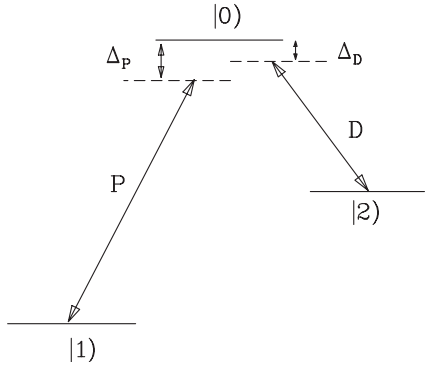

Fig. 4. The three level Λ configuration adiabatic passage scheme.

where $\mu_{0,1}$ is the projection of the dipole matrix element for the $|\psi_1\rangle \leftrightarrow |\psi_0\rangle$ transition on the P polarization, and $\mu_{2,0}$ is the projection of the dipole matrix element for the $|\psi_0\rangle \leftrightarrow |\psi_2\rangle$, transition on the D polarization direction.

Expanding the time dependent wave function in the three bare states,

$$|\Psi(t)\rangle = \sum_{i=1,0,2} b_i(t)|\psi_i\rangle e^{-iE_i t/\hbar}, \tag{62}$$

we can write the Schrödinger equation for the coefficients as

$$\frac{d}{dt}\mathbf{b}(t) = iH \cdot \mathbf{b}(t), \tag{63}$$

where $\mathbf{b} \equiv (b_1, b_0, b_2)$ column vector and

$$H = \begin{pmatrix} 0 & \Omega_P^*(t)e^{-i\Delta_P t} & 0 \\ \Omega_P(t)e^{i\Delta_P t} & 0 & \Omega_D^*(t)e^{i\Delta_D t} \\ 0 & \Omega_D(t)e^{-i\Delta_D t} & 0 \end{pmatrix}, \tag{64}$$

where $\Omega_{P(D)} \equiv \mu_{0,1(2,0)}\varepsilon_{P(D)}$ is the Rabi frequency for "pump" ("dump") process, and $\Delta_{P(D)} \equiv \omega_P - \omega_{0,1(2,0)}$ is the detuning of the "pump" ("dump") pulse relative to the transition frequency $\omega_{0,1(2,0)}$.

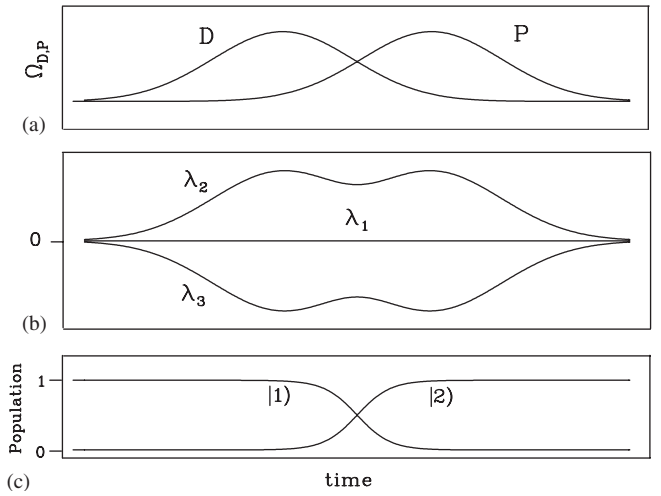

Fig. 5. The pulses (panel (a)), eigenvalues (panel (b)), and populations (panel (c)), as a function of time in the three level adiabatic passage with "counter-intuitive" ordering.

We now diagonalize the H matrix

$$\mathsf{H}\cdot\mathsf{U}=\mathsf{U}\cdot\hat{\lambda}, \tag{65}$$

where $\hat{\lambda}$ is a diagonal matrix, to obtain that

$$\lambda_1=0,\quad \lambda_{2,3}(t)=\pm[|\Omega_P(t)|^2+|\Omega_D(t)|^2]^{1/2} \tag{66}$$

The eigenvector corresponding to the null eigenvalue $\lambda_1=0$ is of the form,

$$\mathsf{U}^{(1)}=\begin{pmatrix}\cos\theta(t)\\ 0\\ -\mathrm{e}^{\mathrm{i}\chi(t)}\sin\theta(t)\end{pmatrix}, \tag{67}$$

where

$$\theta(t)=\arctan\left(\left|\frac{\Omega_P(t)}{\Omega_D(t)}\right|\right), \tag{68}$$

and

$$\chi(t)\equiv(\Delta_P-\Delta_D)t-\phi_D(t)+\phi_P(t)=\phi_P(t)-\phi_D(t),$$

where we assumed two-photon resonance ($\Delta_P-\Delta_D=0$). $\phi_i(t)$ is the phase of the Rabi frequency,

$$\Omega_i(t)\equiv|\Omega_i(t)|\mathrm{e}^{\mathrm{i}\phi_i(t)},\quad i=P,D \tag{69}$$

The adiabatic state associated with the $\lambda_1=0$ eigenvector is

$$|\lambda_1(t)\rangle=\cos\theta(t)\mathrm{e}^{-\mathrm{i}E_1t/\hbar}|\psi_1\rangle-\mathrm{e}^{\mathrm{i}\chi(t)}\sin\theta(t)\mathrm{e}^{-\mathrm{i}E_2t/\hbar}|\psi_2\rangle. \tag{70}$$

We see from Eqs. (67) and (11) that if the system resides initially in $|\psi_1\rangle$ it will correlate exclusively to the $|\lambda_1(t)\rangle$ ("null") eigenvector. It also follows from Eqs. (68) and (11) that if the dump pulse precedes the pump pulse this eigenvector will go smoothly from being entirely $|\psi_1\rangle$ to being entirely $|\psi_2\rangle$, while leaving the state $|\psi_0\rangle$ completely unpopulated throughout the process. Thus, we can achieve as illustrated in Fig. 5 the desired *complete population transfer*. An example of an experiment demonstrating this effect is given in Fig. 6.

Following the initial papers of Bergmann et al. [75–78], the properties of three-state STIRAP have been thoroughly investigated theoretically [74,79–81]. Among the properties examined were the sensitivity of the population transfer

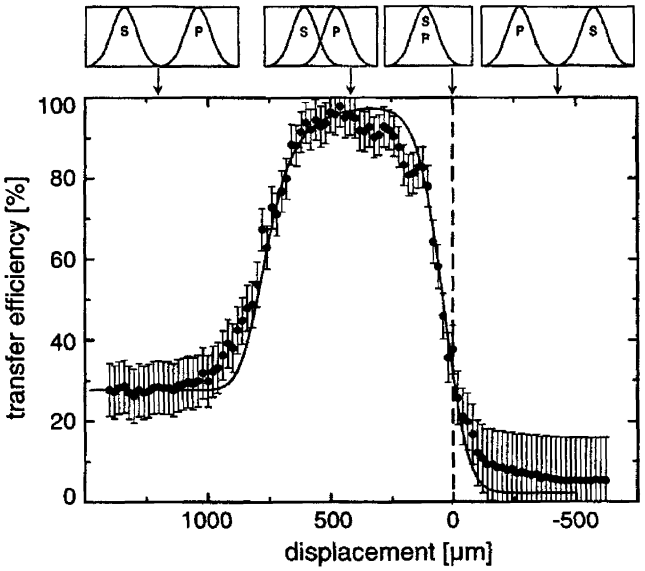

Fig. 6. Experiments on STIRAP in the Ne atom. The degree of population in level $|\psi_2\rangle (=^3 P_2)$ as a function of the delay between the pump and the dump pulses. As the pulses overlap with the dump pulse preceding the pump pulse the population in the $|\psi_2\rangle$ state is seen to approach 100%. Taken from [82].

to the delay between the dump and pump pulse [82]; the effect of one-photon detuning [83]; the effect of two-photon detuning [81]; losses from the intermediate state [84–88]; effects due to the existence of many intermediate states [77,89]; and going beyond the "rotating wave approximation" (RWA) [90,91].

The STIRAP process has been demonstrated experimentally using CW lasers on sodium dimers [76] and meta-stable neon atoms [82,92]. It has been also implemented using pulsed lasers on nitrous oxide molecules [93], sulfur dioxide molecules [94], in a ladder system of a rubidium atom [95], and with degenerate or nearly degenerate states [96].

Generalizations of three state STIRAP to the multi-state chains situation [92,97–101], to adiabatic momentum transfer [92,98,102,103], to branched-chain excitation [104–108], and to population transfer via a continuum of intermediate states [109–114], in direct relation to laser induced continuum structure (LICS) [115–119] have also been made.

New techniques related to STIRAP, such as, hyper-Raman STIRAP (STIHRAP) [91,90,120], stark-chirped rapid adiabatic passage (SCRAP) [121,122], adiabatic passage by light-induced potentials (APLIP) [123–126] and photo-associative STIRAP as a source for cold molecules [127–131] have been developed (Fig. 6).

4.2. The non-degenerate quantum control problem

So far we have dealt separately with the topics of *selectivity control*, i.e., the induction of an active bias in favor of a desired outcome, and the attainment of a *complete population transfer* from one energy eigenstate to another. In the former, the transfer of population between the initial and final states need not be complete. In the latter, the possibility of a number of final outcomes simply does not exist.

In this section we combine the above two objectives by discussing a more general type of quantum control, called "non-degenerate quantum control" (NQC), where the goal is to achieve complete population transfer between two arbitrary superposition states ("wave packets") composed of non-degenerate energy eigenstates. The present emphasis on the non-degenerate nature of the constituent states stems from the fact that in this case frequency discrimination allows for an easy and simple addressing of each constituent state. Such simple means of addressing is not possible if degeneracies exist and we postpone the discussion of the more complicated case of quantum control between superpositions of *degenerate* energy eigenstates to Section 4.3.

In spite of the above limitations, NQC is of interest in many atomic and molecular systems [see e.g., [132–134]]. Although a theorem asserting that a solution to the "Non-Degenerate Quantum Control Problem" (NQP) exists under

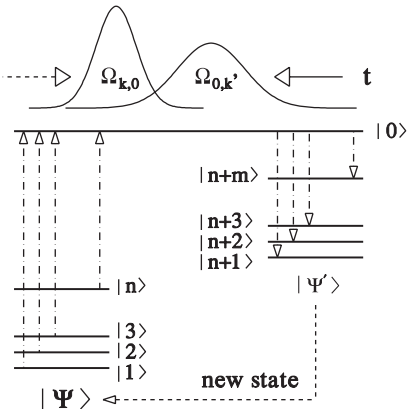

Fig. 7. An illustration of a transfer process in which $|\Psi\rangle \to |0\rangle \to |\Psi'\rangle$. The first (dump) laser pulse, with Rabi frequencies $\Omega_{0,l}(t)$, couples all the initially empty $|l\rangle$ final states $l = n+1, \ldots, n+m$ to state $|0\rangle$, while the second (pump) pulse, with Rabi frequency $\Omega_{0,k}(t)$, couples state $|0\rangle$ to the initially populated $|k\rangle$ states, with $k = 1, \ldots, n$. This process can be repeated again and again.

certain conditions has been published early on [135], this "existence theorem" provides no clue as to the nature of the external fields which actually bring about this type of population transfer.

Solutions of the NQP for some particular weak-field cases [2,52], the three state STIRAP [73,76,78,81,82,108] and its generalization to a few more final states [77,104–106,136,137] have been known for quite some time. The construction of fields which solve the NQP in general has been achieved relatively recently [138]. Although this construction is not the only one possible, its existence is enough to establish that the general NQP is solvable. As it turns out, this construction is also simple and analytic, making it especially attractive and useful for laboratory implementations.

The solution of Ref. [138] is a generalization of the three-state STIRAP discussed in Section 4.1 above. It has evolved from an intermediate result [139] dealing with the transfer of population from a *single* energy eigenstate $|1\rangle$ to a wave packet composed of an *arbitrary number* of non-degenerate energy eigenstates with arbitrary coefficients $|\Psi'\rangle = \sum_k c_k e^{-i\omega_k t}|k\rangle$ $(k \neq 1)$. As in three state STIRAP, the population transfer proceeds via an intermediate energy eigenstate $|0\rangle$, which acts as a virtual unpopulated "stepping stone". The method was applied to the preparation of "coherent" wave packets of material states, in direct analogy with the construction of similar light states by other means [140,141].

Based on the above, the solution of the full NQP, i.e., the achievement of the $|\Psi^i\rangle = \sum_k c_k^i e^{-i\omega_k t}|k\rangle \to |0\rangle \to |\Psi^f\rangle = \sum_{l'} c'_{lf} e^{-i\omega_{l'} t}|l'\rangle$ transfer process, can be accomplished in a straight-forward manner [138]. As discussed below, it is also possible to control the *extent* of population transfer, from 0 to 100%. [In a different context, control over the extent of transfer can also be achieved in other ways, e.g., by successive hops using a chain of states [99]].

Fig. 7 illustrates the method of Ref. [138]. It consists of the application of two pulses in a "counter-intuitive" order, i.e., the "dump" pulse, characterized by a set of Rabi frequencies $\Omega_{0,l'}$, coupling the intermediate $|0\rangle$ state to the final $l' = n+1, \ldots, n+m$ states, is made to *precede* (while partially overlapping) the "pump" pulse, whose constituent Rabi frequencies $\Omega_{k,0}$ couple the initially populated $k = 1, \ldots, n$ states and the intermediate $|0\rangle$ state.

We now describe the NQP solution in greater detail. We consider the action of two pulses, the scalar part of whose electric field is given as

$$\varepsilon(t) = R_e \sum_{k=1}^{n+m} \varepsilon_k(t) e^{-i\omega_{0,k} t}, \tag{71}$$

on a wave packet composed of $|1\rangle, \ldots, |n\rangle$ states with eigenenergies $\omega_1, \ldots, \omega_n$. In the above, $\varepsilon_k(t)$ are the (slowly varying) envelopes of the $\omega_{0,k}$ mode frequencies. The latter are tuned to be in resonance with the $\omega_0 - \omega_k$ transition frequencies.

The first n components of $\varepsilon(t)$ describe the "pump" pulse, and the last m components—the "dump" pulse. The time-dependence of the "dump" ("pump") pulse envelope are controlled by a function, $0 < f_{D(P)}(t) < 1$, according to, $\varepsilon_l(t) = f_D(t)\varepsilon_l$ for $l = n+1, \ldots, n+m$ and $\varepsilon_k(t) = f_P(t)\varepsilon_k$ for $k = 1, \ldots, n$.

In the rotating wave approximation (RWA), in which we also neglect the off-resonance terms, we can write the radiation-matter Hamiltonian, expressed in atomic units ($\hbar = 1$), as

$$H = \sum_{i=0}^{n+m} \omega_i |i\rangle\langle i| + \sum_{k=1}^{n+m} [\Omega_{0,k}(t) e^{-i\omega_{0,k}t} |0\rangle\langle k| + \text{h.c.}].$$

Here,

$$\Omega_{0,k}(t) \equiv \mu_{0,k}\, \varepsilon_k(t) \equiv O_{0,k} f_{D(P)}(t) = \mu_{0,k} \varepsilon_k\, f_{D(P)}(t)$$

are the complex Rabi frequencies, with $\mu_{0,k}$ being the electric-dipole matrix-elements between the $|0\rangle$ and $|k\rangle$ states.

The system evolution is described by the wave function $|\Psi(t)\rangle$, expanded as $|\Psi\rangle = \sum_{i=0}^{n+m} c_i(t) e^{-i\omega_i t} |i\rangle$. Denoting by $\mathbf{c}(t) \equiv (c_0, c_1, \ldots, c_n, c_{n+1}, \ldots, c_{n+m})$ the *column* vector of expansion coefficients, we have that,

$$\dot{\mathbf{c}}(t) = -i\, \mathsf{H}(t)\, \mathbf{c}(t), \tag{72}$$

where the effective time-dependent Hamiltonian is

$$\mathsf{H}(t) = \begin{bmatrix} 0 & \Omega_{0,1} & \ldots & \Omega_{0,n} & \Omega_{0,n+1} & \ldots & \Omega_{0,n+m} \\ \Omega_{1,0} & 0 & \ldots & 0 & 0 & \ldots & 0 \\ \ldots & \ldots & \ldots & \ldots & \ldots & \ldots & \ldots \\ \Omega_{n,0} & 0 & \ldots & 0 & 0 & \ldots & 0 \\ \Omega_{n+1,0} & 0 & \ldots & 0 & 0 & \ldots & 0 \\ \ldots & \ldots & \ldots & \ldots & \ldots & \ldots & \ldots \\ \Omega_{n+m,0} & 0 & \ldots & 0 & 0 & \ldots & 0 \end{bmatrix}.$$

In the counter-intuitive scheme, the pump pulse with the $\varepsilon_1, \ldots, \varepsilon_n$ components follows the dump pulse with the $\varepsilon_{n+1}, \ldots, \varepsilon_{n+m}$ components.

Of the $n + m + 1$ λ_i eigenvalues of $\mathsf{H}(t)$, $n + m - 1$ are zero, $\lambda_1 = \lambda_2 = \cdots = \lambda_{n+m-1} = 0$, and two are non-zero, $\lambda_{n+m}(t) = -\lambda_{n+m+1}(t) = \left(\sum_{k=1}^{n+m} |\Omega_{0,k}(t)|^2\right)^{1/2}$. The crucial zero eigenvalues correspond to *three* types of "null" states, which we term the "initial null states" (INS), the "mixed null states" (MNS) and the "final null states" (FNS). Absorbing the temporal phase factors by re-defining the basis states as, $|j\rangle \equiv e^{-i\omega_j t} |j\rangle$, the three types of null states can be written as

$$\begin{aligned} |D^I_{kk'}\rangle &= \Omega_{0,k'} |k\rangle - \Omega_{0,k} |k'\rangle, \\ |D^M_{kl}\rangle &= \Omega_{0,l} |k\rangle - \Omega_{0,k} |l\rangle, \\ |D^F_{ll'}\rangle &= \Omega_{0,l'} |l\rangle - \Omega_{0,l} |l'\rangle, \\ (k \neq k' &= 1, \ldots, n;\ l \neq l' = n+1, \ldots, n+m). \end{aligned} \tag{73}$$

This construction generates $n(n-1)/2$ INS, nm MNS, and $m(m-1)/2$ FNS, out of which only $n + m - 1$ states are linearly independent.

We first examine the MNS states and show that we can combine them to obtain a state that correlates (in the counter-intuitive pulse ordering) at $t = 0$ with the initial state $|\Psi^i\rangle = \sum_k c^i_k |k\rangle$, and at $t = t_{\text{end}}$ with the final state $|\Psi^f\rangle = \sum_l c^f_l |l(t_{\text{end}})\rangle$. The particular combination that satisfies these asymptotic conditions is

$$|D^M\rangle = \sum_{k,l} t_{kl} |D^M_{kl}\rangle = \sum_{k=1}^{n} |k\rangle \sum_{l=n+1}^{n+m} t_{kl} \Omega_{0,l} - \sum_{l=n+1}^{n+m} |l\rangle \sum_{k=1}^{n} t_{kl} \Omega_{0,k}, \tag{74}$$

where the t_{kl} coefficients are chosen, so that

$$\sum_{l=n+1}^{n+m} t_{kl} \Omega_{0,l} \propto c^i_k, \quad \sum_{k=1}^{n} t_{kl} \Omega_{0,k} \propto c^f_l. \tag{75}$$

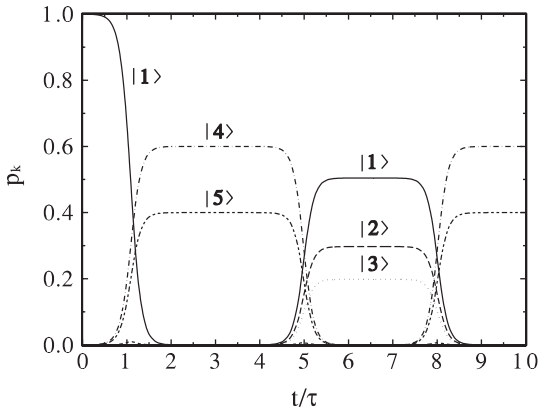

Fig. 8. The populations, $p_k(=|c_k|^2)$, of the $|k\rangle$, $k=1$ to 5, energy eigenstates as a function of time in the chain of transfer processes described in the text. The phases of the c_k coefficients were chosen as zero.

Eqs. (75) can be satisfied by choosing ($\Omega_{0,k}(t) \equiv O_{0,k}\, f_{D(P)}(t)$),

$$t_{kl} = O_{0,k} O_{0,l} \quad \text{and} \quad O_{0,k} = C c_k^i, \quad O_{0,l} = C^{'} c_l^f, \tag{76}$$

where C, $C^{'}$ are arbitrary complex numbers. These numbers are chosen such that the (slowly varying) Rabi frequencies be large enough so as to guarantee the adiabaticity of the transfer process.

Since the particular MNS thus generated is an eigenstate of the light-matter Hamiltonian, $|\Psi^i\rangle$ which correlates initially with it will continue to evolve adiabatically along this eigenstate, executing a smooth AP to the desired final state $|\Psi^f\rangle$. The success of AP depends on the goodness of the adiabatic approximation, which roughly speaking demands that $\Omega\Delta t \gg 1$ where Ω is an average Rabi frequency and Δt is the pulse duration. This criterion is complementary to the demand that the separation between the λ_i eigenvalues be larger than the non-adiabatic coupling terms. In the present case, all the MNS of Eq. (74) are degenerate with other null states, and adiabaticity appears to be easily broken. However, when we orthogonalize all the MNS, these couplings become zero [139], thereby guaranteeing the robustness of the $|\Psi^i\rangle \to |\Psi^f\rangle$ transfer.

Fig. 8 illustrates the validity of Eq. (74) for a chain of population transfers:

$$|1\rangle \to c_4|4\rangle + c_5|5\rangle \to c_1|1\rangle + c_2|2\rangle + c_3|3\rangle \to c_4'|4\rangle + c_5'|5\rangle.$$

In the first link of the transfer-chain, $|1\rangle \to c_4|4\rangle + c_5|5\rangle$, which is seen to exhibit 100% transfer probability, the multi-mode Rabi frequencies were chosen as, $\Omega_{0,1}(t) = O_{0,1} \exp[-(t-t_0)^2/\tau^2]$ and $\Omega_{0,4(5)}(t) = O_{0,4(5)} \exp[-t^2/\tau^2]$, with $t_0 = 2\tau$ being the delay between the pulses. The coefficients of Eq. (76) are chosen to be $C = C^{'} = 50/\tau$. The next transfer-link is realized by repeating the pulses with different central times and amplitudes $O_{0,k}$, in accordance with Eq. (76).

We can briefly investigate the INS states defined in Eq. (73). Given the initial state $|\Psi^i\rangle = \sum_k c_k^i |k\rangle$, the INS will dominate the adiabatic dynamics if we choose the vector of Rabi frequencies of the pump pulse $\mathbf{\Omega}^i \equiv (\Omega_{0,1}, \ldots, \Omega_{0,n})$ to be orthogonal to the vector of initial coefficients $\mathbf{c}^i \equiv (c_1^i, \ldots, c_n^i)$, i.e., $\mathbf{\Omega}^i \cdot \mathbf{c}^i = 0$. If we form a linear combination INS, $|D^I\rangle = \sum_{k,k'} t_{kk'} |D^I_{kk'}\rangle$, with the $t_{k,k'}$ coefficients chosen to make $|D^I\rangle$ correlate at $t=0$ with $|\Psi^i\rangle$, we guarantee that population will remain at the end of the process in the same $|\Psi^i\rangle$ state. In other words, the choice of $\mathbf{\Omega}^i \cdot \mathbf{c}^i = 0$ guarantees that the extent of transfer is 0.

As an example we consider a population transfer from the state $|\Psi^i\rangle = c_1^i\,|1\rangle + c_2^i\,|2\rangle$ to the state $|3\rangle$. Choosing the pump $O^i\left[\equiv \mathbf{\Omega}^i(t)/f_P(t)\right]$ vector to be,

$$O_{0,1}^i = (c_1^i)^* \cos\varphi + c_2^i \sin\varphi,$$

$$O_{0,2}^i = (c_2^i)^* \cos\varphi - c_1^i \sin\varphi, \tag{77}$$

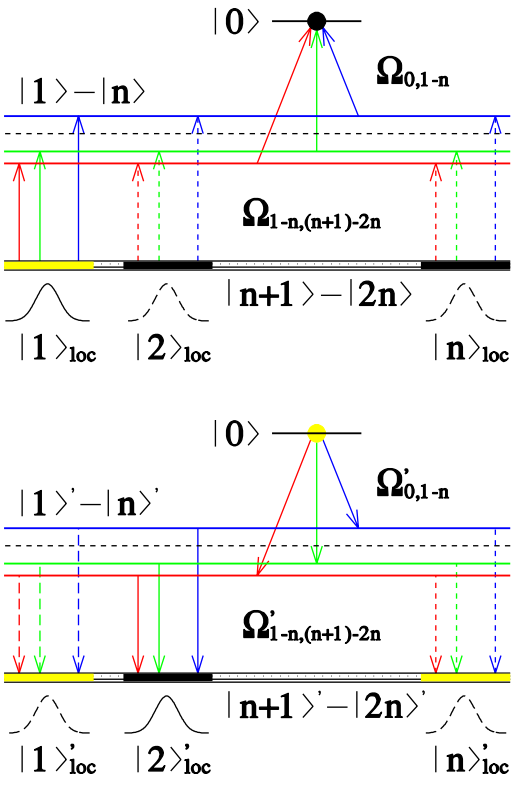

Fig. 9. The DQC scheme. (upper panel) The first step: population in an initial wave packet $|\Psi^i\rangle$, also called $|1\rangle_{\rm loc}$, composed of *n nearly-degenerate* eigenstates is transferred to a single state $|0\rangle$, by a two-photon adiabatic passage via *n non-degenerate* intermediate states. (lower panel) The second step: population transfer by a time reversed process with different Rabi frequencies from $|0\rangle$ to the target wave packet $|\Psi^f\rangle$, also called $|2\rangle'_{\rm loc}$, composed of another set of nearly-degenerate eigenstates. The process can be repeated to generate other ($|n\rangle'_{\rm loc}$) localized states.

we can make the MNS of Eq. (74) correlate with $|\Psi^i\rangle$, by choosing $\varphi = 0$ or π, giving rise to a complete population transfer. In contrast, the $\varphi = \pi/2$ choice causes the INS, for which the transfer probability is zero, to correlate with $|\Psi^i\rangle$. The *extent* of population transfer is thus controlled by the angle φ.

In complete analogy with the INS, the FNS span a subspace defined by the vectors $|D^F\rangle = \sum_{l,l'} t_{ll'}|D^F_{ll'}\rangle$, where $t_{ll'}$ are chosen by the demand that $|D^F\rangle$ correlates at $t = t_{\rm end}$ with the "final" state $|\Psi^f\rangle = \sum_l c^f_l |l\rangle$. Choosing the dump pulses $\mathbf{\Omega}^f \equiv (\Omega_{0,n+1}, \ldots, \Omega_{0,n+m})$ such that $\mathbf{\Omega}^f \cdot \mathbf{c}^f = 0$, where $\mathbf{c}^f \equiv (c^f_{n+1}, \ldots, c^f_{n+m})$ guarantees that population will remain in $|\Psi^f(t)\rangle$.

4.3. The quantum control problem in the presence of degenerate states

In the "degenerate quantum control" (DQC) problem the objective is to control population transfer between wave packets with arbitrary coefficients, $|\Psi^i\rangle = \sum_k c^i_k |k\rangle e^{-i\omega_k t} \to |\Psi^f\rangle = \sum_{k'} c^f_{k'} |k'\rangle e^{-i\omega_{k'} t}$, in which some component energy eigenstates are degenerate (or "nearly-degenerate"). The problem is more demanding than the non-degenerate one because it is no longer possible to use the different frequency components of the field to address different component states. Addressing of the component energy eigenstates in this AP process must therefore be based on *phase-interferences* of one form or another.

In spite of the above difficulty, we have shown [142] that when the "Rabi-frequency vectors" (defined below) are linearly-independent, DQC can be executed by merging the AP and CC techniques. As illustrated in Fig. 9 this is done in two steps: In the first step (upper panel), one uses a pair of laser pulses to adiabatically transfer the population of an initial wave packet $|\Psi^i\rangle$, composed of the nearly-degenerate energy eigenstates $|k\rangle$ ($k = n+1, \ldots, 2n$), to a

single ("parking") state $|0\rangle$, using the non-degenerate auxiliary states $|j\rangle$ ($j = 1, \ldots, n$) as intermediates. As in NQC, the use of non-intuitive pulse ordering guarantees complete population transfer to the "parking" state $|0\rangle$. In the first step the non-intuitive pulse ordering means that the "dump" (D) pulse, characterized by Rabi frequencies $\Omega_{0;1,\ldots,n}$, linking all the $|j\rangle$ states to the $|0\rangle$ state, is made to precede the "pump" (P) pulse, characterized by $\Omega_{n+1,\ldots,2n;1,\ldots,n}$ Rabi frequencies, linking all the $|k\rangle$ states to all the $|j\rangle$ states. In the second step (Fig. 9 lower panel), the population in the "parking" state $|0\rangle$ is transferred to the target wave packet $|\Psi^f\rangle$, composed of the same (or different) set of nearly-degenerate eigenstates $|k'\rangle$. The transfer is executed in an adiabatic fashion, with the "pump" (P) pulse, now linking the $|j\rangle$ states and the $|0\rangle$ state, following the "dump" (D) pulse, linking the final $|k^{'}\rangle$ states with all the $|j\rangle$ states.

The electric field of the combined "pump" and "dump" pulses used in the first step is

$$\vec{E}(t) = \vec{E}_D(t) + \vec{E}_P(t), \tag{78}$$

where

$$\vec{E}_D(t) = R_e \sum_{j=1}^{n} \hat{\epsilon}_{0,j}\varepsilon_{0,j}(t)\mathrm{e}^{-\mathrm{i}\omega_{0,j}t},$$

$$\vec{E}_P(t) = R_e \sum_{j=1}^{n}\sum_{i=n+1}^{2n} \hat{\epsilon}_{j,i}\varepsilon_{j,i}(t)\mathrm{e}^{-\mathrm{i}\omega_{j,i}t}. \tag{79}$$

In the second step the form assumed by the "dump" (D) and "pump" (P) pulses is being *reversed*.

The "dump" and "pump" field components are characterized by the polarization directions $\hat{\epsilon}_{0,j}$ and $\hat{\epsilon}_{j,i}$ and the slowly varying amplitudes $\varepsilon_{0,j}(t)$ and $\varepsilon_{j,i}(t)$. The central frequencies of the field components are chosen to be in near resonance with the system's transition frequencies, $\omega_{0,j} = \omega_0 - \omega_j$ and $\omega_{j,i} = \omega_j - \omega_i$.

The complex Rabi frequencies are $\Omega_{j,i}(t) \equiv \vec{\mu}_{j,i} \cdot \hat{\epsilon}_{j,i}\varepsilon_{j,i}(t)$, where $\vec{\mu}_{j,i}$ are the transition-dipole matrix elements. As in the NQC case, we choose all the Rabi frequencies to have a *common* time envelopes, $\Omega_{j,i}(t) = O_{j,i}\, f_{D(P)}(t)$, with f_D preceding f_P in both steps.

The system's wave function can be expanded in each step as, $|\Psi\rangle = \sum_{i=0}^{2n} c_i(t)\mathrm{e}^{-\mathrm{i}\omega_i t}|i\rangle$, where the column vector $\mathbf{c}(t) = (c_0, c_1, \ldots, c_n, c_{n+1}, \ldots, c_{2n})$ of coefficients is obtained by solving the matrix Schrödinger equation, $\dot{\mathbf{c}}(t) = -\mathrm{i}\,\mathsf{H}(t)\cdot\mathbf{c}(t)$. Here, $\mathsf{H}(t)$ denotes the effective Hamiltonian in the rotating waves approximation,

$$\mathsf{H}(t) = \begin{pmatrix} 0 & \mathbf{\Omega}_0 & \mathbf{0} \\ \mathbf{\Omega}_0^\dagger & \mathbf{0} & \mathbf{H}_F \\ \mathbf{0} & \mathbf{H}_F^\dagger & \mathbf{0} \end{pmatrix}, \quad \mathbf{H}_F = \begin{pmatrix} \mathbf{\Omega}_1 \\ \ldots \\ \mathbf{\Omega}_n \end{pmatrix}, \tag{80}$$

and

$$\mathbf{\Omega}_0 = (\Omega_{0,1}, \ldots, \Omega_{0,n}),$$

$$\mathbf{\Omega}_j = (\Omega_{j,n+1}, \ldots, \Omega_{j,2n}), \quad j = 1, \ldots, n, \tag{81}$$

with † denoting the adjoint operation. The $\mathbf{\Omega}_{0-n}$ vectors of Rabi frequencies are different in the two steps, because they control the population transfer between different wave packets.

We now show that in order to address in the two DQC steps arbitrary wave packets, the Rabi-frequency vectors $\{\mathbf{\Omega}_1, \ldots, \mathbf{\Omega}_n\}$, must be *linearly-independent* of one another. This must be so because when the linear-independence is assured, $D \equiv \det(\mathbf{H}_F) \neq 0$ and the Hamiltonian $\mathsf{H}(t)$ has just *one* zero eigenvalue, with the corresponding "null" eigenvector being given as $(1, \mathbf{0}, \mathbf{x})$, where $\mathbf{0}$ denotes an n-dimensional zero vector and $\mathbf{x}$ is an n-dimensional vector given as, $\mathbf{x} = -\mathbf{H}_F^{-1}\mathbf{\Omega}_0^\dagger$. Direct operation of $\mathsf{H}(t)$ on $(1, \mathbf{0}, \mathbf{x})$ confirms that this is the null state.

By constructing the $\mathbf{\Omega}_0$ vector of Eq. (81) to be proportional to the kth column of the Hermitian $\mathbf{H}_F = \mathbf{H}_F^\dagger$ matrix, i.e., $\mathbf{\Omega}_0^\dagger \propto \mathbf{\Omega}_k^\dagger$ ($k = 1, \ldots, n$), we guarantee that the $(1, \mathbf{0}, \mathbf{x})$ vector correlates at the start of the first step (end of the second step) with $|k\rangle$ ($|k^{'}\rangle$) states, and at the end of the first step (the start of the second step) with the $|0\rangle$ state. Hence, it follows from the linearity of the above equations that with the choice $\mathbf{\Omega}_0^\dagger \propto \sum_{k=1}^{n} c_k\mathbf{\Omega}_k^\dagger$, where $c_k = c_k^i$ (c_k^f) at the start of the first step (end of the second step), the null state correlates at the start of the first step (end of the second step) with the $|\Psi^i\rangle$ ($|\Psi^f\rangle$) superposition state.

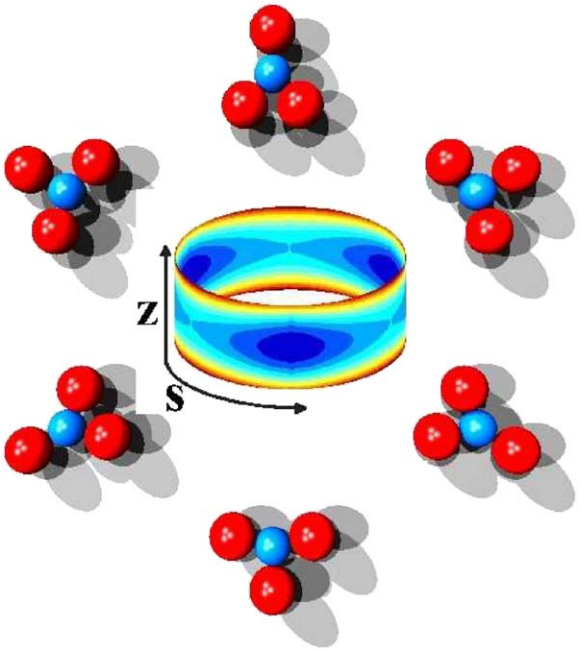

Fig. 10. The three Jahn–Teller-distorted stable T-shaped configurations of the Al_3O molecule and the three equi-lateral transition-states saddle points which separate them. In the center, we display the potential along s—the pseudo-rotation (isomerization) and z—the out-of-plane motion of O relative to the Al_3 plane.

Thus, *complete control* over the population transfer between arbitrary wave packets, composed of nearly-degenerate states, can be achieved. As we show below, even if all $i = n+1, \ldots, 2n$ states are degenerate, it is possible to guarantee the linear-independence of the Rabi-frequencies vectors. Such linear independence may be achieved if the degenerate states are part of a multi-channel continuum, where each Rabi frequency has a different (complex) phase, as in the CC of current directionality discussed in Section 3, or if the dipole-moment vectors $\vec{\mu}_{j,i}$ are pointing in different directions, so that independent polarization-vector $\hat{\epsilon}_{j,i}$ directions can be used, as in the control of the Al_3O isomerization, discussed below. We also note that the efficiency of the two DQC steps does not suffer from the *non-orthogonality* of the linearly-independent $\mathbf{\Omega}_j^\dagger$ $(j = 1, \ldots, n)$ vectors. This is because the non-orthogonality is compensated for in the null vector, where $\mathbf{\Omega}_0^\dagger (\propto \sum_{k=1}^n c_k \mathbf{\Omega}_k^\dagger)$ gets multiplied by the $\mathbf{H}_F^{-1}$ matrix, which, according to Eq. (80), is the inverse of the $\mathbf{\Omega}_k^\dagger$ $(k = 1, \ldots, n)$ matrix.

We now illustrate the versatility of the above DQC method by applying it to the control of isomerization processes of the "Jahn–Teller distorted" Al_3O molecule [143]. As shown in Fig. 10, the Jahn–Teller effect results in the formation of three identical broken-symmetry minima ("isomers") corresponding to T-shaped configurations in which the distance between two of the oxygens is smaller than their distance to the third oxygen [144]. The *in-plane* vibrational motion about each T-shaped configuration minimum gives rise to three sets of highly stable wave packets localized about each minimum. The "*in-plane*" vibrational motion of the molecule between the three minima, which is aided by tunneling, is known as "pseudo-rotation". In addition, the molecule can execute *out-of-plane* vibrations of the O atom relative to the Al_3 triangle.

Our control objective is to transfer population between the localized states of the three minima in as complete a fashion as possible. The control objective falls under the DQC category because each triplet of low-lying localized states is nearly three-fold degenerate. In order to simplify the dynamics we consider hindering the overall rotation of the molecule, by e.g., depositing it on a planar surface. The *in-plane* (x–y) and *out-of-plane* (z) motions will now occur in well defined laboratory directions that are, respectively, parallel and perpendicular to the surface, allowing us to choose the polarization directions of the field components that will couple with the various dipole-moment components so as to make the Rabi-frequencies vector linearly independent. This necessitates the use of one of the *out-of-plane* vibrational modes [142].

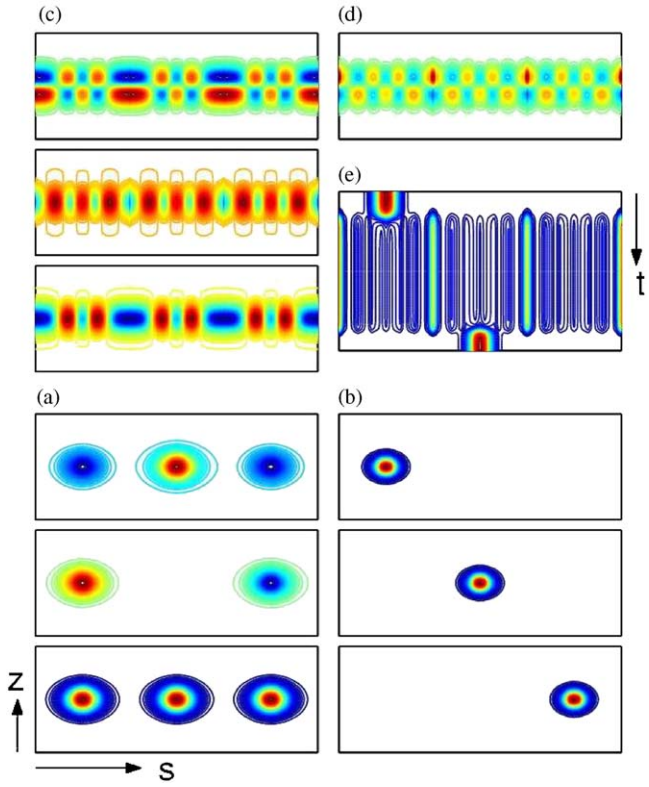

Fig. 11. (a) The three lowest {0, 0} energy eigenstates of Al_3O as a function of the s and z coordinates. (b) Superpositions of these eigenstates to form localized wave packets about each T-shaped minimum. (c) The $|j\rangle$ intermediate states. (d) The $|0\rangle$ parking state. (e) The time-dependence of the DQC dynamics, showing the controlled transfer between two T-shaped minima.

In order to simulate the control dynamics, we have obtained [142], using ab initio methods, the potential surface and electric dipole moments in a two dimensional (2D) subspace of the full (6D) configuration space of Al_3O, containing the pseudo-rotation (s) and the out-of-plane (z) modes (see Fig. 10). The relevant eigenstates and eigenenergies are obtained using well established methodologies [145–147] for solving the 2D nuclear Schrödinger equation $[E_k - H_M]\phi_k(s, z) = 0$.

Because of the high barrier for the pseudo rotation we can neglect Berry-phase effect [148–151]. As a result, the eigenenergies of our 2D model are characterized by the $\{v_s, v_z\}$ numbers of nodes along the s and z directions in each T-shaped minimum, (see also Fig. 11). The low lying $\{v_s, v_z\}$ states appear as triplets, each triplet is composed of two degenerate eigenstates separated in energy from a third, non-degenerate, state.

The three eigenstates in the lowest ($\{0, 0\}$) triplet are shown in panel (a) of Fig. 11. We take linear combinations of these states to form the initial and final wave packets, $|\Psi^i\rangle = \sum_k c_k^i |k\rangle$, $(i = 1, 2, 3)$, localized in the three Jahn–Teller wells, as displayed in panel (b). The three non-degenerate *delocalized* components of the $\{4, 0\}$, $\{6, 0\}$ and $\{4, 1\}$ triplets, shown in the (c) panel, are chosen as the $|j\rangle$ intermediate states. Finally, the non-degenerate component of the $\{6, 1\}$ triplet, presented in panel (d), is used as the "parking" state $|0\rangle$. The three non-degenerate intermediate states belonging to the $\{4, 0\}$, $\{6, 0\}$ and $\{4, 1\}$ triplets are coupled to the localized states $|\Psi^i\rangle$ by pulses polarized in the x, y and z directions, respectively. The same states are coupled to the parking $|0\rangle$ state by pulses polarized in the z, z and $y(x)$ directions, respectively. In this way we are able to choose the field polarizations to achieve the required linear-independence of the $\mathbf{\Omega}_1$, $\mathbf{\Omega}_2$, and $\mathbf{\Omega}_3$ Rabi-frequency vectors.

The Rabi frequencies for *both* DQC steps are

$$\Omega_{j,k}(t) = \Omega_{j,k}^{\max}\{\exp[-(t+\tau)^2/\tau^2] + \exp[-(t-\tau)^2/\tau^2]\},$$

$$\Omega_{k,0}(t) = \Omega_{k,0}^{\max}\{\exp[-(t+3\tau)^2/\tau^2 + \exp[-(t-3\tau)^2/\tau^2\}],$$

with $\Omega_{j,k}^{\max} = \Omega_{k,0}^{\max} = 0.2\,\mathrm{cm}^{-1}$ and $\tau = 5$ ns. The dipole-moment matrix elements are of the order 10^{-3}–10^{-1} Debye. The duration of the laser pulses is roughly $8\tau \ll \tau_i$, so that the $|\Psi^i\rangle$, $i = 1, 2, 3$ states remain localized in their corresponding T-shaped minima for sufficiently long times to be used as legitimate initial and final states.

In panel (e) of Fig. 11, we display the time evolution of the system, during the two steps of the DQC process. The z-integrated probability density $\int \mathrm{d}z|\langle s, z|\Psi(t)\rangle|^2$ is presented as a function of s and t. We start with the localized $|\Psi^1\rangle$ state being initially populated. At the end of the first step, its population is "parked" on the excited delocalized $|0\rangle$ state, using as intermediate the $|j\rangle = |1\rangle - |3\rangle$ states (which remain unpopulated throughout the process). After a parking time, short enough so that no population is lost due to relaxation, the bulk of the probability density is symmetrically concentrated near the three saddle points. Finally, at the end of the second step, the parked population is transferred to the localized $|\Psi^2\rangle$ state.

5. Resonantly enhanced two-photon association

The AP method can be used to address another significant problem; that of resonantly enhanced two photon *association*, depicted schematically in Fig. 12.

The significance of resonantly enhanced 2-photon association stems from the possibility of using it to form ultra-cold molecules, a topic of considerable interest. Those laser cooling schemes that work for atoms [152–154] tend to fail for molecules, mainly due to the presence of many near-resonance lines and the fact that other degrees of freedom, in addition to translation (rotations, vibrations, etc.), must be cooled. Thus, so far all the suggestions to cool warm molecules using light [155,156] have not be realized because of various difficulties.

Rather than cooling warm molecules one can try to *synthesize* cold molecules by associating cold atoms. The molecules thus formed are expected to maintain the translational temperature of the recombining atoms, because the center-of-mass motion remains unchanged in the association process (save for the little momentum imparted by the photon). This idea was first proposed by Julienne et al. [157,158] who envisioned a multi-step association, first involving the continuum-to-bound excitation of translational continuum states of cold trapped atoms to an excited vibrational level in an excited electronic molecular state. This step was followed by a bound–bound spontaneous emission to the ground electronic state.

An undesirable feature of this scheme is that the spontaneous nature of the second step allows the molecules to end up in a large range of vibrational levels. As a consequence, the use of *stimulated* emission [128,130,131,159–165], discussed below, is preferable because it allows population transfer to a particular final molecular state of interest.

5.1. Theory of photo-association of a coherent wave packet

In photoassociation the initial state is the scattering state and the goal is to transfer the population to the final *bound* state $|E_1\rangle$. We therefore consider a pair of colliding atoms described by scattering states $|E, \mathbf{n}^+\rangle$ with $\mathbf{n}$ incorporating

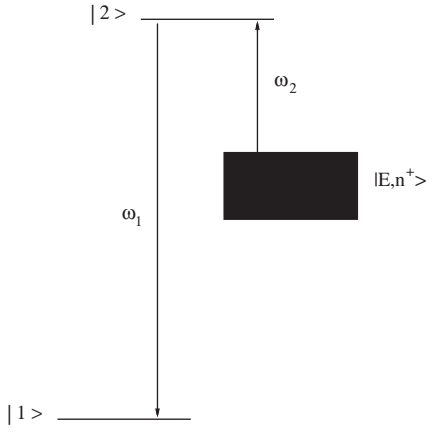

Fig. 12. Energy levels pertinent to the photoassociation process.

the quantum indices specifying the electronic states of the separated atoms and E being the total collision energy. The plus notation signifies, in contrast with the minus states that were previously used to describe dissociation processes, that the *initial* state of the fragments is known.

Following Ref. [159],we focus attention on a Λ-type system, shown in Fig. 12, subjected to the combined action of two laser pulses of central frequencies ω_1 and ω_2. Here ω_2 is in near-resonance with the transition from the $|E, \mathbf{n}^+\rangle$ continuum to an intermediate bound state $|E_2\rangle$ and ω_1 is in near-resonance with the transition from $|E_2\rangle$ to $|E_1\rangle$.

We then solve the Schrödinger equation by expanding the total wave function as in Eq. (18), with the notable exception that here the *incoming* solutions $|E, \mathbf{n}^-\rangle$ are replaced by the outgoing solutions $|E, \mathbf{n}^+\rangle$,

$$|\Psi(t)\rangle = b_1(t)|E_1\rangle \exp(-\mathrm{i}E_1 t/\hbar) + b_2(t)(t)|E_2\rangle \exp(-\mathrm{i}E_2 t/\hbar) + \sum_{\mathbf{n}} \int \mathrm{d}E b_{E,\mathbf{n}}(t)|E, \mathbf{n}^+\rangle \exp(-\mathrm{i}Et/\hbar). \tag{82}$$

We obtain a set of first-order differential equations, which is now of the form

$$\frac{\mathrm{d}}{\mathrm{d}t} b_1(t) = \mathrm{i}\Omega_1^*(t) \exp(-\mathrm{i}\Delta_1 t) b_2(t), \tag{83a}$$

$$\frac{\mathrm{d}}{\mathrm{d}t} b_2(t) = \mathrm{i}\Omega_1(t) \exp(\mathrm{i}\Delta_1 t) b_1(t) + \mathrm{i} \int \mathrm{d}E \sum_{\mathbf{n}} \Omega_{2,E,\mathbf{n}}(t) \exp(-\mathrm{i}\Delta_E t) b_{E,\mathbf{n}}(t), \tag{83b}$$

$$\frac{\mathrm{d}}{\mathrm{d}t} b_{E,\mathbf{n}} = \mathrm{i}\Omega_{2,E,\mathbf{n}}^*(t) \exp(\mathrm{i}\Delta_E t) b_2(t)(t) \quad \text{for all } E \text{ and } \mathbf{n}, \tag{83c}$$

where

$$\Omega_1(t) \equiv \langle \psi_2 | \vec{\mu}_1 \cdot \hat{\epsilon}_1 | E_1 \rangle \varepsilon_1(t)/\hbar, \quad \Omega_{2,E,\mathbf{n}}(t) \equiv \langle \psi_2 | \vec{\mu}_2 \cdot \hat{\epsilon}_2 | E, \mathbf{n}^+ \rangle \varepsilon_2(t)/\hbar,$$
$$\Delta_1 \equiv (E_2 - E_1)/\hbar - \omega_1, \quad \Delta_E \equiv (E - E_2)/\hbar - \omega_2. \tag{84}$$

Contrary to photo-dissociation, in photo-association, the continuum is initially populated. Therefore, the formal solution of Eq. (83c) is of the form,

$$b_{E,\mathbf{n}}(t) = b_{E,\mathbf{n}}(t=0) + \mathrm{i} \int_0^t \mathrm{d}t' \Omega_{2,E,\mathbf{n}}^*(t') \exp(\mathrm{i}\Delta_E t') b_2(t'). \tag{85}$$

Substituting this solution into Eq. (83b) gives

$$\frac{\mathrm{d}}{\mathrm{d}t} b_2(t) = \mathrm{i}\Omega_1(t) \exp(\mathrm{i}\Delta_1 t) b_1(t) + \mathrm{i} \sum_{\mathbf{n}} \int \mathrm{d}E \Omega_{2,E,\mathbf{n}}(t) \exp(-\mathrm{i}\Delta_E t) b_{E,\mathbf{n}}(t=0) - \sum_{\mathbf{n}} \int \mathrm{d}E \int_0^t \mathrm{d}t' \Omega_{2,E,\mathbf{n}}(t) \Omega_{2,E,\mathbf{n}}^*(t') \exp[-\mathrm{i}\Delta_E (t - t')] b_2(t'). \tag{86}$$

When the molecular continuum is unstructured we can invoke the SVCA and replace the energy-dependent bound-continuum dipole matrix-elements by their value at the pulse center, given (in the Λ configuration of Fig. 12) as $E_L = E_2 - \hbar\omega_2$. This is the case, for example, for Na_2 at threshold energies, where the bound-continuum dipole matrix-elements vary with energy by less than 1% over a typical nsec-pulse bandwidth. Within the SVCA, Eq. (86) becomes

$$\frac{\mathrm{d}b_2(t)}{\mathrm{d}t} = \mathrm{i}\Omega_1(t) \exp(\mathrm{i}\Delta_1 t) b_1(t) - \Gamma_2(t) b_2(t) + \mathrm{i}F(t), \tag{87}$$

where

$$F(t) \equiv \varepsilon_2(t) \bar{\mu}_2(t)/\hbar, \tag{88}$$

with

$$\bar{\mu}_2(t) \equiv \sum_{\mathbf{n}} \int \mathrm{d}E \langle \psi_2 | \vec{\mu}_2 \cdot \epsilon_2 | E, \mathbf{n}^+ \rangle \exp(-\mathrm{i}\Delta_E t) b_{E,\mathbf{n}}(t=0). \tag{89}$$

$\Gamma_2(t)$ of the above is defined (in analogy to the CW case of Eq. (27)) as

$$\Gamma_2(t) \equiv (\pi/\hbar)\varepsilon_2^2(t) \sum_{\mathbf{n}} \langle E_j|\hat{\epsilon}\cdot\vec{\mu}|\bar{E},\mathbf{n}^+\rangle\langle\bar{E},\mathbf{n}^+|\hat{\epsilon}\cdot\vec{\mu}|E_i\rangle. \tag{90}$$

Eq. (87) can be expressed in matrix notation as

$$\frac{\mathrm{d}}{\mathrm{d}t}\underline{c} = \mathrm{i}\underline{\underline{H}}(t)\cdot\underline{c}(t) + \mathrm{i}\underline{f}, \tag{91}$$

where $\underline{f}$ and $\underline{c}$ are column vectors defined as, $\underline{f}(t) = (0, F(t))$, $\underline{c} \equiv (\exp(\mathrm{i}\Delta_1 t)b_1, b_2(t))$, and

$$\underline{\underline{H}}(t) = \begin{pmatrix} \Delta_1 & \Omega_1^* \\ \Omega_1 & \mathrm{i}\Gamma_2 \end{pmatrix}. \tag{92}$$

The "*net association rate*" $R(t)$ is the rate of population-change in the bound manifold, given by $\mathrm{d}/\mathrm{d}t\,(|b_1|^2+|b_2(t)|^2)$. It can be written, using Eq. (91) and its complex conjugate, as

$$\begin{aligned} R(t) &= \frac{\mathrm{d}}{\mathrm{d}t}(|b_1|^2+|b_2(t)|^2) = \frac{\mathrm{d}}{\mathrm{d}t}|\underline{c}|^2 = \underline{c}^\dagger\cdot\left(\frac{\mathrm{d}}{\mathrm{d}t}\underline{c}\right) + \left(\frac{\mathrm{d}}{\mathrm{d}t}\underline{c}^\dagger\right)\cdot\underline{c} \\ &= \mathrm{i}\{\underline{c}^\dagger\cdot(\underline{\underline{H}}(t) - \underline{\underline{H}}(t)^\dagger)\cdot\underline{c} + \underline{c}^\dagger\cdot\underline{f} - \underline{f}^\dagger\cdot\underline{c}\} = 2I_m[F^*(t)b_2(t)] - 2\Gamma_2(t)|b_2(t)|^2. \end{aligned} \tag{93}$$

The first term in Eq. (93) represents the association rate,

$$R_{\mathrm{rec}}(t) \equiv 2I_m[F^*(t)b_2(t)], \tag{94}$$

and the second term is the back-dissociation rate,

$$R_{\mathrm{diss}}(t) \equiv 2\Gamma_2(t)|b_2(t)|^2. \tag{95}$$

As expected, the net association rate [Eq. (93)] is the difference between the association rate and the back-dissociation rates.

We can solve Eq. (91) adiabatically by diagonalizing the $\underline{\underline{H}}(t)$ matrix,

$$\underline{\underline{U}}^{\mathsf{T}}(t)\cdot\underline{\underline{H}}(t)\cdot\underline{\underline{U}}(t) = \underline{\underline{\lambda}}(t), \tag{96}$$

where $\underline{\underline{U}}^{\mathsf{T}}$ is the transpose of $\underline{\underline{U}}$. Operating with $\underline{\underline{U}}^{\mathsf{T}}$, on Eq. (91), and defining $\underline{a}(t) \equiv \underline{\underline{U}}^{\mathsf{T}}(t)\cdot\underline{c}$, we obtain that

$$\dot{\underline{a}} = (\mathrm{i}\underline{\underline{\lambda}}(t) + \underline{\underline{A}})\cdot\underline{a} + \mathrm{i}\underline{g}, \tag{97}$$

where $\underline{\underline{A}} \equiv (\mathrm{d}\underline{\underline{U}}^{\mathsf{T}}/\mathrm{d}t)\cdot\underline{\underline{U}}$ is the non-adiabatic coupling matrix. $\underline{g}$ is a column ("source") vector whose transpose is given as

$$\underline{g}^{\mathsf{T}}(t) = (F(t)U_{1,2}(t), F(t)U_{2,2}(t)) = (F(t)\sin\theta(t), F(t)\cos\theta(t)). \tag{98}$$

When $\underline{\underline{A}}$ is neglected (the adiabatic approximation) we obtain from Eq. (97) that

$$\dot{\underline{a}} = \mathrm{i}\underline{\underline{\lambda}}(t)\cdot\underline{a}(t) + \mathrm{i}\underline{g}(t). \tag{99}$$

In the association process the initial conditions are such that

$$\underline{a}(t=0) = 0, \tag{100}$$

so that the adiabatic solutions are

$$\underline{a}(t) = \underline{\underline{v}}(t)\cdot\underline{q}(t), \tag{101}$$

where

$$\underline{\underline{v}}(t) = \exp\left(\mathrm{i}\int_0^t \underline{\underline{\lambda}}(t')\,\mathrm{d}t'\right), \tag{102}$$

and

$$\underline{q}(t) = \mathrm{i}\int_0^t \underline{\underline{v}}^{-1}(t')\cdot\underline{g}(t')\,\mathrm{d}t'. \tag{103}$$

The $b_1(t)$ and $b_2(t)$ coefficients are thus given in the adiabatic approximation as

$$\begin{aligned} b_1(t) &= \mathrm{i}\left\{\cos\theta(t)\int_0^t \exp\left[\mathrm{i}\int_{t'}^t \lambda_1(t'')\,\mathrm{d}t''\right]F(t')\sin\theta(t')\,\mathrm{d}t'\right. \\ &\quad \left. -\sin\theta(t)\int_0^t \exp\left[\mathrm{i}\int_{t'}^t \lambda_2(t'')\,\mathrm{d}t''\right]F(t')\cos\theta(t')\,\mathrm{d}t'\right\}\exp(-\mathrm{i}\Delta_1 t), \\ b_2(t) &= \mathrm{i}\left\{\sin\theta(t)\int_0^t \exp\left[\mathrm{i}\int_{t'}^t \lambda_1(t'')\,\mathrm{d}t''\right]F(t')\sin\theta(t')\,\mathrm{d}t'\right. \\ &\quad \left. +\cos\theta(t)\int_0^t \exp\left[\mathrm{i}\int_{t'}^t \lambda_2(t'')\,\mathrm{d}t''\right]F(t')\cos\theta(t')\,\mathrm{d}t'\right\}, \end{aligned} \tag{104}$$

with $\lambda_{1,2}$ being the solutions of Eq. (96). Given $b_2(t)$, the (channel-specific) continuum coefficients $b_{E,\mathbf{n}}(t)$ are obtained directly via Eq. (85).

It is instructive to study the adiabatic solution when there is insignificant temporal overlap between the two laser pulses. Assuming in that case that the ω_2 pulse precedes the ω_1 pulse, we have during the ω_2 pulse that $\varepsilon_2 \gg \varepsilon_1$, hence by Eq. (96) $\lambda_1 \approx \Delta_1$, $\lambda_2 \approx \mathrm{i}\Gamma_2(t)$ and $\theta(t) = 0$. Substituting these values into Eq. (104), gives, that during the ω_2 pulse (when the ω_1 pulse is off):

$$b_1(t) = 0; \quad b_2 = \mathrm{i}\int_0^t \exp\left(-\int_{t'}^t \Gamma_2(t'')\,\mathrm{d}t''\right)F(t')\,\mathrm{d}t'. \tag{105}$$

From Eq. (88) it is clear that the source term $F(t)$ is linearly proportional to the pulse amplitude. On the other hand, since $\Omega_2 > 0$ and $t' < t$, the $\exp(-\int_{t'}^t \Gamma_2(t'')\,\mathrm{d}t'')$ factor (describing dissociation back to the continuum) decays exponentially with increasing intensity. Thus, merely increasing the laser power does not necessarily increase the association yield. There exists some optimal intensity, beyond which the association probability decreases. Below we display some pulse configurations for a realistic case of photo-association.

As an example of this formulation we consider pulsed photo-association of a coherent wave packet of cold Na atoms [159]. The colliding atoms are described by an (energetically narrow) normalized Gaussian packet of $J = 0$ radial waves:

$$|\Psi(t=0)\rangle = \int \mathrm{d}E\, b_E(t=0)|E, 3s+3s\rangle, \tag{106}$$

where $|E, 3s+3s\rangle$ are the translational Na − Na s-waves with the atoms in the $3s$ state, and b_E at time zero is taken as

$$b_E(t=0) = (\delta_E^2\pi)^{-1/4}\exp\{-(E-E_{\mathrm{col}})^2/2\delta_E^2 + \mathrm{i}\Delta_E t_0\}. \tag{107}$$

Here, t_0 denotes the instant of maximum overlap of the Na + Na wave packet with the $|E_2\rangle$ state. In the simulations, E_{col}, the mean collision energy, varies between $E_{\mathrm{col}} = 0.00695 - 0.0695\,\mathrm{cm}^{-1} \approx 0.01 - 0.1\,\mathrm{K}$ and the wave packet widths, δ_E, vary over the range $\delta_E = 10^{-4}$–$10^{-3}\,\mathrm{cm}^{-1}$. State $|E_1\rangle$ is chosen as the $(X^1\Sigma_g^+, v=0, J=0)$ state and $|E_2\rangle$ as the $(A^1\Sigma_u^+, v'=34, J=1)$ state, as shown in Fig. 13. Thus, the combined effect of the two laser pulses is the transfer of population from the continuum to the ground vib-rotational state $(X^1\Sigma_g^+, v=0, J=0)$, with the bound $(A^1\Sigma_u^+, v'=34, J=1)$ state acting as an intermediate state. In order to minimize spontaneous emission losses we concentrate on the "counter-intuitive" [75,82] scheme where the "dump" pulse $\varepsilon_1(t)$ is applied *before* the $\varepsilon_2(t)$ "pump" pulse.

The appearance of an imaginary Rabi frequency, such as $\mathrm{i}\Gamma_2(t)$, which is due to the presence of a continuum, may change the range of validity of the adiabatic approximation. A "large area" ($\int \Omega\,\mathrm{d}t$) pulses no longer guarantees that we can neglect the non-adiabatic coupling matrix $\underline{\underline{A}}$ [58,166]. Despite this fact, we show below that with the proper choice of pulse parameters, an effective "dark state" can be formed. Using its parametric change induced by the two pulses it is possible to transfer the entire population contained in the continuum wave packet to the ground state, while

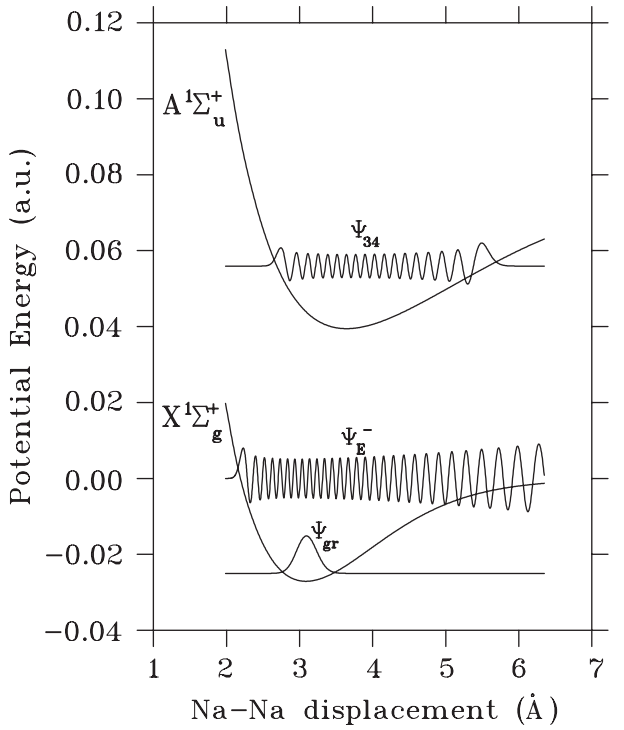

Fig. 13. Potentials and vibrational wave functions used in the simulation of the Na + Na two-photon association. Taken from Fig. 2, Ref. [159].

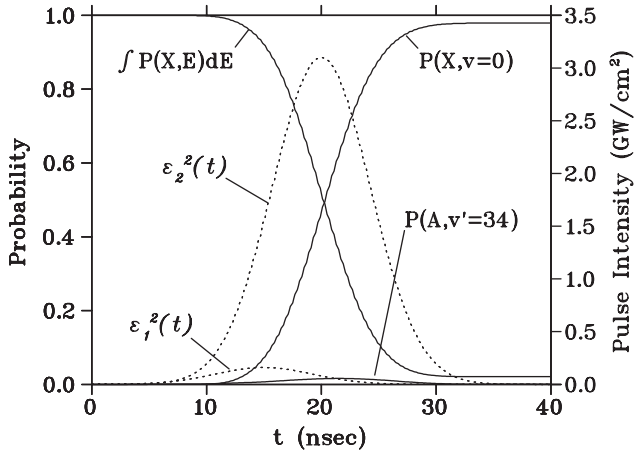

Fig. 14. Results of the "counter-intuitive" pulse sequence. Shown, as a function of time, are integrated population of the wave packet of initial continuum states, the population of the $v = 34$, $J = 1$ intermediate state, and the population of the $v = 0$, $J = 0$ final ground-state. Dashed lines are the intensity profiles of the two Gaussian pulses whose central frequencies are $\omega_1 = 18,143.775\,\mathrm{cm}^{-1}$ and $\omega_2 = 12,277.042\,\mathrm{cm}^{-1}$, (i.e., $\Delta_1 = \Delta_{E_{\mathrm{col}}} = 0$). The maximum intensity of the dump pulse is 1.6×10^8 W/cm^2 and that of the pump pulse is 3.1×10^9 W/cm^2. Both pulses last 8.5 ns. The pump pulse peaks at $t_0 = 20$ ns, the peak time of the Na + Na wave packet. The dump pulse peaks 5 ns before that time. The initial kinetic energy of the Na atoms is $0.0695\,\mathrm{cm}^{-1}$ (or 0.1 K). Taken from Fig. 4, Ref. [159].

keeping the intermediate state population virtually zero at all times. Moreover, for such pulse parameters the adiabatic solutions [Eqs. (104)] are in perfect agreement with exact-numerical solutions [159].

A typical population evolution is shown in Fig. 14 which is obtained with pulse intensities of order $10^8\,\mathrm{W/cm}^2$ and pulse durations of several nsec. Such pulse intensities are sufficiently small to avoid unwanted photoionization,

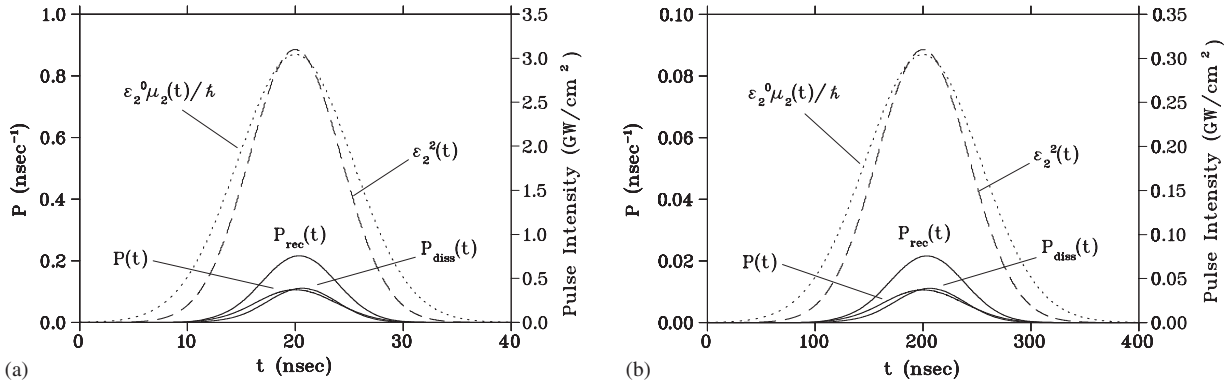

Fig. 15. Rates of association, ($P_{\rm rec}$) back-dissociation ($P_{\rm diss}$) and total molecule-formation (P) vs. t in the "counter-intuitive" scheme. Dashed lines are pulse intensity profile, dotted lines denote the effective Rabi frequency $\varepsilon_2^0\bar{\mu}_2(t)/\hbar$, where ε_2^0 is the peak pulse intensity. (a) Initial wave packet width of $\delta_E = 10^{-3}\,\mathrm{cm}^{-1}$ and other pulse parameters as in Fig. 14. (b) The dynamics scaled by $s = 10$: Initial wave packet width of $\delta_E = 10^{-4}\,\mathrm{cm}^{-1}$; both pulses lasting 85 ns; the pump pulse peaking at $t_0 = 200$ ns and the dump pulse peaking at 50 nsec before that time. Peak intensity of the dump pulse is $1.6 \times 10^6\,\mathrm{W/cm}^2$ and of the pump pulse is $3.1 \times 10^8\,\mathrm{W/cm}^2$. Taken from Fig. 5, Ref. [159].

photodissociation and other strong field parasitic processes. However, working with pulses requires that the atoms be sufficiently close to one another during the laser pulse that they can be recombined. In other words, the initial wave packet of continuum states considered here must be synchronized in time and in duration with the recombining pulses. It is therefore of interest to see whether it is possible to employ longer pulses (of lower intensity) in order to increase the absolute number of recombining atoms and the overall duty cycle of the process.

Use of pulses of different intensity and different durations is illustrated for the "counter-intuitive" scheme in Fig. 15a,b, where the rates of association [$R_{\rm rec}$ of Eq. (94)], back-dissociation [$R_{\rm diss}$ of Eq. (95)], and the net association rate [$R(t)$ of Eq. (93)], are plotted as a function of time. A short-pulse case is shown in Fig. 15a and a long-pulse case, with a more spread out wave packet, is shown in Fig. 15b. Both figures appear identical, though in Fig. 15b the abscissa is scaled up by a factor of 10 and the ordinate is scaled down by a factor of 10.

The scaling behavior demonstrated in Fig. 15 is due to the existence of exact scaling relations in Eq. (91). This scaling is obtained when the initial wave packet-width and the pulse intensities are scaled down as

$$\delta_E \to \frac{\delta_E}{s}, \quad \varepsilon_1^0 \to \frac{\varepsilon_1^0}{s}, \quad \varepsilon_2^0 \to \frac{\varepsilon_2^0}{\sqrt{s}}, \tag{108}$$

and the pulse durations are scaled up as

$$\Delta t_{1,2} \to \Delta t_{1,2} s. \tag{109}$$

It follows from the definition of $F(t)$ that under these transformations

$$F(t) \to \bar{F}_2(t) = \frac{F(t/s)}{s}; \quad \frac{\Omega_{1,2}(t/s)}{s},$$

and Eq. (91) becomes

$$\frac{\mathrm{d}\underline{c}'}{\mathrm{d}t/s} = \mathrm{i}\underline{\underline{H}}(t)(t/s)\cdot\underline{c}' + \mathrm{i}\underline{f}(t/s), \tag{110}$$

where $\underline{c}'$ denotes the vector of solutions of the scaled equations. Thus, the scaled coefficients at time t are identical to the un-scaled coefficients at times t/s.

One of the results of the above scaling relations is that the pulses' durations can be made longer and their intensities concomitantly scaled down, without changing the final population-transfer yields. As noted above, lengthening of the pulses is beneficial because it causes more atoms to recombine within a given pulse.

There is a range of pulse parameters (such as the pulse area, $\Omega_{2,E_L}\Delta t_2$) that maximizes the association yield for a *fixed* initial wave packet. For both the "intuitive" and the "counter-intuitive" schemes there is a clear maximum at

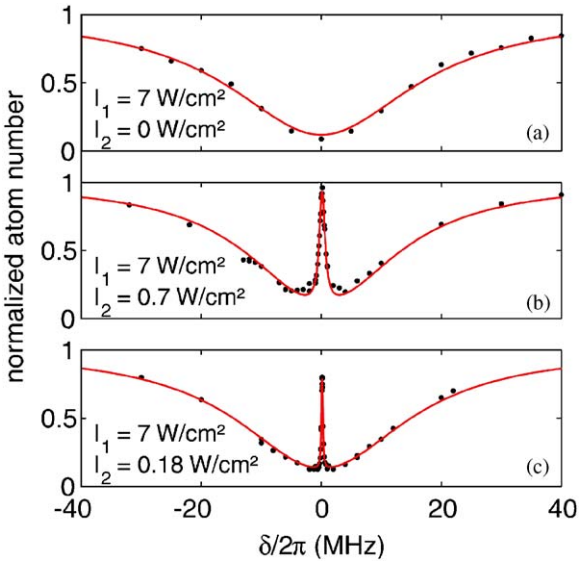

Fig. 16. Experimental evidence for the formation of a dark state in the photoassociation of Rb + Rb (BEC) to form a Rb_2 BEC. Shown is the number of remaining Rb atoms as a function of the detuning of the pump pulse (I_1) relative to the free-bound transition frequency to the intermediate bound state. As one switches on I_2, the dump laser intensity, a dark state whose signature is the decoupling of the system from the external field and the termination of the photoassociation process is seen to be formed. Taken from Fig. 5, Ref. [174].

a specific pulse area; merely increasing the pulse intensity does not lead to an improved association yield. We can attribute this behavior to the fact that the association rate [R_{rec} of Eq. (94)], increases linearly with increasing pulse intensity, whereas dissociation rate [R_{diss} of Eq. (95)] increases exponentially with the intensity. Hence, as long as the energetic width of the initial wave packet stays fixed, the association yield turns over with increasing pulse area. The turn-over point is different for the two pulse schemes: in the "counter-intuitive" case it occurs at a much higher intensity (area).

The existence of a window of intensities for efficient association explains why it is not possible to increase the pulse durations ad infinitum, i.e., to work with cw light. As $\Delta t_{1,2}$ increases, it follows from Eq. (108) that $|\varepsilon_2/\varepsilon_1|^2$ must also increase. Since $|\varepsilon_1|^2$ cannot vanish, $|\varepsilon_2|^2$ must diverge if one is to stay within the windows of intensities for efficient association in the cw limit. Hence radiative association as described in this section cannot take place in the cw regime.

Experimental confirmations of photoassociation via two photon transition as discussed above have been obtained [167–174]. Evidence that counter-intuitive pulse ordering might result in large photo-association cross-sections as suggested above has also been presented [173]. Of especial significance is the experiment of Winkler et al. [174] where a dark state such as the one predicted above has been observed in the photoassociation of Rb BEC to form Rb_2 BEC. As shown in Fig. 16 as the intensity of the dump laser is raised a dark state causing the system to "decouple" from the laser fields is seen to be formed.

6. Suppression of spontaneous emission

The possibility of suppressing spontaneous emission has been a source of great interest in recent years [175–183]. More recently [184,185] we have proposed a new method of completely suppressing spontaneous emission utilizing the interference between resonances. The same method is applicable to any decay process, provided it is governed by overlapping resonances.

The method is based on the fact that one can excite coherently a set of overlapping resonances such that their decay exhibits a step-like behavior: the system starts in a quiescent period in which no spontaneous emission occurs, followed by a "photon-burst" in which spontaneous emission is greatly accelerated, followed by another quiescent period, etc. The quiescent period (and subsequent photon bursts) are due to destructive and constructive interferences between

the overlapping resonances. The reason it is impossible to suppress the decay over all times in this fashion is that the phase and magnitude relations that guarantee at a given time the suppression of decay, change as the system evolves in time, until at a certain time-point the interference for decay becomes constructive and the system experiences the "photon-burst".

In order to achieve suppression of decay at all times, we then suggested irradiating the system before it reaches the photon-burst phase by an external laser field which re-shuffles the phases of the coefficients of the superposition of overlapping resonances. For the two overlapping resonances case this pulse is simply a π pulse which inverts the populations between levels, thereby effectively sending the system "backwards" in time into the quiescent period. Additional external pulses ("interruptions") must be applied periodically just before the system reaches the photon-burst phases as it moves backwards and forwards in time. In this way the system is forced to forever live on the quiescent period ledge.

As explained below, this approach is not limited to the case of pre-existing overlapping resonances. It is possible to suppress the decay of any system, even that of a *single* decaying resonance. This is achieved by (Autler–Townes) splitting [186] a given decaying state into two overlapping field-dressed resonances using an external cw field. Below we describe computational applications of this method to the suppression of the decay of a variety of realistic atomic [e.g., H($2p$) and Pb($6p7s^3P_1^0$)] and molecular [e.g., $Na_2(A^1\Sigma_u^+)$] excited states.

6.1. The decay of overlapping resonances

The decay of and interference between overlapping resonances is best explained using "partitioning" theory [187–191]. Assuming that we have a situation in which bound states interact with a continuum of states, we define two projection operators Q and P, satisfying the equalities $QQ = Q,\ PP = P,\ PQ = QP = 0,\ P + Q = I$, where I is the identity operator. The Q and P operators are chosen to project out the subspaces spanned by bound states and continuum states, respectively.

The full scattering incoming states $|E, \mathbf{n}^-\rangle$, are eigenstates of the Schrödinger equation, written as

$$[E - i\epsilon - H]|E, \mathbf{n}^-\rangle = 0, \tag{111}$$

where the $-i\epsilon$ serves to remind us of the incoming boundary conditions. Using the completeness and orthogonality of P and Q, we obtain from the Schrödinger equation two coupled equations,

$$\begin{aligned}
&[E - i\epsilon - PHP]P|E, \mathbf{n}^-\rangle = PHQ|E, \mathbf{n}^-\rangle,\\
&[E - i\epsilon - QHQ]Q|E, \mathbf{n}^-\rangle = QHP|E, \mathbf{n}^-\rangle.
\end{aligned} \tag{112}$$

We define two basis sets, $|E, \mathbf{n}\rangle$ and $|\alpha\rangle$, which are the solutions of the *homogeneous* (decoupled) parts of Eqs. (112). That is

$$[E - i\epsilon - PHP]|E, \mathbf{n}\rangle = 0, \tag{113}$$

$$[E_s - QHQ]|\alpha\rangle = 0. \tag{114}$$

Implicit in Eqs. (113) and (114) is that $|E, \mathbf{n}\rangle \in P$ and $|\alpha\rangle \in Q$ and as such they are orthogonal to one another. We, in fact, assume that each basis set spans the entire subspace to which it belongs, hence we can write an explicit representation of Q and P as

$$Q = \sum_s |\alpha\rangle\langle\alpha|, \tag{115}$$

$$P = \sum_{\mathbf{n}} \int dE |E, \mathbf{n}\rangle\langle E, \mathbf{n}|. \tag{116}$$

Following Fano [189] we can use Eqs. (115) and (116) to write $|E, \mathbf{n}^-\rangle = [P + Q]|E, \mathbf{n}^-\rangle$ in terms of Q and P as

$$|E, \mathbf{n}^-\rangle = \sum_s |\alpha\rangle\langle\alpha|E, \mathbf{n}^-\rangle + \sum_{\mathbf{n}'} \int dE' |E', \mathbf{n}'\rangle\langle E', \mathbf{n}'|E, \mathbf{n}^-\rangle. \tag{117}$$

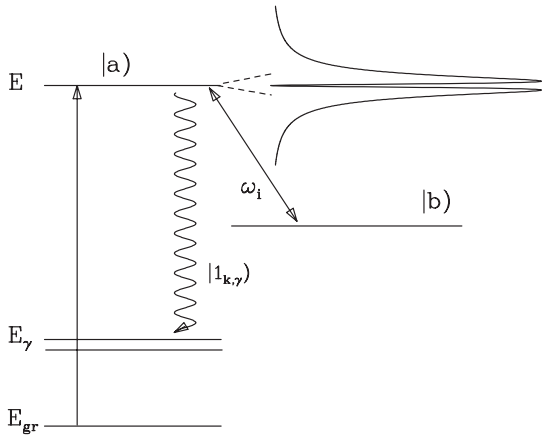

Fig. 17. The energy levels and spontaneous emission pathways of an Autler–Townes split resonance. Shown is a resonance $|a\rangle$ of energy E_a, coupled by a monochromatic light of frequency ω_i to a lower lying state $|b\rangle$. As a result of this coupling, the resonance splits, displaying a hole at the center of the absorption line at $E = E_a$. The wiggly line represents spontaneously emitted photons to lower lying states of energies E_γ. Also shown is the ground state of energy $E_{\rm gr}$ which is excited, using a shaped pulse, to form a superposition of the split components of $|a\rangle$ such that the decay is delayed.

We now solve for $P|E, \mathbf{n}^-\rangle$ by writing it as a sum of the homogeneous solution of Eq. (113) and a particular solution of the first of Eq. (112) obtained by inverting $[E - \mathrm{i}\epsilon - PHP]$,

$$P|E, \mathbf{n}^-\rangle = P|E, \mathbf{n}\rangle + [E - \mathrm{i}\epsilon - PHP]^{-1} PHQ|E, \mathbf{n}^-\rangle. \tag{118}$$

Substituting this solution into the second Eq. (112) we obtain that

$$Q|E, \mathbf{n}^-\rangle = [E - \mathrm{i}\epsilon - Q\mathsf{H}(E)Q]^{-1} QHP|E, \mathbf{n}\rangle. \tag{119}$$

where

$$Q\mathsf{H}(E)Q \equiv QHQ + QHP[E - \mathrm{i}\epsilon - PHP]^{-1} PHQ. \tag{120}$$

We now consider the case of *optically induced* overlapping resonances. We consider therefore an isolated resonance $|a\rangle$ which acquires its width due to spontaneous emission to a manifold of lower lying states denoted as $|\gamma\rangle$. In order to create more resonances we [186] split this resonance by coupling it to a lower lying state $|b\rangle$ using a monochromatic source of frequency ω_i. The situation is described in Fig. 17.

The total Hamiltonian assumes the form,

$$H = H_M + H_R + H_{\rm MR}, \tag{121}$$

where H_M is the matter Hamiltonian, H_R is the radiative Hamiltonian, and $H_{\rm MR}$ is the matter–radiation interaction. For the two material levels $|a\rangle$ and $|b\rangle$ we write H_M as

$$H_M = \tfrac{1}{2}\hbar\omega_{\alpha,b}\sigma_z, \tag{122}$$

where $\omega_{\alpha,b} \equiv (E_a - E_b)/\hbar$ and

$$\sigma_z|a\rangle = |a\rangle, \quad \sigma_z|b\rangle = -|b\rangle, \tag{123}$$

The free radiative Hamiltonian is written as

$$H_R = \sum_{\mathbf{k}} \hbar\omega_k \left[a^\dagger_{\mathbf{k}} a_{\mathbf{k}} + \frac{1}{2}\right]. \tag{124}$$

The $|a\rangle|0,\ldots,0,n_i,0,\ldots,0\rangle$ state, denoted for simplicity as $|a,n_i,0\rangle$, and the $|b\rangle|0,\ldots,0,n_i+1,0,\ldots,0\rangle$ state, denoted for simplicity as $|b,n_i+1,0\rangle$, are eigenstates of H_0, the un-coupled Hamiltonian, defined as, $H_0=H_M+H_R$. Fixing the zero of energy to be mid-way between E_a and E_b we have that

$$\begin{cases} H_0|a,n_i,0\rangle=(E_{n_i}+\frac{1}{2}\hbar\Delta)|a,n_i,0\rangle, \\ H_0|b,n_i+1,0\rangle=(E_{n_i}-\frac{1}{2}\hbar\Delta)|b,n_i+1,0\rangle, \end{cases} \tag{125}$$

where $E_{n_i}\equiv n_i\hbar\omega_i+\frac{1}{2}\hbar\omega_{\alpha,b}-\frac{1}{2}\hbar\Delta$ with $\Delta\equiv\omega_{\alpha,b}-\omega_i$, is the energy of these states relative to the vacuum energy.

The matter-radiation Hamiltonian within the dipole approximation is given as

$$H_{\mathrm{MR}}=-\vec{\mu}\cdot\boldsymbol{\epsilon}_{\mathbf{L}}(R) \tag{126}$$

where

$$\vec{\mu}=\vec{\mu}_{ab}(\sigma_+ +\sigma_-),$$

$$\boldsymbol{\epsilon}_{\mathbf{L}}(R)=\left(\frac{\hbar\omega_i}{2\varepsilon_0 V}\right)^{1/2}\boldsymbol{\epsilon}_{\mathbf{L}}(a+a^\dagger). \tag{127}$$

Neglecting non-resonant coupling (i.e. rotating wave approximation), we obtain that,

$$H_{\mathrm{MR}}=\hbar g_i(\sigma_+ a+a^\dagger\sigma_-). \tag{128}$$

Therefore,

$$\begin{cases} H_{\mathrm{MR}}|a,n_i,0\rangle=\hbar g_i(n_i+1)^{1/2}|b,n_i+1,0\rangle, \\ H_{\mathrm{MR}}|b,n_i+1,0\rangle=\hbar g_i(n_i+1)^{1/2}|a,n_i,0\rangle, \end{cases}$$

where

$$g_i=-\left(\frac{\hbar\omega_i}{2\varepsilon_0 V}\right)^{1/2}\frac{\boldsymbol{\epsilon}_{\mathbf{L}}\cdot\vec{\mu}_{ab}}{\hbar}$$

Taking the Q operator as

$$Q\equiv|a,n_i,0\rangle\langle a,n_i,0|+|b,n_i+1,0\rangle\langle b,n_i+1,0|, \tag{129}$$

we have (in matrix form) that,

$$\underline{\underline{QHQ}}=\begin{pmatrix} E_{n_i}+\frac{1}{2}\hbar\Delta & \hbar g_i(n_i+1)^{1/2} \\ \hbar g_i(n_i+1)^{1/2} & E_{n_i}-\frac{1}{2}\hbar\Delta \end{pmatrix}. \tag{130}$$

The eigenvalues of $\underline{\underline{QHQ}}$ are given as,

$$E^{\pm}_{n_i}=E_{n_i}\pm\hbar\Omega_{n_i}/2, \tag{131}$$

where $\Omega^2_{n_i}=\Delta^2+4g_i^2(n_i+1)$. The ("dressed") eigenstates corresponding to these eigenvalues are given [192] as

$$\begin{cases} |+n_i,0\rangle=\sin\theta|b,n_i+1,0\rangle+\cos\theta|a,n_i,0\rangle, \\ |-n_i,0\rangle=\cos\theta|b,n_i+1,0\rangle-\sin\theta|a,n_i,0\rangle, \end{cases} \tag{132}$$

where

$$\tan 2\theta=-\Omega_i/\Delta \quad \text{where } \hbar\Omega_i\equiv-\vec{\mu}_{ab}\cdot\mathsf{E}_i \text{ and}$$

$$\mathsf{E}_i\equiv 2\boldsymbol{\epsilon}_{\mathbf{L}}\left(\frac{n_i\hbar\omega_i}{2\varepsilon_0 V}\right)^{1/2}. \tag{133}$$

The two orthogonal states $|+n_i,0\rangle, |-n_i,0\rangle$ of the Q manifold and the states $|E,m_i,1_\beta\rangle$ of the P manifold satisfy,

$$\langle\alpha',n_i,0|QHQ|\alpha,n_i,0\rangle = E_\alpha\delta_{n_i',n_i}\delta_{\alpha',\alpha} \quad \text{where } \alpha,\alpha' = \pm, \tag{134}$$

$$\langle E',n_i,1_{\beta'}|PHP|E,m_i,1_\beta\rangle = (E+n_i\hbar\omega_i)\delta(E'-E)\delta_{n_i,m_i}\delta_{\beta'\beta}. \tag{135}$$

The $|1_\beta\rangle$ state of the above is a (spontaneously emitted) one photon state in the β mode. The excited $|a,n_i,0\rangle$ state emits a photon and decays into the P space, with the ω_i photons acting as spectators [193], which means that their number does not change in the process.

Assuming that the lower lying $|b,n_i+1,0\rangle$ state is a non-decaying (or a slowly decaying) state, and denoting the matter-radiation matrix elements as

$$V^{(n)}(a,0|E,1_\beta) \equiv \langle a,n,0|QHP|E,n,1_\beta\rangle,$$

we have that

$$V^{(n)}(+,0|E,1_\beta) = \cos\theta V^{(n)}(a,0|E,1_\beta),$$

$$V^{(n)}(-,0|E,1_\beta) = -\sin\theta V^{(n)}(a,0|E,1_\beta), \tag{136}$$

where we have for brevity denoted n_i as n.

The fully interacting $|E,n,1_\beta^-\rangle$ states, obtained from Eq. (117), form a complete basis set and can be used to expand $|\Psi(t)\rangle$, the full time dependent wave function. Assuming that initially (at $t=0$) we populate a superposition of zero-photon states and a coherent state in the ω_i mode,

$$|\Psi(t=0)\rangle = \sum_{\alpha,n} c_{\alpha,n}|\alpha,n,0\rangle, \tag{137}$$

where $c_{\alpha,n_i} = c_\alpha c_n$, with $c_n = \sum_n \alpha^n/n!$, the wave function at time t is given by,

$$|\Psi(t)\rangle = \sum_{\alpha,n,\beta} c_{\alpha,n}\int_{E_i}^{E_f} \mathrm{d}E\mathrm{e}^{-\mathrm{i}Et/\hbar}|E,n,1_\beta^-\rangle\langle E,n,1_\beta^-|\alpha,n,0\rangle. \tag{138}$$

Applying Eq. (119) to the present case we obtain that $a_{\alpha,n,\beta,m}(E)$ the amplitude function is given as

$$\begin{aligned} a_{\alpha,n,\beta,m}(E) &\equiv \langle\alpha,n,0|E,n,1_\beta^-\rangle \\ &= \sum_{\alpha'}\langle\alpha,n,0|(E-\mathrm{i}\epsilon-Q\mathsf{H}(E)Q)^{-1}|\alpha',n,0\rangle\langle\alpha',n,0|QHP|E,n,1_\beta\rangle, \end{aligned} \tag{139}$$

where $Q\mathsf{H}(E)Q$ is defined in Eq. (120). Using the well known identity, $[E-\mathrm{i}\epsilon-PHP]^{-1} = \mathsf{P}_\upsilon[E-PHP]^{-1} + \mathrm{i}\pi\delta(E-PHP)$, with P_υ denoting the Cauchy principal value integral, we can write the matrix elements of $Q\mathsf{H}(E)Q$ as

$$\langle\alpha,n,0|Q\mathsf{H}(E)Q|\alpha',n,0\rangle = E_\alpha\delta_{\alpha\alpha'} + \hbar\Delta^{(n)}_{\alpha,\alpha'}(E) + \mathrm{i}\frac{\hbar}{2}\Gamma^{(n)}_{\alpha,\alpha'}(E) \tag{140}$$

where

$$\Gamma^{(n)}_{\alpha,\alpha'}(E) \equiv \frac{2\pi}{\hbar}\sum_\beta V^{(n)}(\alpha|E,\beta)V^{(n)}(E,\beta|\alpha'),$$

$$\Delta^{(n)}_{\alpha,\alpha'}(E) \equiv \frac{1}{2\pi}\mathsf{P}_\upsilon\int_{E_i}^{E_f}\mathrm{d}E'\Gamma^{(n)}_{\alpha,\alpha'}(E')/(E-E'). \tag{141}$$

The amplitudes of the $|\alpha',n,0\rangle$ states at time t equal,

$$\langle\alpha,n,0|\Psi(t)\rangle = \sum_\alpha c_{\alpha,n}\int_{E_i}^{E_f}\mathrm{d}E\mathrm{e}^{-\mathrm{i}Et/\hbar}\sum_\beta\langle\alpha,n,0|E,n,1_\beta^-\rangle\langle E,n,1_\beta^-|\alpha,n,0\rangle = \sum_\alpha c_{\alpha,n}M^{(n)}_{\alpha'\alpha}(t). \tag{142}$$

where

$$M^{(n)}_{\alpha'\alpha}(t) = \sum_{\beta} \int_{E_i}^{E_f} \mathrm{d}E \mathrm{e}^{-\mathrm{i}Et/\hbar} a^{(n)}_{\alpha',\beta}(E) a^{(n)*}_{\alpha,\beta}(E). \tag{143}$$

The total population in the zero-photon material states with n spectator photons in the ith mode, at time t, $P^{(n)}(0, \mathbf{c}, t)$, is given by

$$P^{(n)}(0, \mathbf{c}, t) = \sum_{\alpha'} |\langle \alpha', n, 0|\Psi(t)\rangle|^2, \tag{144}$$

where $\mathbf{c} \equiv \{c_{\alpha,n}\}$.

In order to delay the decay we need to find the set of initial coefficients $\mathbf{c}$ which maximizes $P^{(n)}(0, \mathbf{c}, t)$ over a given time interval τ after preparation. Once such a set of coefficients is found, the overlapping resonances thus populated exhibit a step-like decay pattern [184,185], a sample of which is shown in Fig. 21. Indeed, after a quiescent period in which a photon emitted by one resonance gets immediately re-absorbed by the other, the system undergoes a period of rapid decay in which a burst of photons escapes the atom. The "photon-burst" phase is followed by another quiescent phase, etc.

The delay in the emission afforded by the quiescent phase may be of great practical importance for many laser applications by itself. However, we usually want to go one step further and suppress the emission at all times. It is possible to do so in the 2×2 case [184] by applying a π pulse at, or close to, the end of the quiescent period. The effect of the π pulse which transforms the system according to the transformation matrix, $\begin{pmatrix} 0 & i \\ i & 0 \end{pmatrix}$, is to interchange the populations between the two levels. Such an interchange of population in a two level system is known to effectively reverse the direction of time. As a result, after the application of the π pulse, the system moves away from the onset of the "photon burst" phase until it reaches the $-\tau$ time, at which point another photon burst is about to be launched. We avoid such a burst by applying another π pulse which reverses the flow of time once again, sending the system back in the positive time sense. We continue applying a π pulse every 2τ interval, thus confining the system forever to the quiescent phase, making it shuttle back and forth between $-\tau$ and τ. As shown e.g., in Fig. 21, to be discussed in greater detail below, spontaneous emission is thereby effectively blocked. The above analysis also applies to the $N_\alpha > 2$ case, where the transformation is slightly more complicated [184].

We now turn our attention to the application of the above strategy for the Autler–Townes split resonance case. The radiative couplings to the $\beta = \mathbf{k}, \gamma$ mode, where $\omega_\gamma = (E - E_\gamma)/\hbar$ are [194],

$$V(\alpha, 0|E, \gamma, 1_{\mathbf{k},\gamma}) = \begin{cases} \mathrm{i}e\left(\dfrac{\hbar\omega_{\mathbf{k}}}{2\varepsilon_0 V_0}\right)^{1/2} \hat{\varepsilon}_{\mathbf{k},j} \cdot \Delta_{\alpha,\gamma}, & E > E_\gamma, \\ 0 & \text{otherwise.} \end{cases} \tag{145}$$

In the above we have dropped the (n) superscript denoting the number of ω_i spectator photons because the dipole matrix elements for spontaneous emission do not depend on this number.

Integrating over the directions of emission of the photons and summing over the two possible photon polarization directions, we obtain that

$$\Gamma_{\alpha\alpha'}(E) = \frac{e^2}{3\pi\varepsilon_0\hbar^4 c^3} \sum_{\{\gamma: E > E_\gamma\}} \Delta_{\alpha,\gamma} \cdot \Delta^*_{\alpha',\gamma} (E - E_\gamma)^3. \tag{146}$$

The level-shifts $\Delta_{\alpha\alpha'}(E)$ can be calculated from $\Gamma_{\alpha\alpha'}(E)$ using Eq. (141).

The decay matrix elements in the dressed state basis (dropping the energy argument for brevity) can be expressed in the $|a\rangle$, $|b\rangle$ basis as

$$\begin{aligned} \Gamma_{++}(\theta) &= \sin^2\theta\Gamma_{bb} + \cos^2\theta\Gamma_{aa} + \sin 2\theta \ \mathrm{Re}[\Gamma_{ab}], \\ \Gamma_{--}(\theta) &= \cos^2\theta\Gamma_{bb} + \sin^2\theta\Gamma_{aa} - \sin 2\theta \ \mathrm{Re}[\Gamma_{ab}], \\ \Gamma_{+-}(\theta) &= \tfrac{1}{2}\sin 2\theta(\Gamma_{bb} - \Gamma_{aa}) + \cos 2\theta \ \mathrm{Re}[\Gamma_{ab}] - \mathrm{i}\,\mathrm{Im}[\Gamma_{ab}]. \end{aligned} \tag{147}$$

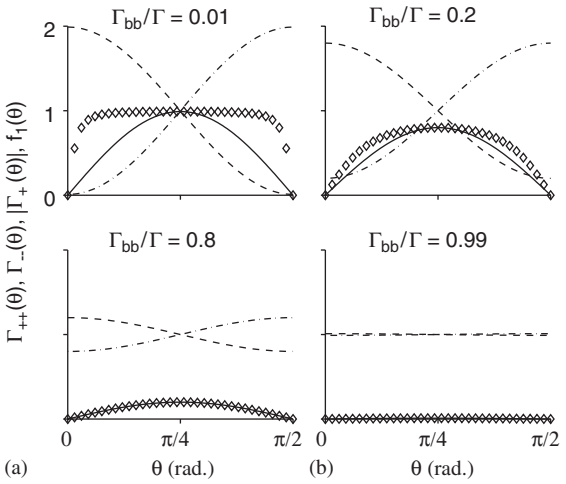

Fig. 18. Γ_{++} (dashed), Γ_{--} (dot–dashed), $|\Gamma_{+-}|$ (solid) and $f \equiv |\Gamma_{+-}|/(\Gamma_{++}\Gamma_{--})^{1/2}$ ($\langle\rangle$).

Since the bare states $|a\rangle$ and $|b\rangle$ have *opposite symmetries*, they emit into different sets of levels, resulting in $\Gamma_{ab} = 0$. Therefore the above expressions can be written as

$$\begin{cases} \Gamma_{++}(\theta) = \overline{\Gamma} - \cos 2\theta \hat{\Gamma}, \\ \Gamma_{--}(\theta) = \overline{\Gamma} + \cos 2\theta \hat{\Gamma}, \\ \Gamma_{+-}(E, \theta) = \sin 2\theta \hat{\Gamma}(E). \end{cases} \tag{148}$$

where $\overline{\Gamma} = \frac{1}{2}(\Gamma_{aa} + \Gamma_{bb})$ and $\hat{\Gamma} = \frac{1}{2}(\Gamma_{bb} - \Gamma_{aa})$.

The possibility of delaying the spontaneous emission is governed by the ratio,

$$f_1(E, \theta) \equiv \frac{|\Gamma_{+-}(E)|}{[\Gamma_{++}(E)\Gamma_{--}(E)]^{1/2}}, \tag{149}$$

which (due to the Schwartz inequality) can assume values between 0 and 1. The unity value leads to maximal delay and the null value to the complete loss of control over spontaneous emission. The ratio reaches its maximum value when $\theta = \pi/4$, i.e. when the field is on-resonance. It then equals

$$f_1(\pi/4) = \frac{|\Gamma_{bb} - \Gamma_{aa}|}{\Gamma_{aa} + \Gamma_{bb}} = \left| \frac{\Gamma_{aa}}{\overline{\Gamma}} - 1 \right|. \tag{150}$$

The maximal degree of delay of the spontaneous emission is attained when $\Gamma_{bb} \approx 0$, i.e. the $|b\rangle$ state is a meta-stable excited state; in that case $\Gamma_{++}(E) = \Gamma_{--}(E) = |\Gamma_{--}(E)| = \frac{1}{2}\Gamma_{aa}(E)$.

The ability to control the spontaneous emission resulting from the introduction of the cw field is demonstrated by a series of computations presented below. In all these computations we have assumed that the energy-dependence of the widths can be neglected over the integration range, which is of the order of magnitude of the width itself. In Fig. 18 we show Γ_{++}, Γ_{--}, $|\Gamma_{+-}|$ and f_1 which result from the introduction of a cw coupling field as a function of the mixing angle θ. The results are shown for several different values of $\Gamma_{bb}/\overline{\Gamma}$.

In Fig. 18(a), $\Gamma_{bb}/\overline{\Gamma} = 0.01$, which means that state $|b\rangle$ is a meta-stable state. The degree of delay of emission we achieve in this case reaches the maximum value it possibly can: $f_1(\theta) \approx 1$. This degree of control is maintained over a wide range of the mixing angle θ. Essentially control is degraded only when the detuning is very large, causing almost no mixing between the $|a\rangle$ and the $|b\rangle$ states ($\theta \approx 0$ or $\theta \approx \pi/2$).

In the next case, shown Fig. 18(b), $\Gamma_{bb}/\overline{\Gamma} = 0.2$. It shows slightly less control, with our ability to delay the decay now being more dependent on the field tuning. The optimal control is achieved, as discussed above, exactly on resonance, where $f_1 = 0.8$ (see Eq. (150)). The possibility of control is being completely eliminated as we increase the $\Gamma_{bb}/\overline{\Gamma}$ ratio, as shown in the lower panel of Fig. 18.

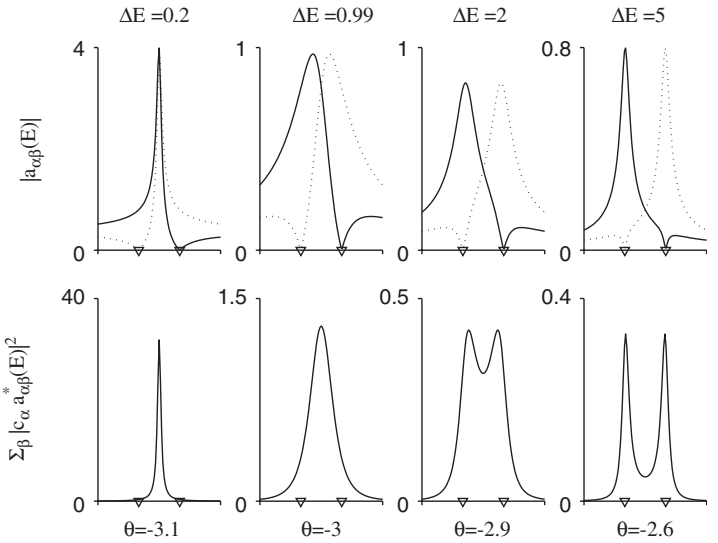

Fig. 19. (Upper panel) The $|a_{\pm,\beta}(E)|$ amplitudes in the 2×2 case, for several values of the levels spacing ΔE for a constant Γ. The x-axis is scaled to encompass $3\Delta E$. The $|a_{+,\beta}(E)|$ is seen to dip to zero at $E_{n_i}^-$ and the $|a_{-,\beta}(E)|$ is seen to dip to zero at $E_{n_i}^+$. The $E_{n_i}^{\pm}$ positions are denoted by the triangles. Each amplitude, are automatically normalized, i.e., they satisfy $\int \mathrm{d}E a_{\alpha\beta}(E)a_{\alpha'\beta}(E)=\delta_{\alpha,\alpha'}$ (lower panel). The same as the upper panel for the $\sum_\beta|\sum_{\alpha=\pm}c_\alpha a_{\alpha,\beta}(E)|^2$ lineshapes.

Another important control variable is the ratio between Γ_{aa}, the resonance widths, and $\Delta E\equiv|E_{n_i}^+-E_{n_i}^-|=\hbar|\Omega_{n_i}|$, the energy spacings between Autler–Townes split resonances. According to Eq. (131), the Autler–Townes splitting enables the tuning of the energy spacings between the resonances by varying the Rabi frequency Ω_{n_i} of the "spectator" cw field. Sample $a_{\alpha,n,\beta,m}(E)$ amplitudes for overlapping resonances with $\Delta E/(\hbar\Gamma)$ varying between 0.2 and 5 are shown in Fig. 19.

The signature of the interference is the appearance of a "dark state" i.e., a continuum energy where the lineshape $(=|a_{\alpha,n,\beta,m}(E)|^2\ )$ dips to zero, occurring at the peaks ($E_{n_i}^+$ or $E_{n_i}^-$) of the neighboring resonance for each lineshape. These dark states, first discovered in Ref. [191], bring about the phenomenon of "Electromagnetically Induced Transparency" [195] hole, midway between the resonances, shown in Fig. 17, for a particular linear combination of the resonances. In the optimized case studied here the $\sum_\beta|\sum_{\alpha=\pm}c_\alpha a_{\alpha,\beta}(E)|^2$ lineshapes shown in the lower panel of Fig. 19 do not necessarily dip to zero.

6.2. Suppression of spontaneous emission in sample systems

6.2.1. The hydrogen atom

We first study the suppression of the spontaneous emission of a hydrogen atom in the $|2P_0\rangle$ state, which can only decay to a *single* (the ground $|1S_0\rangle$) state. We do so by coupling the $|2P_0\rangle$ state, which is identified with state $|a\rangle$ of Fig. 17, with the $|3S\rangle$ state (identified with the $|b\rangle$ state of that Figure) using a resonant cw field. Contrary to Fig. 17, here $E_b>E_a$, which means that $\Gamma_{bb}\neq 0$.

All the parameters needed for this case are known analytically. Thus, the energy differences between the material states are, $E_{2P}-E_{1S}=\frac{3}{4}\frac{me^4}{2\hbar^2(4\pi\varepsilon_0)^2}=\frac{3}{8}$ a.u., and $E_{3S}-E_{2P}=\frac{5}{72}$ a.u. We obtain that,

$$\begin{aligned}\Gamma_{2P_0,2P_0}(E)&=\frac{2^{15}}{3^{11}}\frac{4\pi\varepsilon_0}{m^2e^2c^3}(E-E_{1S}-(n_i+1)\hbar\omega_i)^3\\&=626.8\,\mu\mathrm{s}^{-1},\\\Gamma_{3S,3S}(E)&=3\times\frac{2^{15}3^6}{5^{12}}\frac{4\pi\varepsilon_0}{m^2e^2c^3}(E-E_{2P}-n_i\hbar\omega_i)^3\\&=6.32\,\mu\mathrm{s}^{-1}.\end{aligned}\tag{151}$$

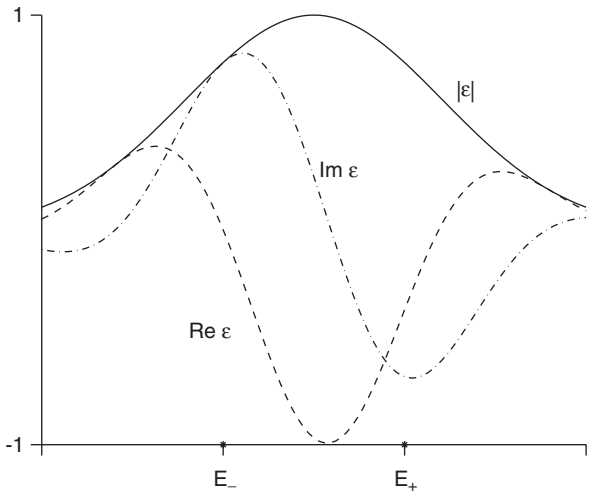

Fig. 20. The light pulse (in frequency space) used to excite the Autler Townes split $|2P_0\rangle$ state from the ground $1S$ state to produce the optimal c_α coefficients. This choice of coefficients is the one most effective in delaying the emission (in the absence of the interruptions) over the optimization time of 2.4 ns.

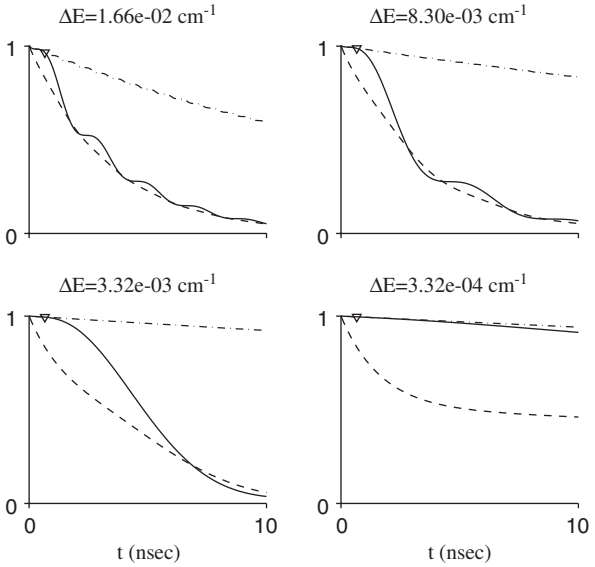

Fig. 21. Suppression of the $2P$-$1S$ spontaneous emission in the hydrogen atom, for which the natural line-width is $\hbar\overline{\Gamma} = 1.66 \times 10^{-3}\,\mathrm{cm}^{-1}$. The solid lines display the decay of the optimized superposition of the Autler–Townes split levels with no interruptions. The dot–dashed lines are the decay curves of the same superposition states in the presence of interruptions. The dashed lines display the average decay of the two Autler–Townes split components. The optimization time τ (marked by a triangle) is $0.2/\Gamma = 0.65$ ns, and the total time range displayed is 0 to $3/\Gamma = 10$ ns.

The corresponding lifetimes are $\tau_{2P_0} = 1.586$ ns and $\tau_{3S} = 157.4$ ns. Using Eq. (148), we obtain for the on-resonance Autler–Townes split states, $|\pm, n\rangle = (|2P, n+1\rangle \pm |3S, n\rangle)/\sqrt{2}$, that $\Gamma_{++}(E) = \Gamma_{--}(E) = 316.6\,\mu\mathrm{s}^{-1}$, and $|\Gamma_{+-}(E)| = 310.2\,\mu\mathrm{s}^{-1}$.

Delaying the spontaneous emission is achieved by exciting the ground-state Hydrogen atom with a light pulse (linearly polarized in the x direction) whose shape, as determined according to the procedure outlined in the previous section, for an optimization time of 2.4 ns, is shown in Fig. 20.

The result of exciting with an optimized pulse (a sample of which is given in Fig. 20) is displayed in Fig. 21 for four different splittings (ΔE). We see a step-like decay: the system starts with a quiescent period which lasts longer

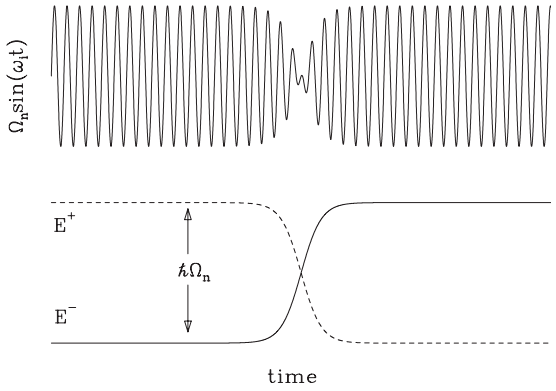

Fig. 22. The train wave of the spectator cw field of frequency ω_i near an interruption which switches Ω_{n_i} to $-\Omega_{n_i}$, thereby exchanging the order of the $E^{\pm}_{n_i}$ levels, as shown in the lower panel.

and longer the smaller the Autler Townes splitting (i.e. Ω_{n_i}) is. As mentioned above, the onset of the photon burst can be avoided by exchanging the population between levels, thereby sending the time *backwards* until the next onset of the photon burst phase at which point another exchange of population is executed. In Ref. [184] the application of a π pulse was suggested as a means of achieving this population exchange. However because in atoms and homonuclear diatomic molecules the $|+n_i, 0\rangle$ and $|-n_i, 0\rangle$ states are not coupled optically to one another, the π pulse in question would have to arise from a two-photon (e.g. Raman) process. Rather than do this we can within the framework of the present setup achieve the same reversal of time by switching the levels while keeping the population of the levels intact. According to Eq. (131), we can switch the order of the $E^{\pm}_{n_i}$ levels by adiabatically changing the sign of Ω_{n_i}. A schematic illustration as to the kind of interruption needed in the spectator cw field to achieve this is displayed in Fig. 22.

The result of the kind of interruptions displayed in Fig. 22 is shown as the dot–dash curve of Fig. 21. We see that the spontaneous emission has been effectively suppressed, with the suppression becoming more effective, the smaller is the Autler–Townes splitting. Also shown in Fig. 21 (as the dashed line) are the natural decay curves, arising when we start with one of the eigenstates, i.e. $c_{\alpha'} = \delta_{\alpha\alpha'}$. As can be seen, this decay, which is *non-exponential* due to the interaction between the resonances, is still much faster than the suppressed decay aided by the interruptions.

6.3. Suppression of the spontaneous emission in the Pb Atom

We now show that the above method works equally well in the presence of more than one final state to which the system can emit. We study the Pb atom and take as the $|a\rangle$ state the $6p\,7s\,^3P_1^0$ excited state which emits [196] to the

$$|1\rangle = 6p^2\,^3P_0 \;\; \lambda_1 = 283.31\,\text{nm} \;\; A_{a,1} = 43.0\,\mu\text{s}^{-1},$$
$$|2\rangle = 6p^2\,^1P_1 \;\; \lambda_2 = 363.96\,\text{nm} \;\; A_{a,2} = 32.0\,\mu\text{s}^{-1},$$
$$|3\rangle = 6p^2\,^3P_2 \;\; \lambda_3 = 405.79\,\text{nm} \;\; A_{a,3} = 93.1\,\mu\text{s}^{-1},$$
$$|b\rangle = 6p^2\,^1D_2 \;\; \lambda_4 = 722.90\,\text{nm} \;\; A_{a,b} = 2.6\,\mu\text{s}^{-1}$$

final states. The total decay rate of state $|a\rangle$ is therefore given as

$$\Gamma_{aa}(E_a) = \sum_{\gamma=1,2,3,b} a_{\alpha\gamma} = 171\,\mu\text{s}^{-1}. \tag{152}$$

We assume that the decay rate of $|b\rangle$ is negligible compared with that of $|a\rangle$, hence, $\hbar\Gamma_{++} = \hbar\Gamma_{--} = \hbar\Gamma_{+-} = \frac{1}{2}\Gamma_{\alpha,a} = 4.531 \times 10^{-3}\,\text{cm}^{-1}$. We note that $|a\rangle$ can decay to $|b\rangle$ as well as to the other states noted above.

The suppressed and natural decay curves for this system are shown in Fig. 23. We see that the suppression works extremely well, in fact better than in Hydrogen, especially at the small splitting end.

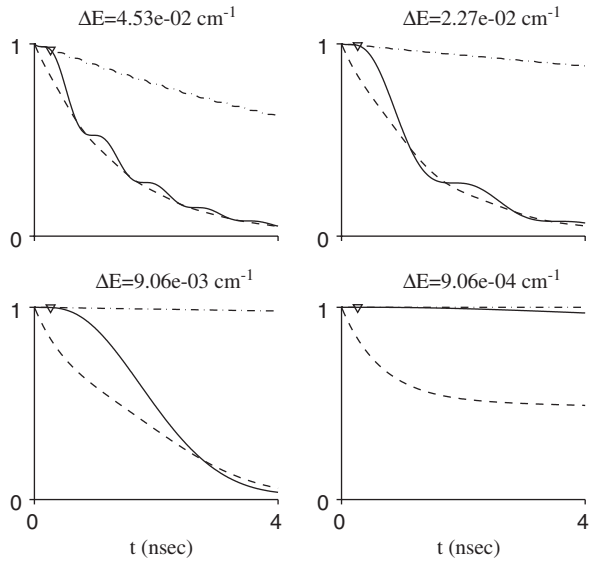

Fig. 23. Suppression of the spontaneous emission in the Pb atom, details are as in Fig. 21. The optimization time τ (marked by a triangle) is $0.2/\Gamma = 2.4$ ns, and the total time range displayed is 0 to $3/\Gamma = 35$ ns.

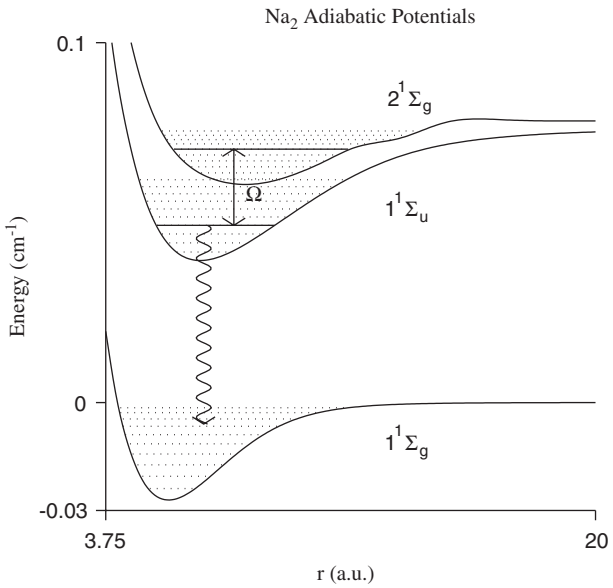

Fig. 24. The three lowest singlet potential energy curves of Na_2: $1^1\Sigma_g$, $1^1\Sigma_u$, and $2^1\Sigma_g$. Every fifth vibrational level is marked with a dashed line. The $|a\rangle$ state is the $v = 20$ vibrational level of the second potential. The $|b\rangle$ state is the $v' = 30$ vibrational level of the third potential. Both are marked by solid lines. The Franck-Condon factor (= overlap integral) between these two states is 0.118.

6.4. *Suppression of the $Na_2(A \to X)$ spontaneous emission*

The suppression of spontaneous emission method works equally well for a molecular system. In molecular systems there is usually a multitude of final states to which the system can emit. In this example we consider suppressing the emission from a particular ($|a\rangle$) vibrational state belonging to the $1^1\Sigma_u$ (A) electronic manifold, aided by a particular vibrational ($|b\rangle$) state belonging to the $2^1\Sigma_g$ electronic manifold. The relevant potentials are displayed in Fig. 24.

Using an average electronic transition-dipole moment μ_e of 7 Debye (=2.756 a.u.) between the $1^1\Sigma_u$ (A) and the ground $1^1\Sigma_g$ (X) states [197], we have calculated the dipole moment matrix elements within the Franck–Condon approximation, according to which

$$\Delta_{v,\gamma} \approx \mu_e \langle v|\gamma\rangle, \tag{153}$$

where $|v\rangle$ and $|\gamma\rangle$ signify vibrational states.

The vibrational wavefunctions needed for this calculation were derived from the potential energy curves of Schmidt and Meyer [198]. In the present rough treatment only the vibrational states (without the rotational sub-levels) were included in the calculations. The inclusion of the rotational factors is not expected to qualitatively change the conclusions drawn here.

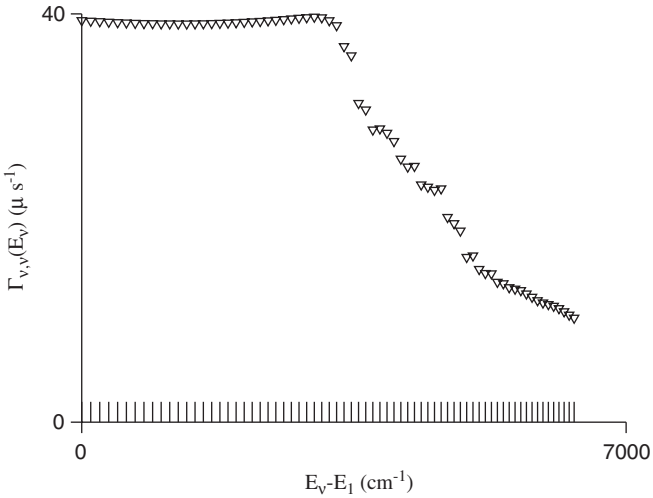

Fig. 25. The decay rates $\Gamma_{vv}(E_v)$ of the 70 lowest vibrational states $|v\rangle$ of the $1\,^1\Sigma_u$ surface.

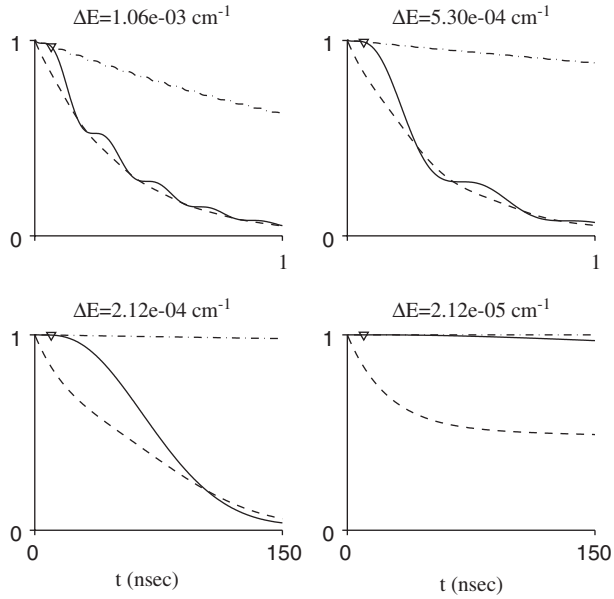

Fig. 26. Suppression of the spontaneous emission of the sodium dimer. The optimization time τ (marked by a triangle) is $0.2/\Gamma = 10$ ns, and the total time range displayed is 0 to $3/\Gamma = 150$ ns.

The lineshape for the vibrational levels (and specifically that of $v=20$) of the excited surface $1^1\Sigma_u$ are much narrower than the energy level spacing, therefore all the resonances are isolated, as in the atomic cases discussed above.

Assuming that the decay rates of the vibrational levels belonging to the $2^1\Sigma_g$ manifold (which can decay to the $1^1\Sigma_u$ manifold) are negligible compared to those of the $1^1\Sigma_u$ surface, we can write $\Gamma_{vv}(E)$ as

$$\Gamma_{vv}(E) = \frac{e^2}{3\pi\varepsilon_0\hbar^4c^3} \sum_{\{\gamma:E>E_\gamma\}} |\Delta_{v,\gamma}|^2 (E - E_\gamma)^3, \tag{154}$$

where γ includes only the vibrational levels in the ground electronic manifold. We obtain that for $0 \leqslant v \leqslant 30$, $\Gamma_{vv}(E_v) \approx 40\ \mu s^{-1}$ or $\hbar\Gamma_{vv} = 2.12 \times 10^{-4}\ cm^{-1}$. The change of $\Gamma_{vv}(E)$ with energy may be neglected, since the relevant integration range around E_v, $\pm\hbar\Gamma = \pm 2.1 \times 10^{-4}\ cm^{-1}$, is much smaller than $E_v - E_\gamma$ for *all* $|\gamma\rangle$ ground states considered.

Fig. 25 displays the decay widths $\Gamma_{vv}(E_v)$ for the 70 lowest vibrational states $|v\rangle$ of the $1^1\Sigma_u$ surface. Also displayed are the energy levels E_v. The decay curves resulting from coupling the $|a\rangle = |v=20\rangle$ with the $|b\rangle = |v'=30\rangle$ are shown in Fig. 26. Again the method is very successful in completely suppressing the decay.

7. The coherent suppression of intramolecular radiationless transitions

In this section we describe the utilization of interference between overlapping resonances in order to achieve control of *intramolecular dynamics*. We show that by appropriately preparing a linear combination of zeroth-order states on one Born–Oppenheimer surface, quantum interference can be invoked to either maximize or minimize the population that undergoes a radiationless transition at a preset target time. Further, we show that this control requires the presence of overlapping resonances. We illustrate the method by performing computations [199] on a four mode model of pyrazine [200,201].

7.1. Theory of the suppression of radiationless transitions

Consider a molecular Hamiltonian

$$H_M = H_{ad} + H_{12}, \tag{155}$$

where H_M is the total material Hamiltonian, H_{ad} is the Born–Oppenheimer (adiabatic) Hamiltonian in which different electronic states are decoupled from one another, and H_{12} is the non-adiabatic coupling between electronic states. Bound eigenstates of the total material Hamiltonian are denoted $|\gamma\rangle$, with

$$H_M|\gamma\rangle = E_\gamma|\gamma\rangle, \tag{156}$$

where the $|\gamma\rangle$ describe both electronic and nuclear motion. Below, we suppress the rotational component of the dynamics, which is of little relevance to the radiationless processes of interest.

It is useful to consider the eigenstates of H_{ad},

$$H_{ad}|i\rangle = (E_i^{(e)} + E_i^{(v)})|i\rangle, \tag{157}$$

which we term the "bare kets" and label with roman letters, e.g., $|i\rangle$,$|i'\rangle$ and $|j\rangle$. Here, $E_i^{(e)}$ is the electronic energy and $E_i^{(v)}$ is the vibrational energy associated with bare ket $|i\rangle$.

We assume that the system is prepared initially in a state belonging to one of the electronic surfaces. The *radiationless transition* process amounts to the flow of populations to other electronic states. In the specific case of pyrazine the initial state belongs to the S_2 electronic state and final state to S_1. The time dependent probability $P_2(t)$ that the system is found in electronic state S_2 is given by

$$P_2(t) = \sum_{j\in S_2} |\langle j|\Psi(t)\rangle|^2, \tag{158}$$

where $|\Psi(t)\rangle$ is the state of the system at time t and the sum is over all bare kets that are in S_2.

Consider then an initial state $|\Psi(0)\rangle$ that has been optically prepared on S_2 [i.e., $P_2(0) = 1$] as

$$|\Psi(0)\rangle = \sum_{i\in S2} c_i|i\rangle, \tag{159}$$

where c_i are the (complex) coefficients for the given initial state. Then with the propagator $U(t) = \mathrm{e}^{-\mathrm{i}Ht/\hbar}$, the state of the system at time t is

$$|\Psi(t)\rangle = U(t)|\Psi(0)\rangle = \sum_{i\in S_2} c_i U(t)|i\rangle. \tag{160}$$

The $P_2(t)$ probability is therefore given as

$$P_2(t) = \sum_{j\in S_2} \left| \sum_{i\in S_2} c_i \langle j|U(t)\right| i\rangle|^2. \tag{161}$$

As we have done in the discussion of spontaneous emission we rewrite the above expression by expanding the square and collecting the coefficients c_i into a vector $\underline{c}$. We obtain that

$$P_2(t) = \underline{c}^\dagger \cdot \underline{\underline{\mathsf{K}}} \cdot \underline{c} \tag{162}$$

where the $\underline{\underline{\mathsf{K}}}$ matrix is given by

$$K_{i'i}(t) = \sum_{j\in S_2} \langle j|U(t)|i\rangle \langle j|U(t)|i'\rangle^*. \tag{163}$$

We consider coherently controlling $P_2(t)$ by preparing an initial vibrational superposition state on S_2 that either maximizes or minimizes $P_2(t)$ at some preselected target time T. Specifically, we seek the coefficients c_i that extremize $P_2(T)$ while preserving the norm of $\underline{c}$. To do so we introduce a Lagrange multiplier, λ, and define

$$\xi(t, \underline{c}) = \underline{c}^\dagger \cdot \underline{\underline{\mathsf{K}}} \cdot \underline{c} - \lambda(\underline{c}^\dagger \cdot \underline{c} - 1). \tag{164}$$

The optimal set of initial coefficients (subject to the constraint on the norm) is then found for stationary $\xi(t, \underline{c})$, i.e. when

$$\frac{\partial\xi(t, \underline{c})}{\partial \mathrm{Re}[c_i]} = 0, \quad \frac{\partial\xi(t, \underline{c})}{\partial \mathrm{Im}[c_i]} = 0 \tag{165}$$

for all i. Eq. (165) is equivalent to the eigenvalue equation

$$\underline{\underline{\mathsf{K}}}(t) \cdot \underline{c} = \lambda \underline{c}. \tag{166}$$

Hence, the optimum initial coefficients for time T are determined by diagonalizing $\underline{\underline{\mathsf{K}}}(T)$.

To understand the nature of the dynamics we expand Eq. (162) and collect appropriate terms to rewrite P_2 as

$$P_2(t) = \sum_i |c_i|^2 g_i(t) + \sum_{i\neq i'} c_{i'}^* c_i f_{ii'}(t), \tag{167}$$

where

$$g_i(t) = \sum_{j\in S_2} |\langle j|U(t)|i\rangle|^2, \quad f_{ii'}(t) = \sum_{j\in S_2} \langle j|U(t)|i\rangle \langle j|U(t)|i'\rangle^*. \tag{168}$$

Eqs. (167) and (168) admit simple interpretations: g_i describes the P_2 dynamics of a system that is initially prepared as the bare ket $|i\rangle$, whereas $f_{ii'}$ provides the effect of interferences between the bare kets comprising the initial superposition state $\Psi(0)$. Comparatively large values of $f_{ii'}(T)$ indicate that interference is playing a significant role in the pyrazine dynamics at the target time, and that Coherent Control is possible. By contrast, if the g_i terms dominate then active control over the P_2 dynamics is not possible for the energy regime spanned by $\Psi(0)$. In this case only "passive" control

is possible, where one weights, in $\Psi(0)$, the specific $|i\rangle$ whose decay is slowest (for suppression of P_2 decay) or fastest (for enhancement of P_2 decay).

Additional insight is obtained by substituting Eqs. (160) into (158) and using $\sum_\gamma |\gamma\rangle\langle\gamma| = 1$ in conjunction with the definition of the propagator. We obtain that

$$\begin{aligned} P_2(t) &= \sum_{j\in S_2} \left| \sum_{i\gamma} c_i \langle j|\gamma\rangle\langle\gamma|i\rangle \exp[-\mathrm{i}E_\gamma t/\hbar] \right|^2 \\ &= \sum_{j\in S_2} \sum_{i\gamma i'\gamma'} c_i c_{i'}^* \langle j|\gamma\rangle\langle\gamma|i\rangle\langle i'|\gamma'\rangle\langle\gamma'|j\rangle \exp[-\mathrm{i}(E_\gamma - E_{\gamma'})t/\hbar]. \end{aligned} \tag{169}$$

Hence, when we perform an infinite time average $\bar{P}$:

$$\bar{P} = \lim_{T->\infty} \frac{1}{T} \int_0^T P(t)\,\mathrm{d}t. \tag{170}$$

we obtain that $\bar{P}_2$ is given by

$$\bar{P}_2 = \sum_{j\in S_2} \sum_{i\gamma i'} c_i c_{i'}^* |\langle j|\gamma\rangle|^2 \langle i'|\gamma\rangle\langle\gamma|i\rangle, \tag{171}$$

because the $\gamma \neq \gamma'$ terms average out. There is also an alternative probability,

$$P_2'(t) = \sum_{j\in A} \left| \sum_{i\in A} c_i \langle j|U(t)|i\rangle \right|^2, \tag{172}$$

where A is a subset of S_2. Here $P_2'(t)$ gives the probability of remaining in the initial subspace I of S_2. The most elementary of these cases is

$$P_2''(t) = |\langle i|U(t)|i\rangle|^2, \tag{173}$$

which provides the probability of staying within just a single created bare ket $|i\rangle$, is also of interest below.

7.1.1. Overlapping resonances in a discrete spectrum

In the simplest radiationless transition model a single bare ket is excited and other S_2 states are regarded as irrelevant, so that Eq. (167) takes the form:

$$P_2(t) = \left| \sum_\gamma |\langle i|\gamma\rangle|^2 \exp(-\mathrm{i}E_\gamma t/\hbar) \right|^2 \tag{174}$$

If the coefficients $|\langle i|\gamma\rangle|^2$ are distributed as a discrete Lorentzian function in E_γ, and the level spacing is tiny, the decay of $P_2(t)$ is exponential. More complex, however, and more relevant to the discussion below, is the case where there are several neighboring resonances that are wider than the adjacent level spacing, so that the resonances overlap. In the discrete case this means that two or more bare kets have non-zero overlap matrix elements with the same $|\gamma\rangle$.

The interference term $f_{ii'}(t)$ of Eq. (168) depends upon

$$\langle j|U(t)|i\rangle\langle j|U(t)|i'\rangle^* = \sum_{\gamma,\gamma'} \langle j|\gamma\rangle\langle\gamma|i\rangle\langle i'|\gamma'\rangle\langle\gamma'|j\rangle \mathrm{e}^{-\mathrm{i}(E_\gamma - E_{\gamma'})/\hbar}. \tag{175}$$

Hence non-zero $f_{ii'}(t)$, and the ability to control the system via the phases of the c_i coefficients, requires that at least two bare kets have non-zero overlap with at least one common exact eigenstate.

7.2. Control over "internal conversion" processes in pyrazine

As an example, consider computations dealing with control over the "internal conversion" (i.e., $S_2 \leftrightarrow S_1$) in pyrazine, a molecule possessing 24 vibrational modes. The dynamics of pyrazine is treated using a model due to Peluso et al. [201] which is a variant of a model of Domcke et al. [200]. Here, the $|i\rangle$ are products of an electronic component, either of the S_1 or S_2 electronic state, and a vibrational part, which is itself a product of harmonic oscillator (HO) eigenstates; one HO eigenstate for each of the 24 normal modes of the molecule. Although all 24 modes are included in the calculation, non-zero quantum numbers are allowed in only four of these modes. Specifically, excitations of the 1, 6a, 8a and 10a modes of up to 10, 9, 8 and 9 quanta, respectively, are included (i.e., we include every HO products that has mode 1 with a quantum number not exceeding 10, and mode 6a with a quantum number not exceeding 9, etc.). The result is often termed a four mode model. The S_1 to S_2 coupling is given by the simple linear term:

$$H_{12} = \beta Q_{10a}, \tag{176}$$

where Q_{10a} is the 10a normal coordinate and

$$\beta = 1.3[\text{eV}\,\text{Å}^{-1}\,\text{AMU}^{-1/2}], \tag{177}$$

obtained via a qualitative fit to experimental data. The difference in electronic energy is taken as

$$|E^{(e)}_{S1} - E^{(e)}_{S_2}| = 0.956\,\text{eV}. \tag{178}$$

Given the basis, the eigenvectors of the total Hamiltonian were determined via standard linear algebra techniques. A total of 9900 bare kets on each of the S_2 and S_1 surfaces were utilized, constructed as described above. States on S_1 are consecutively labeled as $|1\rangle$ to $|9900\rangle$ and those on S_2 are labeled $|9901\rangle$ to $|19800\rangle$. By expanding a bare ket $|i\rangle$ in the exact eigenstates, $|\gamma\rangle$:

$$|i\rangle = \sum_{\gamma} D_\gamma |\gamma\rangle, \tag{179}$$

we obtain the discrete version of a lineshape $|D_\gamma|^2 = |\langle\gamma|i\rangle|^2$ which provides a picture of the resonance.

Figs. 27 and 28 show two typical examples of the resonance shapes observed in these calculations, here for states $|11432\rangle$ and $|10088\rangle$. The former appears sharp and single peaked, being spread out over a few hundred wavenumbers.

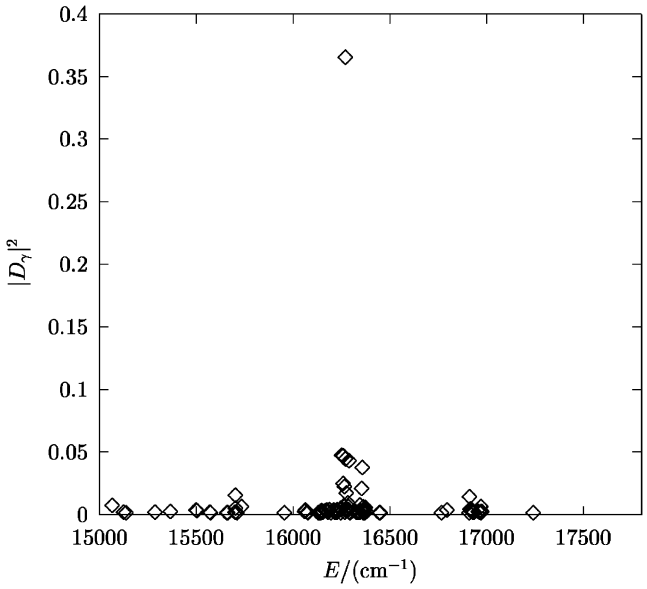

Fig. 27. Narrow resonance shape—ket $|11432\rangle$.

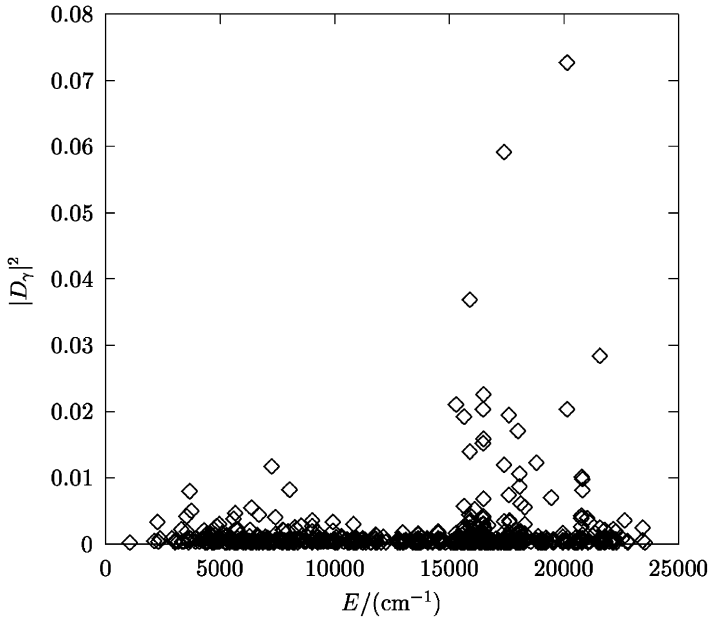

Fig. 28. Wide resonance shape—ket $|10088\rangle$.

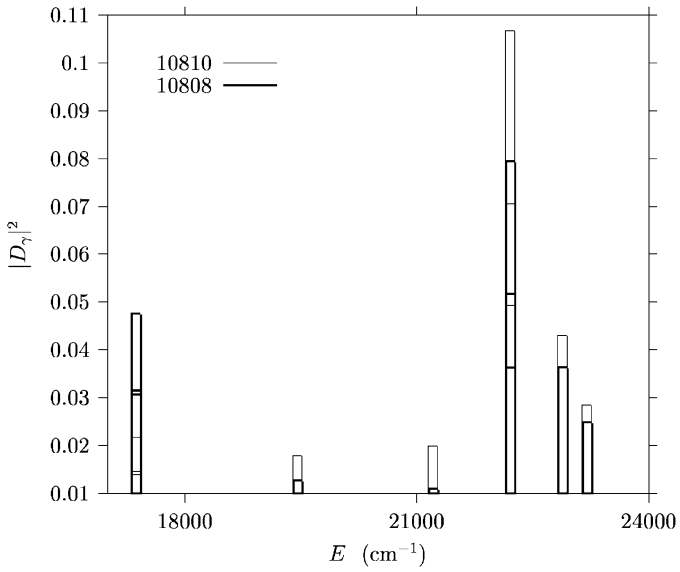

Fig. 29. Overlap of states $|10808\rangle$ and $|10810\rangle$.

By contrast, the latter shows at least two peaks regions and is broadly distributed over several thousand wave numbers, reflective of overlapping resonances. As we will see below, $|11432\rangle$ is also affected by the presence of other bare kets. Overlaps of lines typical of those observed are shown in Fig. 29, which is discussed in further detail below.

Also observed in this model of Pyrazine are the bare kets that almost entirely comprise a single exact Hamiltonian eigenstate, i.e. eigenstates that are comprised of over 90% of one bare ket. The dynamics of these extreme states has been emphasized by Sukharev and Seideman [202].

The calculations of $P_2(t)$ are characterized by two, qualitatively different, temporal regions: a short-time monotonic decay "region *I*", followed by an oscillatory "region *II*". The transition times for passing from region *I* to region *II* depend on the initial state. A specific $P_2(t)$ decay obtained upon laser excitation with an "ultrashort" ($\delta(t)$-like) pulse

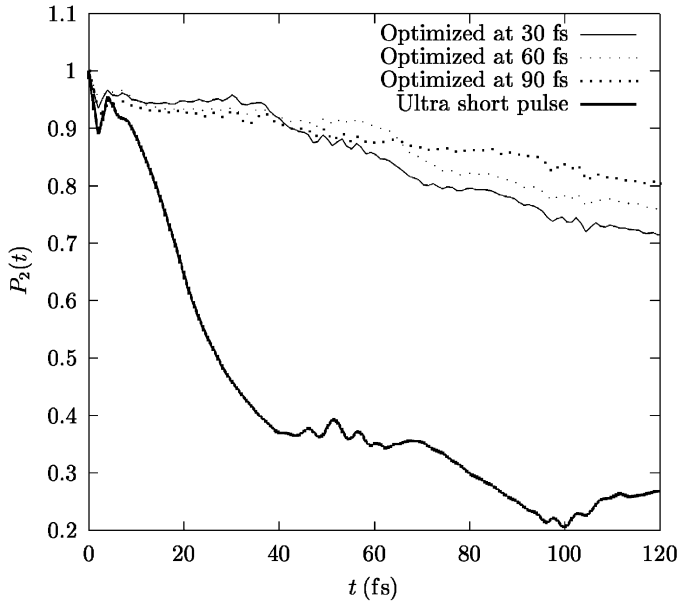

Fig. 30. $P_2(t)$ for a state prepared with an ultra short pulse and for three optimized states.

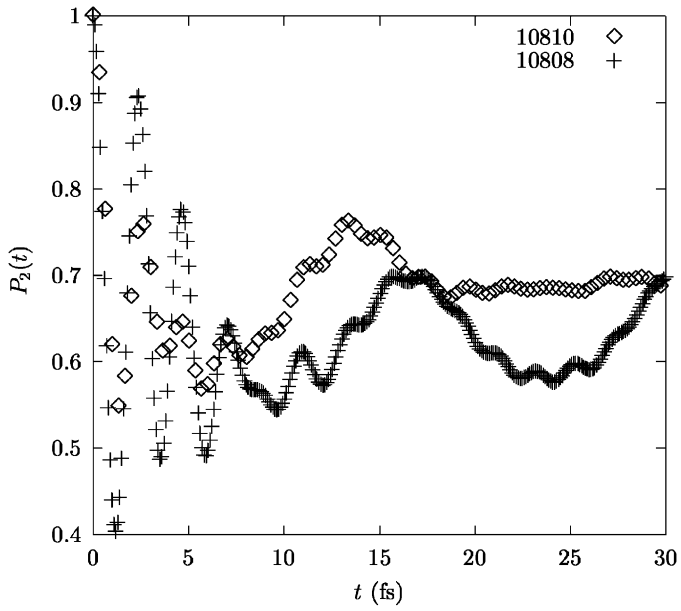

Fig. 31. Individual time evolution of P_2 for each of the levels $|10810\rangle$ and $|10808\rangle$.

creating a superposition of 50 vibrational states of S_2 from S_0 is shown as a solid line in Fig. 30. The intial wave packet is centered at $\approx 9500\,\mathrm{cm}^{-1}$ with a width of $990\,\mathrm{cm}^{-1}$, where the zero of energy is chosen as the the energy of the ground vibrational state in the S_1 electronic manifold (it being 4.95 eV above the ground vibrational state of the S_0 manifold). The decay is rapid, on the time scale of 20–40 fs, which is consistent with experimental results [203].

Fig. 30 also shows the $P_2(t)$ resulting from the maximization of $P_2(T)$ decay for three cases. These results use the same 50 bare kets that comprise the above short pulse initial state, and differ only by the times at which they were maximized: $T = 30$, 60 or 90 fs, respectively. An examination of the composition of these three states shows the origin

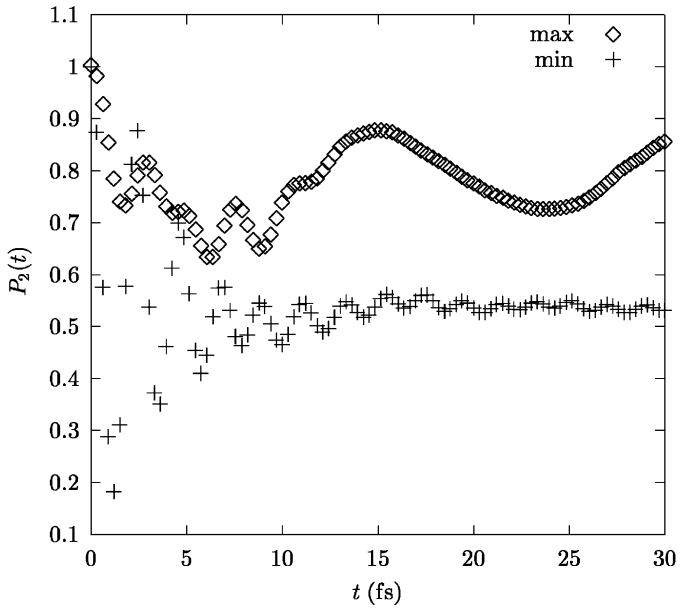

Fig. 32. Superposition of $|10808\rangle$ and $|10810\rangle$: P_2 optimized at $T = 20$ fs.

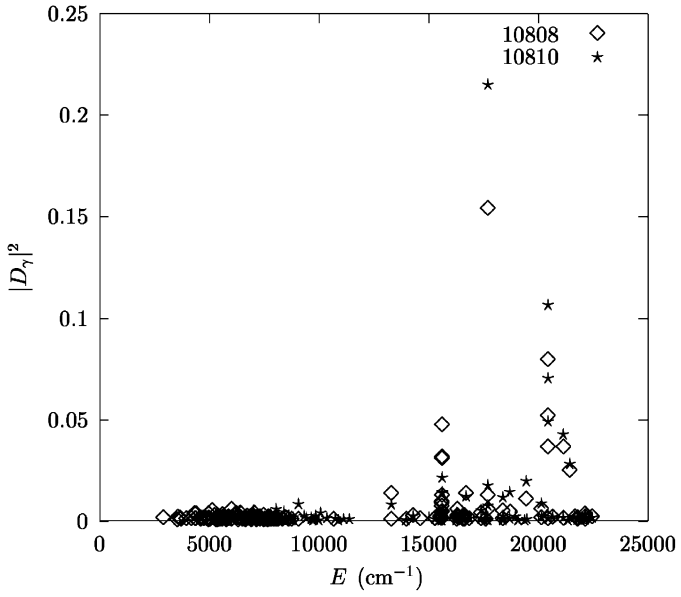

Fig. 33. Resonance shape of $|10808\rangle$ and $|10810\rangle$.

of their similarity: approximately 80% of the amplitude of each initial state lies in only one bare ket—that bare ket with the largest $\bar{P}_2$. Thus, little, if any, active interference-based coherent control participates in these optimizations. Similar observations were made for the case of $P_2(T)$ minimizations.

To demonstrate active control in this model of Pyrazine therefore requires that we focus on those bare kets that have a fairly large $f_{ii'}(t)$ value at the target time of interest. We considered first a case where the initial superposition is comprised only two bare kets, $|i\rangle = |10810\rangle$, $|i'\rangle = |10808\rangle$. The time evolution of each of these kets, regarded independently, is shown in Fig. 31. Note that neither of these states display simple falloff of $P_2(t)$, but rather show

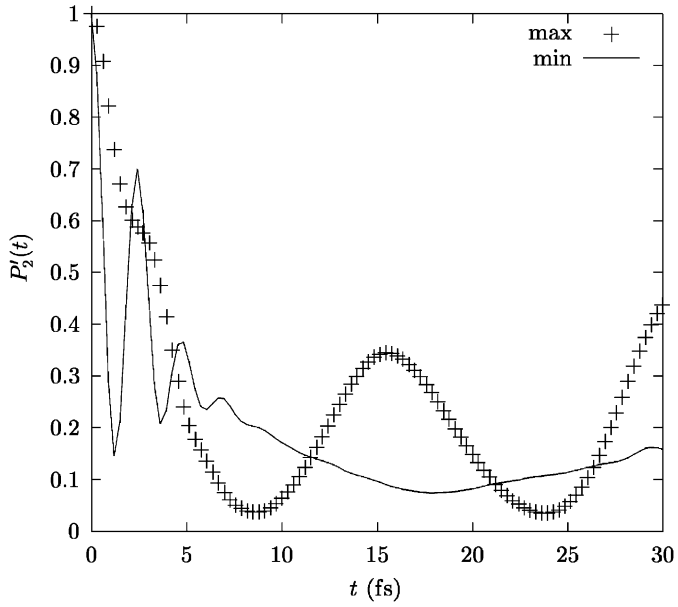

Fig. 34. Optimized P_2' curves for $|10808\rangle$ and $|10810\rangle$. Optimization time $T = 15$ or 20 fs.

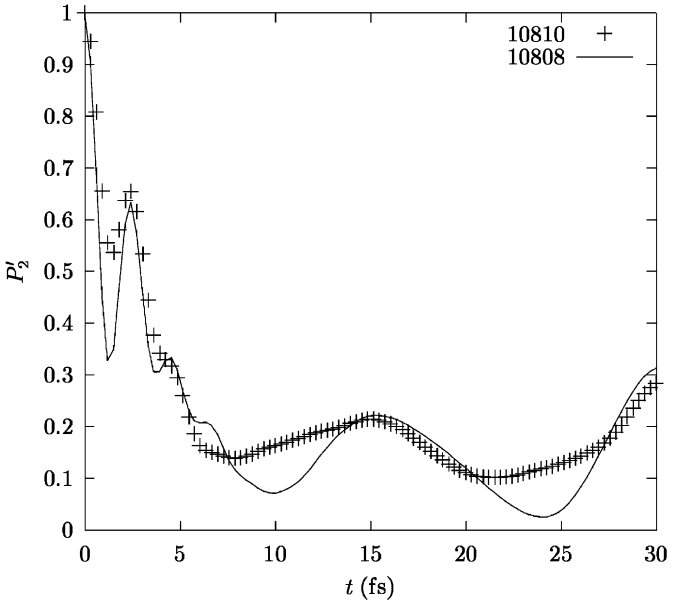

Fig. 35. Individual P_2' curves for $|10808\rangle$ and $|10810\rangle$.

population that oscillates in and out of S_2, leading to a long time value of ≈ 0.68. This type of quasi-periodic dynamics was typical of most of the states studied, and more recent work [204] shows that this is due to the low density of states on the S_1 surface associated with the four mode model.

We next optimized $P_2(t)$ using an initial superposition of two states $|10808\rangle$ and $|10810\rangle$ at $T = 20$ fs. The results shown in Fig. 32. Here the difference between the maximal and minimal $P_2(t)$ at this target time is seen to be significant, but not substantial. Such control arises from the participation of overlapping resonances in the S_2 manifold, with the individual bare states shown in Fig. 33. The primary contributions to the overlap of these two states is shown in Fig. 29,

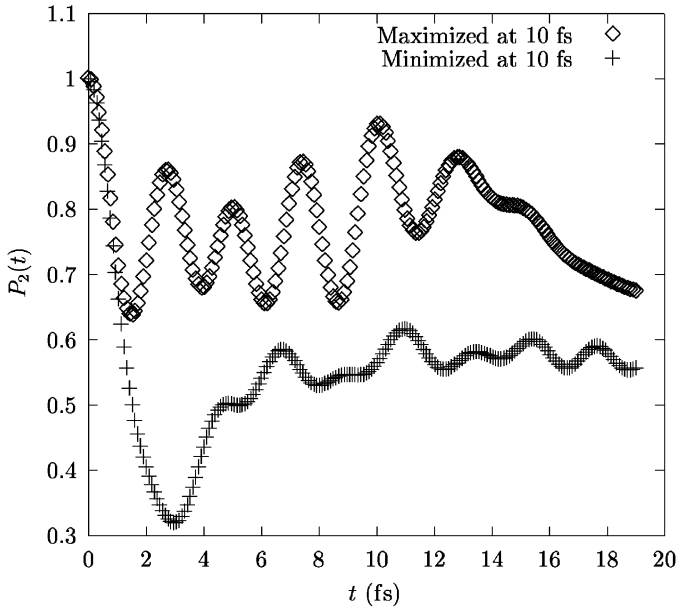

Fig. 36. Maximized and minimized populations at 10 fs for a family of bare kets that have relatively large $\bar{f}_{ii'}$.

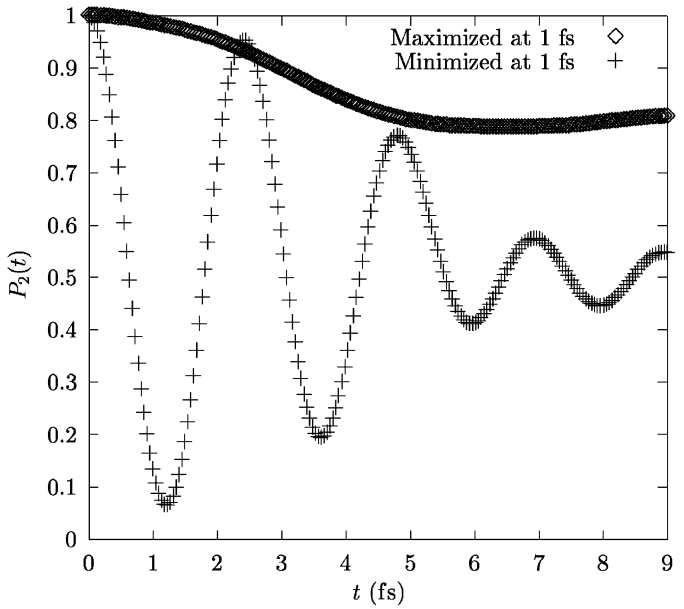

Fig. 37. Same as Fig. 36 except that optimizations where performed at 1 fs.

where the height of the histogram indicates the contribution of each of the bare kets to the exact state at the indicated energy E_γ.

A considerably different degree of control obtains from optimizing the probability, $P_2'(t)$, of remaining within these two states, which we here use to define the subspace A. The result of optimization at either $T = 15$ and 20 fs are visually indistinguishable and are shown in Fig. 34. These results should be compared to the uncontrolled probability of each of the two states $|10808\rangle$ and $|10810\rangle$ remaining solely within this manifold, as shown in Fig. 35. Two things are evident.

First, the individual $P_2'(t)$ curves lie far lower than those in Fig. 32, indicating the participation of many more bare kets in the dynamics of $P_2(t)$ than merely the two bare kets that form this original superposition. Second, with these few states, the extent of control depends heavily on the target time T: control at $T = 15$ fs is clearly far better than that at $T = 20$ fs, a manifestation of the time dependent component of the interference contribution to $f_{ii'}$.

$P_2(t)$ control results are significantly better when a much larger set of initial states forms the superposition state. Two such results, using 100 states centered $\approx 18{,}000\,\mathrm{cm}^{-1}$ with a width of $\approx 2000\,\mathrm{cm}^{-1}$ are shown in Figs. 36 and 37. Optimizations at both $T = 10$ and 1 fs are shown. There is appreciable control in both cases: i.e., there is now a considerable difference between the population of the maximized and minimized curves. This is particularly true for the 1 fs case, where $P_2(t)$ varies over range of 90%. Note also that the maximized $P_2(t)$ persists at high values well beyond 1 fs. Similarly, control in the 10 fs case is large, ranging from $P_2(T = 10)$ of 0.9–0.54.

8. Decoherence and loss of control

Thus far we have dealt with idealized isolated systems which are not subject to external collisions. Further, we have assumed that the system is initially in a pure state (i.e. described by a wavefunction) and that the externally imposed electric field is coherent, i.e. that the field is described by a well defined function of time. Under these circumstances the system is in a pure state before and after laser excitation, and remains so throughout its evolution. However, if the system is initially in a mixed state (e.g. due to prior collisional relaxation), or if the incident radiation field is not fully coherent (e.g., due to fluctuations of the laser phase or of the laser amplitude), or if collisions cause the loss of quantum phase after excitation, then phase information is degraded, interference phenomena are muted and laser control is jeopardized [205].

We use the term "decoherence" to mean loss of quantum information (either the phase or the amplitude of a state) due to the interaction of a system with its environment [208–212]. We consider a system s interacting with an environment (a *bath*). The total Hamiltonian H_{tot} is of the form

$$H_{\mathrm{tot}} = H_s + H_{\mathrm{bath}} + H_{\mathrm{int}}, \tag{180}$$

where H_s is the system Hamiltonian, H_{bath} is the Hamiltonian of the environment, and H_{int} is the interaction between them.

The system plus environment is described by a density operator $\rho_{\mathrm{tot}}(t)$ [206], whose dynamics is given by the quantum Liouville–von Neumann equation;

$$\mathrm{i}\hbar \frac{\partial \rho_{\mathrm{tot}}(t)}{\partial t} = [H_{\mathrm{tot}}, \rho_{\mathrm{tot}}(t)]. \tag{181}$$

Operators which pertain solely to the system, denoted $A_s(t)$, are given by averaging only over environmental variables, i.e. $A_s(t) = Tr_{\mathrm{bath}}[\rho_{\mathrm{tot}}(t)A(t)]$.

By pre-averaging over the environment variables we can obtain an equation of motion for $\rho_s(t)$, the system component of the density matrix. If the correlation time of the environment is much shorter than the typical time scale for the variation of the system then the generalized master equation [205,207] is of the form

$$\frac{\partial \rho_s(t)}{\partial t} = -\mathrm{i}\hbar^{-1}[H_s, \rho_s(t)] + F(\rho_s), \tag{182}$$

where $F(\rho_s)$ is a functional of ρ_s. Its functional form depends upon the nature of the environment and on the coupling H_{int}. The resultant equations are quite complex. As such, a variety of approximations to the generalized master equations have yielded equations which are used to model the effect of the environment on the system dynamics.

8.1. Coherent control in equilibrated condensed phases

8.1.1. The optical bloch equation

Consider coherent control as it would apply to liquid phase chemistry. Here, molecules of species B in solution would be subjected to laser irradiation. Since we are ultimately interested in the fate of the B molecules, B is the system and

the remaining molecules in the solution, and the laser, are the environment. Decoherence effects can then arise from the collisions of the solvent with the molecule of interest, or from incoherence properties of the laser that cause some loss of quantum phase information. Both of these effects are discussed below, along with proposed methods to reduce the effects of collisional or laser induced decoherence effects.

The strong role of collisions in decohering a system is readily seen by considering the density matrix of a system which has reached thermal equilibrium at temperature T through collisional relaxation, i.e. $\rho_s^T = Q\exp(-H_s/k_{\mathrm{B}}T)$. Here H_s is the system Hamiltonian, Q is a normalization factor and k_{B} is Boltzmann's constant. Considerable insight is obtained if we cast the density matrix in the energy representation. Then $\rho_{ij}^T = \langle E_i|\rho_s^T|E_j\rangle = Q\exp(-E_i/k_{\mathrm{B}}T)\delta_{ij}$, where $|E_i\rangle$ are energy eigenstates of H_s. That is, the system shows population in each of the energy levels, but no off-diagonal terms. Non-zero off-diagonal terms would represent quantum coherence between the energy eigenstates of the Hamiltonian. To see this, contrast the equilibrium result with that of the density operator associated with a pure state

$$|\psi\rangle = \sum_k a_k|E_k\rangle. \tag{183}$$

This density operator would be given by

$$\rho_s = |\psi\rangle\langle\psi| = \sum_{k,m} a_k a_m^*|E_k\rangle\langle E_m|, \tag{184}$$

which can be confirmed by substituting in Eq. (181), but with H and ρ_{tot} replaced by H_s and ρ_s. In this case,

$$\rho_{mk} = a_k a_m^*, \tag{185}$$

where here and below $\rho_{m,k}$ denotes the (m,k) element of the density matrix representing ρ_s.

Thus, the fact that there is a well defined phase relationship between the eigenstates of the Hamiltonian, contained in the wavefunction, is manifest in the existence of off-diagonal elements in the energy representation. The absence of off-diagonal matrix elements for the thermally equilibrated case makes clear that collisions have destroyed matter coherence manifest as quantum correlations between energy eigenstates.

With this in mind, we introduce the simplest of models for relaxation and concomitant decoherence. That is, the equation of motion of $\rho_s(t)$ in the energy representation is given the form

$$\mathrm{i}\hbar\frac{\partial\rho_{ij}(t)}{\partial t} = [H,\rho_s(t)]_{ij} - \frac{1}{T_{ij}}\rho_{ij}(t), \tag{186}$$

with $T_{ii} = T_1$ and $T_{ij} = T_2$ for $i \neq j$. Here T_1 and T_2 are phenomenological relaxation times. In this model, where $F(\rho)_{ij} = -\rho_{ij}(t)/T_{ij}$, the coherent terms $\rho_{ij}(t)$, $i \neq j$ decay with a rate $1/T_2$ and populations $\rho_{ii}(t)$ decay with rate $1/T_1$. If the system is in the presence of a radiation field, then H_s in Eq. (186) augmented by the dipole-electric field interaction H_{MR}. The result is the so-called Optical Bloch Equations. Note that this approach focuses explicitly on decoherence in the energy representation.

The simplest Optical Bloch Equations result from a system comprised of two eigenstates $|E_1\rangle$, $|E_2\rangle$ of the molecule Hamiltonian H_M which experience the interaction $H_{\mathrm{MR}} = -\varepsilon\hat{\epsilon}\cdot\vec{\mu}\cos(\omega t+\phi)$. The Hamiltonian H_s in Eq. (186) is $H_s = H_M + H_{\mathrm{MR}}$. Eq. (186) then becomes [where we suppress the t dependence of $\rho(t)$]:

$$\begin{aligned}\mathrm{i}\hbar\frac{\partial\rho_{ij}}{\partial t} &= \sum_k [H_{ik}\rho_{kj} - \rho_{ik}H_{kj}] - \frac{1}{T_{ij}}\rho_{ij},\\ H_{ik} &= E_i\delta_{ik} - \frac{\varepsilon}{2}\exp(-\mathrm{i}\omega t - \mathrm{i}\phi)\mu_{ik}(1-\delta_{ik}).\end{aligned} \tag{187}$$

Here we have used the rotating wave approximation to replace $\cos(\omega t+\phi)$ by $(\varepsilon/2)\exp(-\mathrm{i}\omega t-\phi)$. We now define

$$\begin{aligned}R_1 &\equiv \mathrm{i}\rho_{12}\exp(\mathrm{i}\omega t+\mathrm{i}\phi) + \mathrm{c.c.} = 2\,\mathrm{Im}(\rho_{12}^*),\\ R_2 &\equiv \rho_{12}\exp(\mathrm{i}\omega t+\mathrm{i}\phi) + \mathrm{c.c.} = 2\,\mathrm{Re}(\rho_{12}^*),\\ R_3 &\equiv \rho_{11}-\rho_{22},\end{aligned} \tag{188}$$

where c.c. denotes the complex conjugate of the term that precedes it. With these definitions, Eq. (187) becomes

$$\frac{dR_1}{dt} = \Delta R_2 - \frac{1}{T_2}R_1 + \Omega_{2,1}R_3,$$

$$\frac{dR_2}{dt} = -\Delta R_1 - \frac{1}{T_2}R_2,$$

$$\frac{dR_3}{dt} = -\frac{1}{T_1}R_3 - \Omega_{1,2}R_1. \tag{189}$$

Here $\Delta \equiv (E_2-E_1)/\hbar-\omega \equiv \omega_{21}-\omega$, i.e., the detuning of ω from the $|E_1\rangle$ to $|E_2\rangle$ transition, and $\Omega_{1,2}=\langle E_1|\vec{\mu}\cdot\hat{\epsilon}|E_2\rangle\varepsilon/\hbar$ is the Rabi frequency of the transition. Eq. (189) constitutes the standard form of the two level optical Bloch Equation.

8.1.2. Countering collisional effects

Consider now a scenario that is capable of maintaining coherent control in the presence of collisions for systems that are described by the Optical Bloch Equations. In particular, we reconsider the bichromatic CC scenario, assuming, however, that the molecules are in solution at temperature T. Further, we irradiate the system so as to saturate the $|E_1\rangle$ to $|E_2\rangle$ transition and simultaneously photodissociate the system. The initial state, prior to dissociation, is a mixed state described, in the energy representation, by a 2×2 density matrix with elements ρ_{ij}, $(i, j = 1, 2)$. Photodissociation of this mixed state can be written as a generalization [213] of pure state CC starting from a superposition state (Eq. (183)). Assuming that the initial density matrix is given by Eq. (185), the probability of photodissociation is given as

$$P^{(q)}(E) = (2\pi/\hbar)^2 \sum_{i,j=1}^{N} [\rho_{ij}\bar{\epsilon}(\omega_{E,i})\bar{\epsilon}^*(\omega_{E,j})]\mu^{(q)}(ji). \tag{190}$$

Eq. (190) is, in fact, the correct generalization to the case where the initial state is mixed and represented by ρ_{ij}.

To utilize Eq. (190) we determine ρ_{ij} for the case where two levels $|E_1\rangle$ and $|E_2\rangle$ are continuously subjected to radiation and collisions using the Optical Bloch approach. However, it is necessary to modify Eq. (187) since selection rules in coherent control require that $|E_1\rangle$ and $|E_2\rangle$ be of the same parity. Hence, since one photon absorption does not couple these states, we consider saturating this transition using two photon absorption through an off-resonant intermediate bound state $|0\rangle$ with dipole matrix elements $\mu_{oj} = \langle 0 \mid \vec{\mu}\cdot\hat{\epsilon} \mid E_j\rangle$.

For simplicity we assume that $2\omega = (E_2 - E_1)/\hbar$ so that the transition is two-photon resonant (the non-resonant case is discussed in [213]), and extend [214] Eq. (189) to two photon absorption by replacing $\Omega_{2,1}$ by the proper two photon transition matrix element $D_{2,1}$, given as

$$D_{2,1} = \varepsilon^2\mu_{20}\mu_{01}/[2\hbar^2(\omega - \omega_{01})]. \tag{191}$$

Eq. (189), with the added recognition that at temperature T the quantity R_3 equals the thermodynamic population difference R_3^e, become

$$\frac{dR_1}{dt} = -\frac{D_{1,2}R_3}{2} - \frac{R_1}{T_2},$$

$$\frac{dR_2}{dt} = -\frac{R_2}{T_2},$$

$$\frac{dR_3}{dt} = \frac{D_{2,1}R_1}{2} - \frac{(R_3 - R_3^e)}{T_1}, \tag{192}$$

where

$$R_3^e = [1 - \exp(-\hbar\omega_{21}/k_BT)]/[1 + \exp(-\hbar\omega_{21}/k_BT)]. \tag{193}$$

At long times ($t \gg T_2$, T_1) the system saturates, i.e., $\mathrm{d}R_3/\mathrm{d}t = 0$ and Eq. (192) implies that $\mathrm{d}R_1/\mathrm{d}t = 0$. The equations for R_i can then be readily solved and, in conjunction with Eq. (188), gives $\rho_{1,2}$ at saturation:

$$\rho_{1,2} = R_3^e T_2 D_{1,2} \exp[\mathrm{i}(2\phi - \pi/2)]/(4 + D_{2,1}^2 T_1 T_2),$$

$$\rho_{1,1} = 0.5[1 + R_3^e/(1 + D_{2,1}^2 T_1 T_2/4)],$$

$$\rho_{2,2} = 0.5[1 - R_3^e/(1 + D_{2,1}^2 T_1 T_2/4)]. \tag{194}$$

Consider then excitation of this mixed state with a Gaussian pulse, whose contribution within the rotating wave approximation is given by

$$\varepsilon(t) = A\mathrm{e}^{-\mathrm{i}(\omega_L t+\delta)}\mathrm{e}^{-(t-t_0)^2/\tau^2}. \tag{195}$$

with Fourier transform

$$\epsilon(\omega) = (A\tau/\sqrt{\pi})\mathrm{e}^{-\tau^2(\omega_L-\omega)^2/4}\mathrm{e}^{-\mathrm{i}(\omega_L-\omega)t_0}\mathrm{e}^{-\mathrm{i}\delta} \equiv \varepsilon_\omega \mathrm{e}^{-\mathrm{i}(\omega_L-\omega)t_0}\mathrm{e}^{-\mathrm{i}\delta}. \tag{196}$$

Note that this control arrangement the two frequencies $\omega_1 = (E - E_1)/\hbar$ and $\omega_2 = (E - E_2)/\hbar$ that dissociates the system are components of a single pulse. The temporal width of the pulse is such that $\tau \gg T_1$, T_2.

Inserting the long time ρ_{ij} into Eq. (190) gives (denoting ε_{ω_i} by ε_i) the probability $P^{(q)}(E)$ of forming product in channel q at energy E as

$$P^{(q)}(E) = (\pi^2/\hbar^2)[P_{1,1}^{(q)}(E) + P_{2,2}^{(q)}(E) + P_{1,2}^{(q)}(E)], \tag{197}$$

where

$$P_{1,1}^{(q)}(E) = \rho_{1,1}\varepsilon_1^2\mu^{(q)}(11) = 0.5[1 + R_3^e/(1 + D_{2,1}^2 T_1 T_2/4)]\varepsilon_1^2\mu^{(q)}(11),$$

$$P_{2,2}^{(q)}(E) = \rho_{2,2}\varepsilon_2^2\mu^{(q)}(22) = 0.5[1 - R_3^e/(1 + D_{2,1}^2 T_1 T_2/4)]\varepsilon_2^2\mu^{(q)}(22)$$

and

$$\begin{aligned} P_{1,2}^{(q)}(E) &= 2 \mid \rho_{1,2} \mid\mid \mu^{(q)}(12) \mid \varepsilon_1\varepsilon_2 \cos(\alpha_{12}^{(q)} + \omega_{21}\tau + 2\phi - \pi/2) \\ &= 0.5T_2 D_{1,2} R_3^e/(1 + D_{2,1}^2 T_1 T_2/4)\varepsilon_1\varepsilon_2 \mid \mu^{(q)}(12) \mid \cos(\alpha_{12}^{(q)} + \omega_{21}\tau + 2\phi - \pi/2). \end{aligned} \tag{198}$$

From these equations it is evident that coherent control can be achieved in solution, for example, by varying τ to alter the quantum interference term.

A number of simple qualitative observations are evident. First $P^{(q)}(E)$ depends upon the parameters associated with the saturation through the combinations $D_{2,1}T_1$ and $D_{1,2}T_2$ (or their ratio and product T_1/T_2 and $D_{2,1}^2 T_1 T_2$ used below). Control vanishes if $P_{1,2}^{(q)}(E) = 0$ and this occurs if either $T \to \infty$ (i.e., $R_3^e \to 0$) or $D_{1,2}T_2 \to 0$. Both these limits correspond to complete loss of coherence. Examination of Eq. (198) shows that this is not the case, however, for $D_{2,1}T_1 \to 0$, consistent with the fact that T_1 relates to population, rather than phase, relaxation. Physically [215], however, in collisional environment, $T_1 \gg T_2$ so that the limit $T_1 \to 0$ also implies loss of control. Note also that control vanishes under extremely large pumping rates, $D_{2,1} \to \infty$ for which $\rho_{1,1} = \rho_{2,2}$ and $\rho_{1,2} \to 0$.

Sample computational results are shown in Figs. 38–41 for the case of the photodissociation of CH_3I into $CH_3 + I$ vs. $CH_3 + I^*$. In particular, we show control over the ratio $I^*/(I + I^*)$ for the collision-free case in Fig. 38, and at three successively higher temperatures in the subsequent three figures. The abscissa is $S = \varepsilon_1^2/(\varepsilon_1^2 + \varepsilon_2^2)$ and the ordinate is the angle $\chi_{12} = \omega_{21}\tau + 2\phi - \pi/2$. The results clearly show control for the two lower temperatures, including $T = \hbar\omega_{21}/k_B$ and the total loss of control at the highest temperature, as manifest in the lack of dependence of the yield ratio on the phase angle χ_{12}.

The results clearly show that, although collisional effects do reduce the degree of control relative to the collision-free case, saturation pumping of superposition in the bichromatic control scenario can be used to overcome collisional effects up until some reasonable temperature.

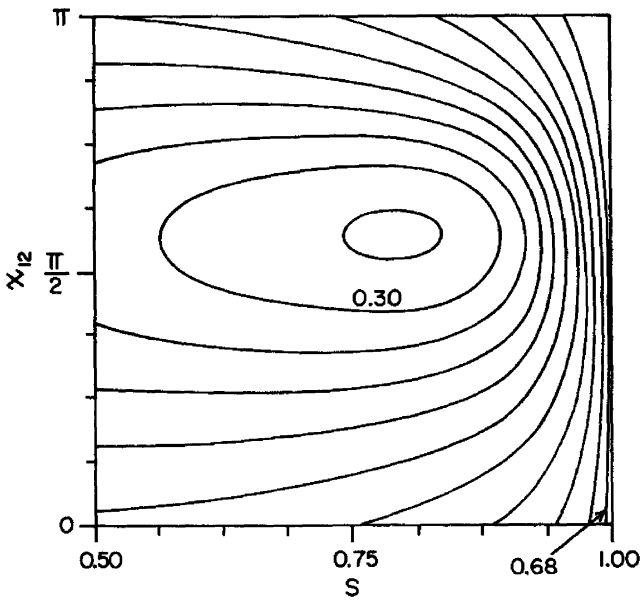

Fig. 38. Contour plot of the I* yield $[I^*/(I+I^*)]$ for two color photodissociation of a pure CH_3I superposition state comprised of bound states with quantum numbers $(v, J) = (0, 2)$ and (1,2) excited with frequencies $\omega_1 = 41579\,\mathrm{cm}^{-1}$ and $\omega_2 = 41163\,\mathrm{cm}^{-1}$. Contours increase, in increments of 0.04, from the "center well". Taken from Fig. 1, Ref. [213].

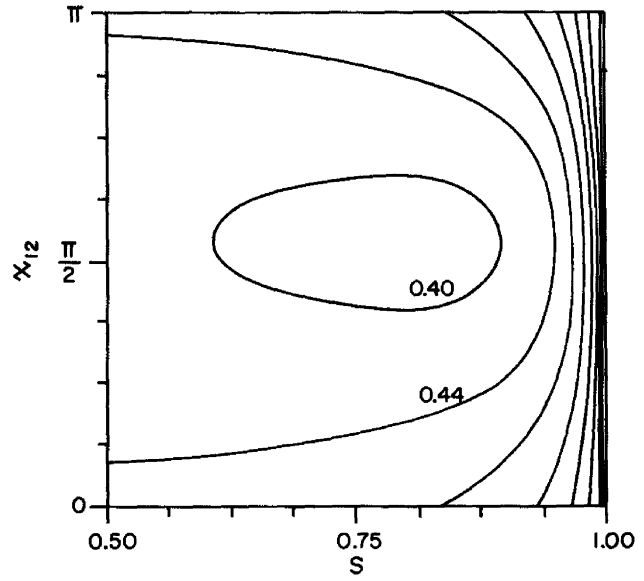

Fig. 39. As in Fig. 38, but at $k_B T = 0.2\hbar\omega_{21}$. Taken from Fig. 2, Ref. [213].

8.2. Countering partially coherent laser effects in pump–dump control

An alternate source of decoherence is in the nature of the laser used to irradiate the system. Specifically, if the laser has random components then it inputs a degree of randomness into the system, reducing the phase information content and hence decohering the system.

For example, consider control of photodissociation of an initial two-level superposition state that is excited to the continuum. If there are sufficiently strong external perturbations, or excessive jitter in the laser phase, then this

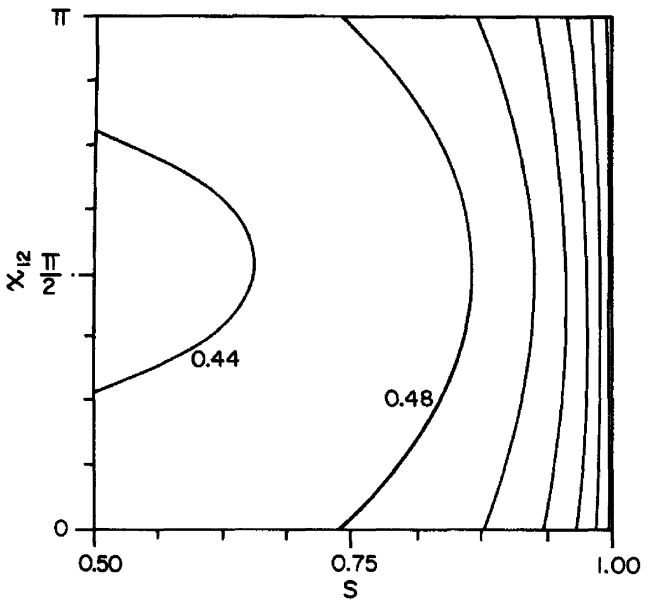

Fig. 40. As in Fig. 38, but at $k_B T = \hbar\omega_{21}$. Taken from Fig. 3 Ref. [213].

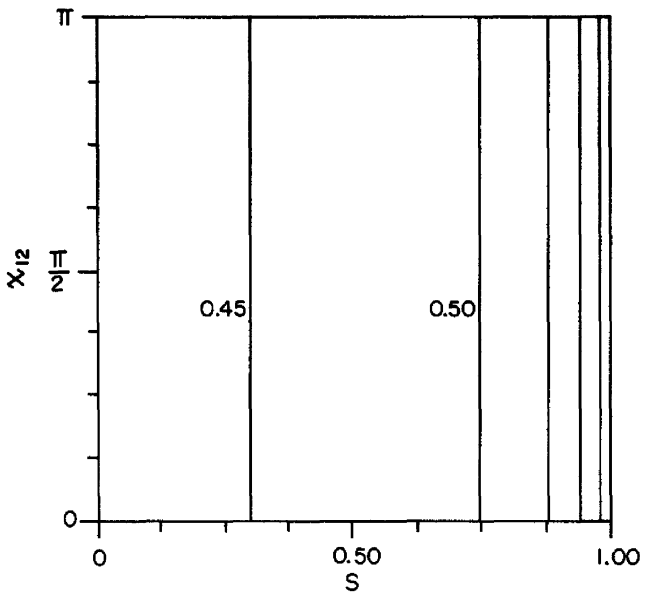

Fig. 41. As in Fig. 38, but at $k_B T = 1000\hbar\omega_{21}$. Contours are spaced by 0.05. Taken from Fig. 4, Ref. [213].

corresponds to a complete average over $\phi_1 - \phi_2$. We obtain that the branching ratio between the q and q' manifold is given as

$$R_{q,q'}(E) \equiv \frac{P^{(q)}(E)}{P^{(q')}(E)} = \frac{|\mu^{(q)}(1,1)| + x^2|\mu^{(q)}(2,2)|)}{|\mu^{(q')}(1,1)| + x^2|\mu^{(q')}(2,2)|}. \tag{199}$$

Thus, there is no longer any dependence on any phase characteristics and all phase control is lost.

Eq. (199) represents an extreme fully incoherent situation. It is enlightening to consider the effect of partially coherent laser sources through the example of the pump–dump CC scenario in the case where the laser is not fully coherent.

To characterize partially coherent pulses [216] consider a Gaussian laser pulse with time profile $\varepsilon_x(t)$ and phase $\delta_x(t)$, i.e.

$$\varepsilon_x(t) = (\epsilon_{x0}/2)\mathrm{e}^{-(t-t_x)^2/\tau_x^2}\mathrm{e}^{-\mathrm{i}[\omega_x t+\delta_x(t)]}. \tag{200}$$

We adopt a phase diffusion model for the partially coherent laser source in which the phase δ_x is allowed to be time dependent and random. Thus, the molecule–laser interaction is modeled by the interaction with an ensemble of lasers, each of different phase. This ensemble is described by a Gaussian correlation for the stochastic phases with a decorrelation time scale τ_{xc}:

$$\langle \mathrm{e}^{\mathrm{i}\delta_x(t_2)}\mathrm{e}^{-\mathrm{i}\delta_x(t_1)}\rangle = \mathrm{e}^{-(t_2-t_1)^2/2\tau_{xc}^2}. \tag{201}$$

Here the angle brackets denote an average over the ensemble of laser phases.

To examine photodissociation given this field requires, as shown below, the frequency–frequency correlation function $\langle \epsilon_x(\omega_2)\epsilon_x^*(\omega_1)\rangle$ where $\epsilon_x(\omega)$ is the Fourier transform of $\varepsilon(t)$ for $\delta_x(t)$ equal to a constant δ_x. Given Gaussian pulses [Eqs. (200)–(201)] we have [216]

$$\langle \epsilon_x(\omega_2)\epsilon_x^*(\omega_1)\rangle = \frac{\epsilon_{x0}^2\tau_x T_x}{8}\,\mathrm{e}^{\mathrm{i}(\omega_2-\omega_1)t_x}\mathrm{e}^{-\tau_x^2(\omega_2-\omega_1)^2/8}\mathrm{e}^{-T_x^2(\omega_2+\omega_1-2\omega_x)^2/8}, \tag{202}$$

where

$$T_x = \tau_x\tau_{xc}/(\tau_x^2+\tau_{xc}^2)^{1/2}. \tag{203}$$

Since the pump–dump control scenario involves two lasers we adopt a similar description for the dump pulse $\varepsilon_d(t)$, with appropriate change in parameter labels, i.e.

$$\varepsilon_d(t) = (\epsilon_{d0}/2)\mathrm{e}^{-(t-t_d)^2/\tau_d^2}\mathrm{e}^{-\mathrm{i}(\omega_d t+\delta_d(t))}, \tag{204}$$

$$\langle \mathrm{e}^{\mathrm{i}\delta_d(t_2)}\mathrm{e}^{-\mathrm{i}\delta_d(t_1)}\rangle = \mathrm{e}^{-(t_2-t_1)^2/2\tau_{dc}^2}, \tag{205}$$

$$\langle \epsilon_d(\omega_2)\epsilon_d^*(\omega_1)\rangle = \frac{\epsilon_{d0}^2\tau_d T_d}{8}\mathrm{e}^{\mathrm{i}(\omega_2-\omega_1)t_d}\mathrm{e}^{-\tau_d^2(\omega_2-\omega_1)^2/8}\mathrm{e}^{-T_d^2(\omega_2+\omega_1-2\omega_d)^2/8}, \tag{206}$$

where $T_d = \tau_d\tau_{dc}/(\tau_d^2+\tau_{dc}^2)^{1/2}$ Here τ_{xc} and τ_{dc} define the degree of field coherence, the two limiting cases being a coherent source ($\tau_{ic}\to\infty, i = x, d$) and fully incoherent source ($\tau_{ic}\to 0, i = x, d$).

The frequency spectrum of the pulse provides a primary means of characterizing the laser-molecule interaction and is given, for the excitation pulse, by

$$I_x(\omega) = \frac{T_x}{\sqrt{2\pi}}\mathrm{e}^{-T_x^2(\omega-\omega_x)^2/2}, \tag{207}$$

whose full width at half maximum (FWHM) is $2\sqrt{2\ln 2}/T_x$. For the coherent pulse $T_x = \tau_x$ giving a FWHM of the intensity spectrum equal to $\Delta_x/\sqrt{2}$ where $\Delta_x \equiv 4\sqrt{\ln 2}/\tau_x$ is the FWHM of the frequency profile of the pulse.

Similar definitions apply to characterize the dump pulse. Further, for consistency we define the partial coherence parameter $\Delta_{xc} = 4\sqrt{\ln 2}/\tau_{xc}$ and similar parameters (Δ_d, Δ_{dc}) for the dump pulse. Note that fitting Eq. (207) to the measured pulse frequency spectrum provides a means of obtaining T_x and ω_x from experimental data [216].

Consider now the pump–dump scenario where, for generality, we assume a pump pulse whose spectral width is sufficiently large to encompass a large number of levels. A molecule with Hamiltonian H_M is subjected to two temporally separated pulses $\varepsilon(t) = \varepsilon_x(t) + \varepsilon_d(t)$. The probability of forming channel q at energy E is now given as

$$P^{(q)}(E) = (2\pi/\hbar^2)\sum_{\mathbf{m}}|\sum_j b_j\langle E,\mathbf{m},q^-|\hat{\epsilon}\cdot\vec{\mu}|E_j\rangle\epsilon_d(\omega_{EE_j})|^2, \tag{208}$$

where $\omega_{EE_j} = (E - E_j)/\hbar$ and b_j is given by

$$b_j = (2\pi \mathrm{i}/\hbar)\langle E_j|\hat{\boldsymbol{\epsilon}}\cdot\vec{\mu}|E_1\rangle\bar{\epsilon}_x(\omega_{j,1}) \equiv c_j\bar{\epsilon}_x(\omega_{j,1}). \tag{209}$$

Eq. (209) also defines c_j as the field independent component of b_j.

Expanding the square allows us to write the probability in a canonical form:

$$\begin{aligned} P^{(q)}(E) &= (2\pi/\hbar^2)\sum_{ij} b_i b_j^* \epsilon_d(\omega_{EE_i})\epsilon_d^*(\omega_{EE_j})\mu^{(q)}(ij) \\ &\equiv (2\pi/\hbar^2)\sum_{ij} c_i c_j^* \epsilon_x(\omega_{ig})\epsilon_x^*(\omega_{jg})\epsilon_d(\omega_{EE_i})\epsilon_d^*(\omega_{EE_j})\mu^{(q)}(ij), \end{aligned} \tag{210}$$

where $\mu^{(q)}(ij) = \sum_{\mathbf{n}}\langle E_j|\hat{\boldsymbol{\epsilon}}\cdot\vec{\mu}|E, \mathbf{n}, q^-\rangle\langle E, \mathbf{n}, q^-|\hat{\boldsymbol{\epsilon}}\cdot\vec{\mu}|E_j\rangle$. To incorporate effects due to a partially coherent source we independently average Eq. (210) over the ensemble of phases of the excitation and dump pulses, giving

$$P^{(q)}(E) = (2\pi/\hbar^2)\sum_{ij} c_i c_j^* \langle\epsilon_x(\omega_{ig})\epsilon_x^*(\omega_{jg})\rangle\langle\epsilon_d(\omega_{EE_i})\epsilon_d^*(\omega_{EE_j})\rangle\mu^{(q)}(ij). \tag{211}$$

Note that despite the excitation of multiple levels the only correlation function required is between ϵ at two frequencies. Assuming the phase diffusion model described above, then the frequency–frequency correlation functions is given by Eq. (202). The probability $P(q)$ of forming product in channel q is then obtained by integrating over the pulse width:

$$P(q) = \int \mathrm{d}E\, P^{(q)}(E) = (2\pi/\hbar^2)\sum_{i,j} c_i c_j^* \langle\epsilon_x(\omega_{ig})\epsilon_x^*(\omega_{jg})\rangle \int \mathrm{d}E\langle\epsilon_d(\omega_{EE_i})\epsilon_d^*(\omega_{EE_j})\rangle\mu^{(q)}(ij). \tag{212}$$

Invoking the ("flat continuum") SVCA, in conjunction with the generalized Parseval's equality (whose conventional form, $\int \mathrm{d}\omega\langle|\epsilon(\omega)|^2\rangle = \int \mathrm{d}t\langle\varepsilon^*(t)\varepsilon(t)\rangle$ is the special case of $\omega_1 = \omega_2$), renders $P(q)$ independent of the coherence properties of the dump pulse. Specifically we have

$$\begin{aligned} \int \mathrm{d}\omega\langle\epsilon^*(\omega-\omega_1)\epsilon(\omega-\omega_2)\rangle &= \frac{1}{2\pi}\int \mathrm{d}\omega \int\int \mathrm{d}t_1\,\mathrm{d}t_2\langle\varepsilon^*(t_1)\varepsilon(t_2)\rangle \mathrm{e}^{\mathrm{i}\omega(t_2-t_1)}\mathrm{e}^{\mathrm{i}(\omega_1 t_1-\omega_2 t_2)} \\ &= \int\int \mathrm{d}t_1\,\mathrm{d}t_2\langle\varepsilon^*(t_1)\varepsilon(t_2)\rangle\delta(t_2-t_1)\mathrm{e}^{\mathrm{i}(\omega_1 t_1-\omega_2 t_2)} \\ &= \int \mathrm{d}t\langle\varepsilon^*(t)\varepsilon(t)\rangle\mathrm{e}^{\mathrm{i}(\omega_1-\omega_2)t}. \end{aligned} \tag{213}$$

Since the right hand side is independent of the phase of $\varepsilon(t)$ then the frequency integrated correlation function is independent of the degree of coherence of the dump pulse.

Assuming that $\mu^{(q)}(ij)$ in independent of E over the pulse width allows us to write Eq. (212) as

$$P(q) = (2\pi/\hbar^2)\sum_{ij} c_i c_j^* \langle\epsilon_x(\omega_{ig})\epsilon_x^*(\omega_{jg})\rangle F(\omega_{ji})\mu^{(q)}(ij), \tag{214}$$

with $F(\omega_{ji}) \equiv \int \mathrm{d}t\langle|\varepsilon_d(t)|^2\rangle\mathrm{e}^{\mathrm{i}(E_j-E_i)t/\hbar}$. Hence,

$$P(q) = (2\pi/\hbar^2)\sum_{ij} c_i c_j^* |\langle\epsilon_x(\omega_{ig})\epsilon_x^*(\omega_{jg})\rangle F(\omega_{ji})\mu^{(q)}(ij)|\mathrm{e}^{\mathrm{i}\omega_{ij}\Delta_t + \mathrm{i}\alpha^{(q)}(ij)(E)}, \tag{215}$$

where $\Delta_t = (t_d - t_x)$. For the simplest case, excitation which encompasses only two levels, $P(q)$ is given by:

$$\begin{aligned} P(q) = (2\pi/\hbar^2)[&|c_1|^2\langle|\epsilon_x(\omega_{1g})|^2\rangle\mu^{(q)}(11)F(\omega_{11}) + |c_2|^2\langle|\epsilon_x(\omega_{2g})|^2\rangle\mu^{(q)}(22)F(\omega_{22}) \\ &+ 2|c_1 c_2^*\mu^{(q)}(12)\langle\epsilon_x(\omega_{1g})\epsilon_x^*(\omega_{2g})\rangle F(\omega_{21})|\cos(\omega_{21}\Delta_t + \alpha^{(q)}(12) + \beta)], \end{aligned} \tag{216}$$

with $\langle E_1|\vec{\mu}\cdot\hat{\epsilon}|E_g\rangle\langle E_g|\vec{\mu}\cdot\hat{\epsilon}|E_2\rangle \equiv |\langle E_1|\vec{\mu}\cdot\hat{\epsilon}|E_g\rangle\langle E_g|\vec{\mu}\cdot\hat{\epsilon}|E_2\rangle|\exp(\mathrm{i}\beta)$.

Since partial laser phase coherence affects both the direct terms as well as the cross terms the extent of control is dependent on the laser properties through the relative magnitudes of $|\langle\epsilon_x(\omega_{1g})\epsilon_x^*(\omega_{2g})\rangle|$ and $\langle|\epsilon_x(\omega_{ig})|^2\rangle$, $i = 1, 2$. To expose the dependence on the coherence of the pump field denote the terms $|c_k c_j^* F(\omega_{jk})\mu^{(q)}(k, j)(E)|$ by $a_{k,j}^{(q)}$ and consider the ratio of the $k \neq j$ term in Eq. (215) to the associated diagonal terms. That is, consider the contrast ratio

$$C_{kj}^{(q)} = \frac{a_{k,j}^{(q)}\langle\epsilon_x(\omega_{kg})\epsilon_x^*(\omega_{jg})\rangle}{a_{k,k}^{(q)}\langle|\epsilon_x(\omega_{kg})|^2\rangle + a_{j,j}^{(q)}\langle|\epsilon_x(\omega_{jg})|^2\rangle}. \tag{217}$$

For the Gaussian model of a partially coherent source Eq. (217) assumes the form

$$C_{kj}^{(q)} = \exp\left[\frac{-\omega_{kj}^2(\tau_x^2 - T_x^2)}{8}\right]\left[\frac{a_{k,j}^{(q)}\exp(-\omega_{jk}T_x^2\delta_{E_{jk}}/2\hbar)}{a_{k,k}^{(q)} + a_{j,j}^{(q)}\exp(-\omega_{jk}T_x^2\delta_{E_{jk}}/\hbar)}\right]. \tag{218}$$

Here $\delta_{E_{jk}} \equiv E_x - E_{\mathrm{av}} \equiv \hbar\omega_x - (E_k + E_j)/2$. The second term in Eq. (218), in brackets, is a function of $T_x^2\delta_{E_{jk}}$. If two bound state levels dominate the pump excitation then this term contributes a scaling characteristic to control plots. That is, if we plot contours of constant dissociation probability as a function of Δ_t and $\delta_{E_{jk}}$ then, barring the first term, plots with different T_x will appear similar, with a new range scaled by $\delta_{E'} = (T_x/T_x')^2\delta_{E_{jk}}$.

The first term in Eq. (218) can be rewritten as

$$A_{kj} = \exp\left[\frac{-\omega_{kj}^2(\tau_x^2 - T_x^2)}{8}\right] = \exp\left[\frac{-\omega_{kj}^2\tau_x^2}{8}\left(1 - \frac{1}{(\tau_x/\tau_{xc})^2 + 1}\right)\right], \tag{219}$$

which affords additional insight into the dependence of control, achieved by varying Δ_t, on coherence characteristics of the pump laser. Note first that Eq. (219) implies that for fixed τ_x control comes predominantly from nearby molecular states, i.e. those with small ω_{kj}. Second, for fixed pulse duration τ_x, control is expected to decrease with decreasing τ_{xc}, i.e. with decreasing pulse coherence. This is reasonable since decreasing τ_x leads to the preparation of mixed molecular states with increasing degrees of state impurity [217] and hence loss of phase information. Somewhat unexpected, however, is the prediction of improved control with decreasing pulse duration τ_x at fixed (τ_x/τ_{xc}), embodied in the $\exp(-\omega_{kj}^2\tau_x^2)$ term.

As an example, consider the dependence of the photodissociation of a model collinear HDH complex H+DH←HDH→HD+H as a function of Δ_t and of the detuning $\delta_E \equiv E_x - E_{av} \equiv \hbar\omega_x - (E_1 + E_2)/2$, where E_1 and E_2 are two selected neighboring energy levels for variable Δ_{xc}. For small Δ_{xc} only two levels are excited but as Δ_{xc} increases the excitation encompasses a larger number of levels below. Each panel of Fig. 42 shows a contour plot of the fractional yield of DH [i.e., P(DH)/(P(DH)+P(H_2))] as a function of Δ_t and δ_E, for different values of Δ_{xc}. Panel a, for comparison, the case of a coherent pulse ($\Delta_{xc} = 0$); the range of control is large with the yield ratio varying from 0.19 to 0.92. Panels b and c shows control in the same system but with differing amounts of pump laser incoherence. Increasing incoherence is clearly accompanied by a reduction in the range of control, with considerable loss of control by $\Delta_{xc} = 80\,\mathrm{cm}^{-1}$ control [panel c]. Note that regions where the yield depends on δ_E but not on Δ_t does not constitute interference based control. Rather this dependence is a consequence of the (generally uninteresting) predisposition of various bound levels of the excited electronic state to preferentially dissociate to particular products. The pattern shown in Fig. 42, where the control plot is dominated by a single well defined peak and valley, is characteristic of the excitation of essentially two levels, i.e., two molecular levels under the laser excitation envelope have significant Franck–Condon factors. More complicated behavior is seen upon excitation of additional levels. Fig. 43 shows results typical of those obtained with the excitation of a large number of levels. The resultant dependence of the yield ratio on δ_E and Δ_t is far more complex than the behavior seen in previous figures. However, the reduction of control with increasing Δ_{xc} is clearly evident; control is lost by $\Delta_{xc} = 1000\,\mathrm{cm}^{-1}$ (not shown).

From these and related studies we find that control in the model DH_2 system is lost when $(\Delta_{xc}/\Delta_x) = (\tau_x/\tau_{xc}) \approx 4-5$. This precludes the use of typical nanosecond lasers, where $(\Delta_{xc}/\Delta_x) > 10^2$, for pump–dump control.

A more complex analysis of the effect of laser phase diffusion has been applied to the case of one photon-vs. three photon absorption (i.e., simultaneous absorption of $3\omega_1$ and ω_3 with $3\omega_1 = \omega_3$) by Lambropoulos and coworkers [218]. They assumed that the ω_3 photon was made by third harmonic generation from the ω_1 laser. Current experiments, vary the relative phase of two laser beams by passing ω_3 and ω_1 through a gas. If the laser frequency is somewhat unstable

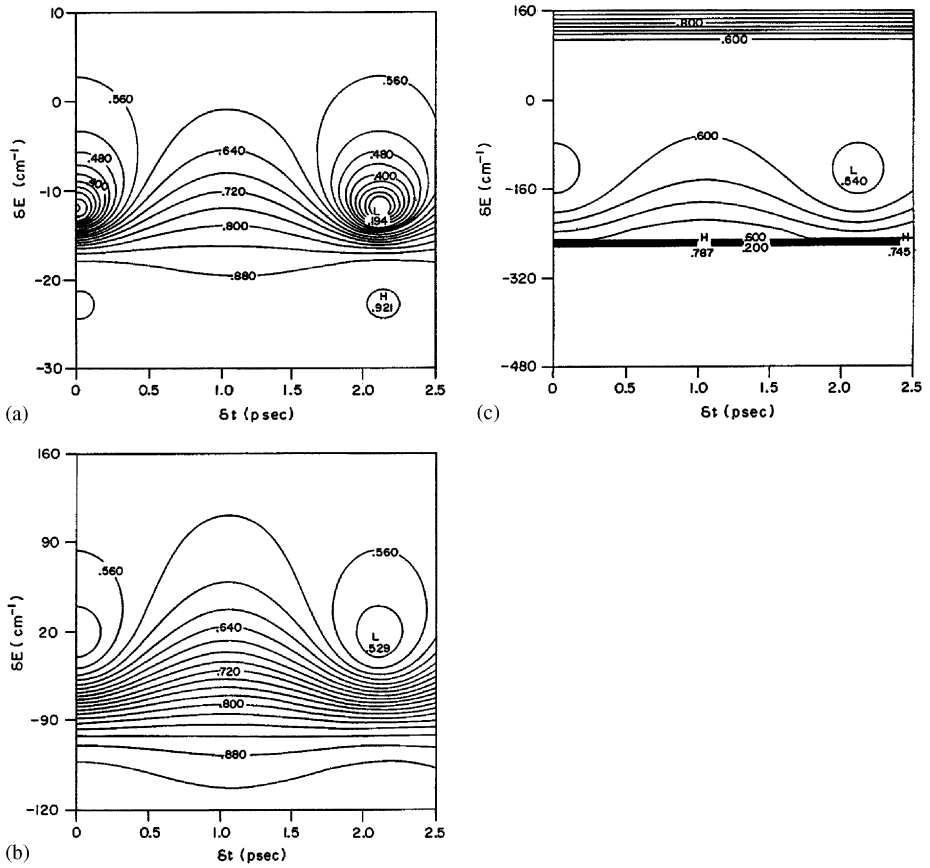

Fig. 42. Contour plots of the fraction of DH yield as a function of the detuning, δE and the time delay $\Delta_t \equiv \Delta_t$ for partially coherent pulsed excitation. Here $\Delta_d = 80\,\mathrm{cm}^{-1}$, $\Delta_x = 20\,\mathrm{cm}^{-1}$, (a) $\Delta_{xc} = 0\,\mathrm{cm}^{-1}$ (upper left), (b) $\Delta_{xc} = 40\,\mathrm{cm}^{-1}$ (lower left) and (c) $\Delta_{xc} = 80\,\mathrm{cm}^{-1}$ (upper right). Taken from Fig. 1 Ref. [222].

then the relative phase of the two beams will acquire a fluctuating phase which is a source of phase loss in the system. The phase fluctuations of the ω_1, denoted $\delta\phi$ are assumed proportional to the fluctuations of ω_1, i.e. $\delta\phi = \alpha\delta\omega_1$. For typical experimental circumstances it is reasonable to model the $\delta\omega_1$ distribution by the Gaussian probability distribution

$$P(\delta\omega_1) = (2\pi\gamma\beta)^{-1/2}\exp[-(\delta\omega_1)^2/(2\gamma\beta)], \tag{220}$$

where γ and β parametrize the laser frequency fluctuations:

$$\langle\delta\omega_1\delta\omega_1(t-\tau)\rangle = \gamma\beta\exp^{-\beta|t|}. \tag{221}$$

For the one vs. three photon scenario as applied to the simple case of He photoionization (i.e. only a single product channel is considered) the ionization probability is given by

$$P^{(q)}(E) = F_q(11) - 2x\cos[\phi_3 - 3\phi_1 + \delta_q(13)]\epsilon_0^2|F_q(13)| + x^2\epsilon_0^4 F_q(33). \tag{222}$$

Assuming that the direct one photon and direct three photon parts are unity and the phase assumes a time dependent fluctuation then the essential part of the Eq. (222) is of the form

$$P^{(q)}(\phi_0, t) = 1 + \cos(\phi_0 + \delta\phi(t)) = 1 \pm \cos(\alpha\delta\omega_1(t)), \tag{223}$$

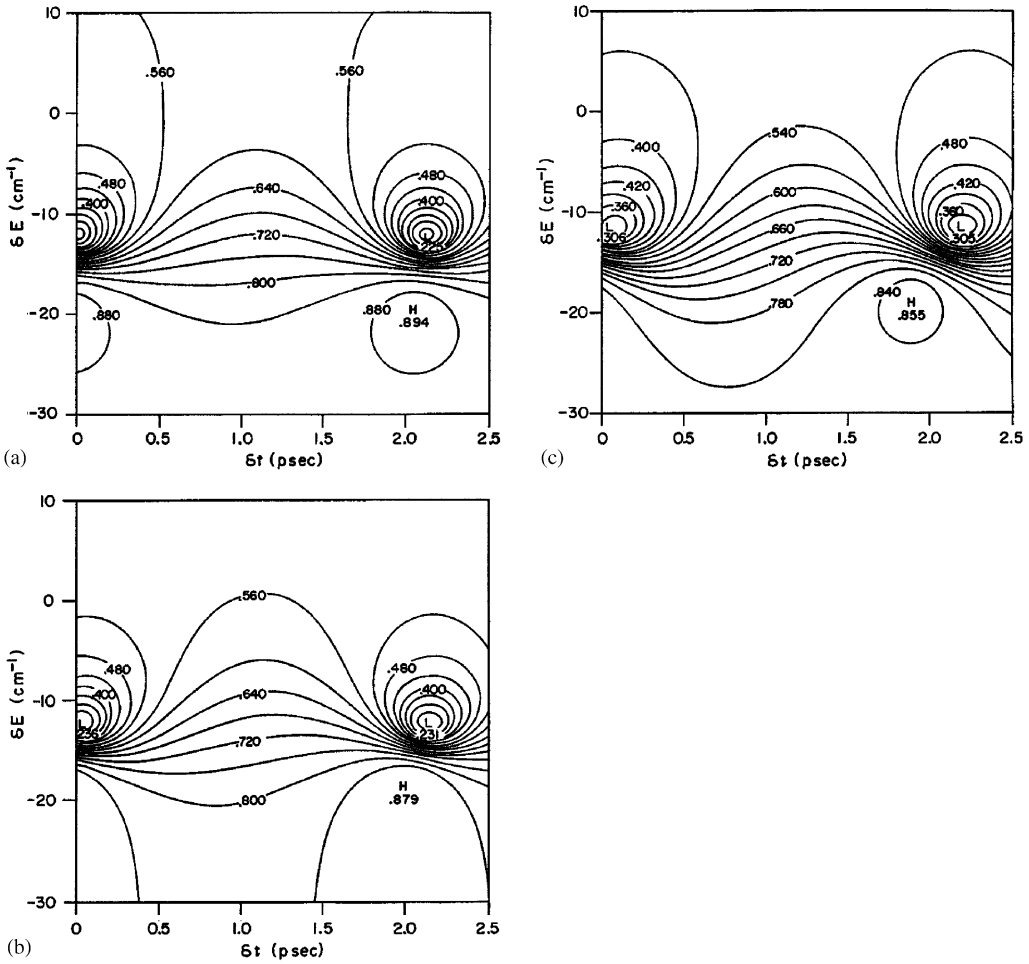

Fig. 43. Same as Fig. 42, but for excitation of denser set of bound states [222]. Here $\Delta_x = 200\,\mathrm{cm}^{-1}$ and (a) $\Delta_{xc} = 0\,\mathrm{cm}^{-1}$ (upper left), (b) $\Delta_{xc} = 200\,\mathrm{cm}^{-1}$ (lower left) and (c) $\Delta_{xc} = 800\,\mathrm{cm}^{-1}$ (upper right). Taken from Fig. 2 Ref. [222].

where $\phi_3 - 3\phi_1 + \delta_q(13) \equiv \phi_0 + \delta\phi(t)$ and where the plus and minus refer to the cases where $\phi_0 = 0$ and π, respectively. The average probability is then obtained as

$$\langle P^{(q)}(E)\rangle = 1 \pm \int P(\delta\omega_1)\cos(\alpha\delta\omega_1)d[\delta\omega_1],$$

$$\langle P^{(q)}(E)\rangle = 1 \pm \exp[-\alpha^2\gamma\beta/2]. \tag{224}$$

A useful criteria for the effect of the partially coherent laser on the control is given by the "contrast ratio", i.e. the ratio of the photoionization signal at its maximum and minimum,

$$\zeta_0 = \log_{10}[\langle P^{(q)}(E)\rangle, \phi = 0/\langle P^{(q)}(E)\rangle = \log_{10}[1 \pm \exp[-\alpha^2\gamma\beta/2]. \tag{225}$$

Numerical studies [218] show that Eq. (225) provides a zeroth order approximation to the results of a full computation, which underestimates the degree of possible control in a realistic system. In addition, these results show that even for phase diffusion fields which have widths on the order of wave numbers, control is still extensive (e.g. $\zeta_0 \approx 5$). Examination of the experimental results on one photon vs. three photon control show, however, contrast ratios on the

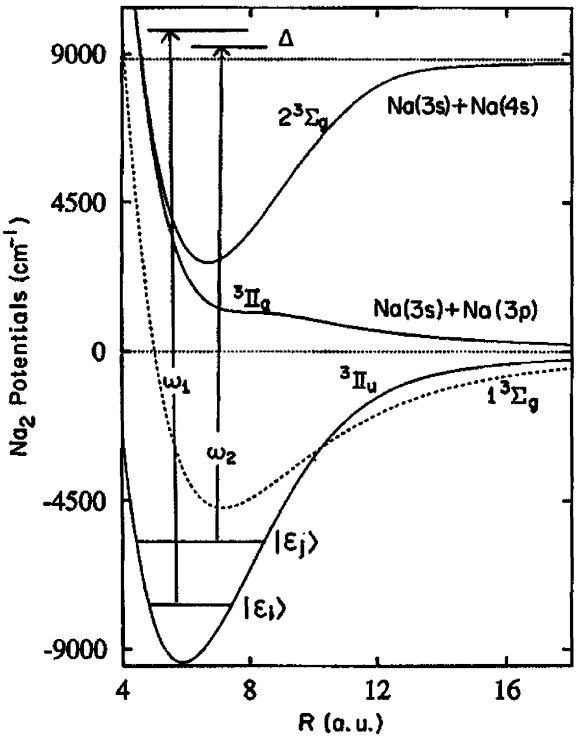

Fig. 44. Sample scenario for the incoherent interference control of the photodissociation of Na_2. Taken from Fig. 1 Ref. [223].

order of 30% [219,220]. That is, the main experimental limitation, thus far, is due to experimental issues other than the partial laser coherence [221].

8.3. Countering cw laser jitter

For cw lasers, laser decoherence appears via the jitter and drift of the laser phase ϕ in the field $\mathbf{E}(z,t)$ with a concomitant reduction in control [See Section 8.2]. However, suitable design of the control scenario can result in a method which is immune to the effects of laser jitter. In particular, we rely upon the way in which the laser phase enters into control scenarios.

The role of the laser phase in controlling molecular dynamics was clear in the examples shown in Section 2. For example, in the one vs. three photon scenario the relative laser phase $(\phi_3 - 3\phi_1)$ enters directly into the interference term, as does the relative phase $\phi_1 - \phi_2$ in the bichromatic control scenario. These results embody two useful general rules about the contribution of the laser phase to coherent control scenarios. The first is that the interference term contains the *difference* between the laser phase imparted to the molecule by one route, and that imparted to the molecule by an alternate route. Second, the phase imparted to the state $|E_m\rangle$ by a light field of the form

$$\hat{\epsilon}\int_{-\infty}^{\infty} \mathrm{d}\omega|\epsilon(\omega)|\exp[\mathrm{i}\phi(\omega)]\exp(-\mathrm{i}\omega\tau) \tag{226}$$

in an excitation from level $|E_1\rangle$ to $|E_m\rangle$ is $\pm\phi(|\omega_{m,1}|)$. The plus sign applies to light absorption $(E_m > E_1)$ and the minus sign to stimulated emission $(E_1 > E_m)$. This observation proves very useful in designing schemes which are insensitive to laser phase.

8.4. Incoherent interference control

Incoherent lasers can still prove useful for interference-based control if the scenario is designed appropriately. Fig. 44 shows a level scheme where a cw field with frequency ω_1 excites the level $|E_i\rangle$ to the photodissociative

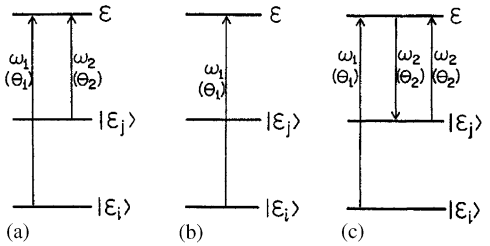

Fig. 45. Interfering pathways from $|E_i\rangle$ to the continuum associated with the scenario in the previous figure.The frequency and phase of the lasers are ω_i and ϕ_i. Taken from Fig. 5 [224].

continuum. Simultaneously, a stronger cw laser field of frequency ω_2 couples the continuum to the initially empty state $|E_j\rangle$. The phases associated with these two fields are ϕ_1 and ϕ_2, respectively. The effect of the strong field is to cause Rabi cycling of population between $|E_j\rangle$ and the continuum. Thus, in this arrangement, population can be transferred from $|E_i\rangle$ to the continuum by a variety of routes, as shown in Fig. 45.

The first panel shows the simplest path to the continuum, consisting of one photon absorption of ω_1. The subsequent panels show the three photon process to the continuum (absorption of ω_1 followed by stimulated emission and reabsorption of ω_2, etc.), and a five photon process (absorption of ω_1 followed by stimulated emission and reabsorption of ω_2, twice). This series goes on ad-infinitum, resulting in an infinite number of interfering pathways.

In accord with Section 8.3 the phase imparted to the continuum state by the first route in Fig. 45 is ϕ_1, and by the second is $\phi_1 - \phi_2 + \phi_2$. The $-\phi_2$ contribution to the latter phase is due to the stimulated emission step, and the following $+\phi_2$ is due to the absorption. Hence both routes impart the overall phase ϕ_1 to the continuum state. It is clear that this is also the case for all additional routes to the continuum, since they must contain an equal number of stimulated emission and absorption steps.

Examination of all previous described scenarios makes clear, however, that it is the *relative* phase imparted to the routes which affects control. In the case described here, the relative phase of the routes is $\phi_1 - \phi_1 = 0$, so that control is independent of the laser phase. As a consequence, even lasers with extreme laser jitter and drift can be used in this scenario. Note, however, that in this scenario, control is achieved by varying the frequencies ω_1 and ω_2. Examples of computations based upon this "incoherent interference control" are given in Refs. [223,224].

9. Decoherence free subspaces: an *S*-matrix approach

In addition to Coherent Control, decoherence is detrimental to other processes that rely on coherence, such as Quantum Computations [225,226]. An approach alternative to those described above, originating in the field of Quantum Information, for minimizing decoherence, is the construction of subspaces that are immune (or are relatively insensitive) to decoherence. Such subspaces are called "decoherence free subspaces" (DFS) [227,228].

Here we describe the use of CC techniques to the construction of DFS. Our construction is based solely on knowledge of the *S*-matrices associated with all the processes contributing to decoherence. Contrary to previous approaches [228], no knowledge of the system-bath Hamiltonian, which is rarely ever known, is needed here.

This construct of a DFS uses additional states to those in a subspace of interest, termed "chaperon" states. Although the coefficients of the chaperon states, which by themselves are susceptible to decoherence, must be reset from time to time, no such resetting needs to be done to the smaller subspace of interest, which, due to interferences with the chaperon states, becomes immune to decoherence. The effectiveness of chaperon states is due to a property known to exist in the context of reactive tunneling [229], namely that if the number of final states that are energetically accessible to a given scattering process is less than the number of initial states in the space of interest, then one can construct subspaces in which the given scattering process is suppressed.

We focus on the *system* states $|A\rangle$ in a Hilbert subspace $\{\alpha\}$ that undergo transitions to states $|B\rangle$ in the Hilbert subspace $\{\beta\}$ due to the action of an external perturbation, such as that exerted by a bath. The subspaces $\{\alpha\}$ and $\{\beta\}$ may be equal, or may differ from one another. We show that by utilizing states in another subspace, which undergo

transitions to $\{\beta\}$ and possibly other states, we can modify $\{\alpha\}$ to be decoherence-free. This, as shown below, is due to quantum interference effects.

We assume that in the absence of the interaction with the bath the system dynamics is described by the system Hamiltonian H_s, whose eigenstates are denoted by $|i\rangle$. Here we focus on *energetically degenerate* subspaces of H_s, i.e., states of the same system energy E_s. For example, we might consider a situation in which the system is comprised of a set of $j = 1, \ldots, N$ $s_j = \pm 1/2$ spinors, kept sufficiently far apart from one another, such that their spin-spin interaction is negligible. In this case we will write states $|i\rangle$ as either

$$|i\rangle = \Pi_{j=1}^{N} |s_j^{(i)}\rangle \tag{227}$$

or as an entangled linear combinations of such states.

Standard scattering theory [230], gives the probability P_{fi} of making a transition to a final state $|f\rangle$ having started in the initial state $|i\rangle$ due to a collision with a bath atom of energy E_b (i.e., at total energy $E = E_s + E_b$), as

$$P_{fi}(E) = |T_{fi}(E)|^2, \tag{228}$$

where $T_{fi}(E) \equiv \langle f|T(E)|i\rangle$. Here $T(E)$ is the transition operator defined as $T(E) \equiv S(E) - I$, where $S(E)$ is the Scattering operator and I is the unit operator. The total probability $P_{\beta\leftarrow i}(E)$ of executing a transition into the entire subspace $\{\beta\}$ that is comprised of M_β energetically degenerate final states, is given by

$$P_{\beta\leftarrow i} = \sum_{f=1}^{M_\beta} |T_{fi}|^2, \tag{229}$$

where, for brevity, we have suppressed the energy index E.

In most situations the decoherence process cannot be described by a single transition operator. Rather, one finds L distinct processes that operate in a completely independent way from one another. For example, we may have collisions at various bath energies E_b, or contributions from many orbital angular momenta. (We do not consider as being distinct, processes that operate simultaneously or in a concerted way. Such processes can be combined within a single T operator.) Scattering theory [230] tells us that for a set of distinct processes, the integral cross-section is given as a simple sum of the cross-sections associated with each independent process. We can therefore generalize Eq. (229) in a straightforward way to read

$$P_{\beta\leftarrow i} = \sum_{\ell=1}^{L} \sum_{f=1}^{M_\beta} |T_{fi}^{(\ell)}|^2, \tag{230}$$

where $T^{(\ell)}$ is the T operator associated with process ℓ.

Consider now a further generalization in which the initial state is not a single eigenstate, but $|\mathbf{c}\rangle$, an entangled superposition of many eigenstates of the same energy E_s

$$|\mathbf{c}\rangle = \sum_{i=1}^{K} c_i |i\rangle = \sum_{i=1}^{K} c_i \Pi_{j=1}^{N} |s_j^{(i)}\rangle. \tag{231}$$

Because all these states have the same energy the probability of forming $|f\rangle$ from this initial state is

$$P_{f\leftarrow \mathrm{c}} = \sum_{\ell=1}^{L} \left| \sum_{i=1}^{K} c_i T_{fi}^{(\ell)} \right|^2, \tag{232}$$

and the total transition probability into subspace $\{\beta\}$, $P_{\beta\leftarrow \mathbf{c}}$, is

$$P_{\beta\leftarrow \mathbf{c}} = \sum_{\ell=1}^{L} \sum_{f=1}^{M_\beta} \left| \sum_{i=1}^{K} c_i T_{fi}^{(\ell)} \right|^2. \tag{233}$$

Note, in Eq. (233), the distinctly different character of the two sums: i.e. the incoherent sum over probabilities to final states and over different processes, and the coherent sum over amplitudes from initial states. The latter sum will, as shown below, allow control over the relaxation process.

Introducing the matrix $\boldsymbol{\sigma} = \sum_\ell \mathbf{T}_\beta^{\dagger(\ell)} \cdot \mathbf{T}_\beta^{(\ell)}$ with elements $\sigma_{ij} = \sum_{\ell=1}^{L} \sum_{f=1}^{M_\beta} T_{fj}^{*(\ell)} T_{fi}^{(\ell)}$ allows us to rewrite Eq. (233) as

$$P_{\beta \leftarrow \mathbf{c}} = \mathbf{c}^\dagger \cdot \boldsymbol{\sigma} \cdot \mathbf{c}, \tag{234}$$

where the dagger denotes the Hermitian conjugate. The β subscript on the $\mathbf{T}^{(\ell)}$ symbol indicates that we are dealing with the sub-matrix of the $\mathbf{T}^{(\ell)}$ containing the transition amplitudes into the $\{\beta\}$ final subspace only.

We now wish to choose optimal sets of $\mathbf{c}$ vectors that minimize the transitions into subspace $\{\beta\}$, consistent with the normalization constraint $\sum_{i=1}^{K} |c_i|^2 = 1$. We obtain the optimal solutions by requiring

$$\frac{\partial}{\partial c_k^*} \left[P_{\beta \leftarrow \mathbf{c}} - \lambda \sum_{i=1}^{K} |c_i|^2 \right] = \frac{\partial}{\partial c_k^*} [\mathbf{c}^\dagger \cdot \boldsymbol{\sigma} \cdot \mathbf{c} - \lambda \mathbf{c}^\dagger \mathbf{c}] = 0, \tag{235}$$

where λ is a Lagrange multiplier. Explicitly taking the derivative gives the result that the optimized coefficients satisfy the eigenvalue equation

$$\boldsymbol{\sigma} \cdot \mathbf{c}^{(\lambda)} = \lambda \mathbf{c}^{(\lambda)}. \tag{236}$$

Note that Eq. (236) also results from taking derivatives in Eq. (235) with respect to c_k, since $\boldsymbol{\sigma}$ is Hermitian.

If there is a zero eigenvalue, i.e., if $\lambda = 0$ is an eigenvalue of Eq. (236), with an eigenvector $\mathbf{c}^{(0)}$ satisfying

$$\boldsymbol{\sigma} \cdot \mathbf{c}^{(0)} = 0 \tag{237}$$

then [by inserting Eq. (237) into Eq. (234)] we have that $P_{\beta \leftarrow \mathbf{c}^{(0)}} = 0$. Therefore, the superposition state with the $\mathbf{c}^{(0)}$ coefficients is completely immune to all scattering processes into subspace $\{\beta\}$, i.e., $|\mathbf{c}^{(0)}\rangle$ is a "decoherence free" state with respect to subspace $\{\beta\}$.

Clearly, $\lambda = 0$ is obtained if

$$\det(\boldsymbol{\sigma}) = \det \sum_\ell (\mathbf{T}_\beta^{(\ell)\dagger} \cdot \mathbf{T}_\beta^{(\ell)}) = \det(\mathsf{T}_\beta^\dagger \cdot \mathsf{T}_\beta) = 0, \tag{238}$$

where T is a super T-matrix, including the ℓ different processes as a subscript,

$$\mathsf{T}_{\ell, f; i} \equiv \mathbf{T}_{f,i}^{(\ell)}. \tag{239}$$

Eq. (238) holds if the number of initial states K comprising the initial superposition [Eq. (231)] is greater than LM_β. To see this result note that, under these circumstances, $\boldsymbol{\sigma}$ is a matrix of order $K \times K$ and the T_β matrix is of order $K \times LM_\beta$. If $K > LM_\beta$ then we can construct a $K \times K$ order matrix $\mathbf{A}_\beta$ by adding a sub-matrix of $(K - LM_\beta)$ rows of zeroes to the lower part of each T_β. Then

$$\det(\boldsymbol{\sigma}) = \det(\mathsf{T}_\beta^\dagger \cdot \mathsf{T}_\beta) = \det(\mathbf{A}_\beta^\dagger \cdot \mathbf{A}_\beta) = \det(\mathbf{A}_\beta^\dagger) \det(\mathbf{A}_\beta) = 0. \tag{240}$$

The last equality holds because the determinants of $\mathbf{A}_\beta$ and $\mathbf{A}_\beta^\dagger$ are zero.

The number of decoherence free states with respect to subspace $\{\beta\}$, i.e. the degeneracy of the $\lambda = 0$ eigenvalue of Eq. (237), is $K - \mathrm{rank}(\boldsymbol{\sigma}) = K - \mathrm{rank}(\mathsf{T}_\beta)$. Given the dimensionality of T_β, and that $K > LM_\beta$, the degeneracy is at least, and typically, $K - LM_\beta$. This result leads immediately to the development of a strategy of constructing a DFS of dimension M_α. That is, we first identify the subspace $\{\beta\}$ of dimension M_β that is coupled to the subspace $\{\alpha\}$ by the L scattering processes considered above. We now use a larger space, of dimension $K = LM_\beta + M_\alpha$, to construct the superposition states $|\mathbf{c}^{(0)}\rangle$ all having, according to Eq. (236), zero eigenvalues and hence zero transition probabilities to subspace $\{\beta\}$. We call the extra LM_β states "chaperon" states.

In order to create the desired DFS we choose the M_α degenerate $\mathbf{c}^{(0)}$ eigenvectors satisfying Eq. (237) to be of the form,

$$\mathbf{c}^{(0,1)^{\mathbf{T}}} = (1, 0, \ldots, 0, c^{(0,1)}_{M_\alpha+1}, c^{(0,1)}_{M_\alpha+2}, \ldots, c^{(0,1)}_{K})$$

$$\mathbf{c}^{(0,2)^{\mathbf{T}}} = (0, 1, \ldots, 0, c^{(0,2)}_{M_\alpha+1}, c^{(0,2)}_{M_\alpha+2}, \ldots, c^{(0,2)}_{K})$$

$$\vdots$$

$$\mathbf{c}^{(0,M_\alpha)^{\mathbf{T}}} = (0, \ldots, 0, 1, c^{(0,M_\alpha)}_{M_\alpha+1}, c^{(0,M_\alpha)}_{M_\alpha+2}, \ldots, c^{(0,M_\alpha)}_{K}), \tag{241}$$

written for typographical convenience in terms of the matrix transpose $^{\mathbf{T}}$.

The $c^{(0,i)}_{M_\alpha+1}, \ldots, c^{(0,i)}_{K}$, $i = 1, \ldots, M_\alpha$ coefficient matrix is determined by substituting Eq. (241) into Eq. (237) and solving it. The resulting set of vectors $\mathbf{c}^{(0,i)}$, $i = 1, \ldots, M_\alpha$ spans a DFS of dimension M_α that is immune to the L bath-induced $\{\alpha\} \to \{\beta\}$ transitions. Note that the structure of Eq. (241) arises from the fact that each vector has LM_β free coefficients plus the number one in one of the entries. This is exactly the number of coefficients (normalization is of no consequence) needed to satisfy Eq. (237). Each of the M_α null eigenvectors thus generated is different from the other, because the one is placed in a different position.

The nature of the elements in the $\mathbf{c}^{(0,i)}$ is of interest. Note that the first M_α coefficients in each of these vectors (which span the original $\{\alpha\}$ subspace) can not change under relaxation processes. This is because they correspond to states which could only go to the subspace $\{\beta\}$ under the decoherence processes, and transitions to $\{\beta\}$ have been eliminated by the above construction. By contrast, the chaperon states can make transitions to states other than those in $\{\beta\}$ and can therefore change under decoherence. If we fail to maintain the original values of the chaperon coefficients, the initial $\{\alpha\}$ subspace will no longer be "protected" and will cease to be immune to relaxation. However, because these coefficients are known to us, we can reset the values of the chaperon coefficients from time to time, as needed, thereby guaranteeing that the DFS constructed remains a DFS for as long as we wish.

In a similar way we can reset the values of the chaperon coefficients for any superposition state in $\{\alpha\}$. Storing classically the $\mathbf{d}$ matrix of chaperon coefficients, $d_{i,j} \equiv c^{(0,i)}_{M_\alpha+j}$, $i = 1, \ldots, M_\alpha$, $j = 1, \ldots, LM_\beta$, we can write a general vector in $\{\alpha\}$, of the form $\mathbf{a} = \sum_{i=1}^{M_\alpha} a_i \mathbf{c}^{(0,i)}$, as

$$\mathbf{a}^{\mathbf{T}} = \left(a_1, a_2, \ldots, a_{M_\alpha}, \sum_i a_i d_{i,1}, \sum_i a_i d_{i,2}, \ldots \sum_i a_i d_{i,LM_\beta} \right). \tag{242}$$

In order to maintain the protective effect of the chaperon states, thereby guaranteeing that we retain a true DFS, all we need is to reset from time to time the values of the chaperon coefficients to be the vector product of the first M_α qbits, whose values need not be determined, times the (classically stored) $\mathbf{d}$ matrix. Because the first M_α coefficients are expected to be very stable, as they can begin to change only after the chaperon coefficients change, this resetting can be done at a rate which is expected to be much smaller than the relaxation rates themselves. Thus, for example, to do quantum computing in the DFS we would perform operations on vectors in the entire space, but use for computing only the first M_α elements of the vectors. Like other error corrections methods, one need never measure anything about the first M_α coefficients with which computations or information storage are done. Rather, whatever operation was performed on the M_α dimensional dfs subspace can be performed on a vector prepared with the pre-stored chaperon coefficients of the $d_{i,j}$ matrix to reset the coefficients, without measuring the a_i values.

In order for the procedure to work in practice we need to know the $\boldsymbol{\sigma}$ relaxation matrix, or more specifically, the $T^{*(\ell)}_{fj} T^{(\ell)}_{fi}$ products. Traditional scattering experiments yield directly only the absolute values $|T^{(\ell)}_{fi}|$. As a consequence, the phases of $T^{*(\ell)}_{fj} T^{(\ell)}_{fi}$ must be extracted using one of a number of methods. For example, one can obtain the complex transition amplitudes from differential cross sections using "inverse-scattering" methods and generalized unitarity relations [231,232], or by using coherently controlled scattering [233] which is sensitive to the phases of T matrix elements. Alternatively, one may perform a "forward" fitting procedure, in which one optimizes a set of parameter-dependent phases to fit all the experimentally available differential cross-sections data. Although this is not a trivial task, it is one that is achievable.

10. Summary

Coherent control of bound and continuum processes has seen rapid development over the past two decades, both theoretically and computationally. This review has focused on some of the most recent theoretical developments, many of which followed earlier work summarized in two monographs [1,2]. Considerations of developments thus far indicate that quantum based control of such processes is often robust and effective. We can anticipate future efforts directed towards the study of more complex systems, towards control in condensed phases and towards applications in areas such as quantum computing and molecular electronics.

Acknowledgments

Years of scientific collaboration and many helpful discussions with Pete Christopher, Einat Frishman, Jiangbin Gong, Petr Král, and Ioannis Thanopoulos are hereby gratefully acknowledged.

References

[1] For a recent review of optimal control methodologies, see, S.A. Rice, M. Zhao, Optical Control of Molecular Dynamics, Wiley, New York, 2000.
[2] M. Shapiro, P. Brumer, Principles of the Quantum Control of Molecular Processes, Wiley, New York, 2003.
[3] R.J. Gordon, S.A. Rice, Ann. Rev. Phys. Chem. 48 (1997) 595.
[4] D. Tannor, S.A. Rice, J. Chem. Phys. 83 (1985) 5013.
[5] D.J. Tannor, R. Kosloff, S.A. Rice, J. Chem. Phys. 85 (1986) 5805.
[6] S. Shi, A. Woody, H. Rabitz, J. Chem. Phys. 88 (1988) 6870;
A.P. Peirce, M.A. Dahleh, H. Rabitz, Phys. Rev. A 37 (1988) 4950.
[7] D.J. Tannor, S.A. Rice, Adv. Chem. Phys. 70 (1988) 441.
[8] S. Shi, H. Rabitz, Chem. Phys. 139 (1989) 185.
[9] R. Kosloff, S.A. Rice, P. Gaspard, S. Tersigni, D.J. Tannor, Chem. Phys. 139 (1989) 201.
[10] A.P. Peirce, M.A. Dahleh, H. Rabitz, Phys. Rev. A 42 (1990) 1065.
[11] W. Jakubetz, J. Manz, H.-J. Schreier, Chem. Phys. Lett. 165 (1990) 100.
[12] J.E. Combariza, B. Just, J. Manz, G. Paramonov, J. Phys. Chem. 95 (1991) 10 351.
[13] S. Shi, H. Rabitz, Comput. Phys. Commun. 63 (1991) 71.
[14] B. Amstrup, R.J. Carlson, A. Matro, S.A. Rice, J. Phys. Chem. 95 (1991) 8019.
[15] W. Jakubetz, E. Kades, J. Manz, H.J. Schreier, J. Phys. Chem. 97 (1993) 12609.
[16] M. Demiralp, H. Rabitz, Phys. Rev. A 47 (1993) 809.
[17] W.S. Warren, H. Rabitz, M. Dahleh, Science 259 (1993) 1581.
[18] Y. Yan, R.E. Gillilan, R.M. Whitnell, K.R. Wilson, J. Phys. Chem. 97 (1993) 2320;
J.L. Krause, R.M. Whitnell, K.R. Wilson, Y. Yan, S. Mukamel, J. Chem. Phys. 99 (1993) 6562.
[19] B. Amstrup, S.A. Rice, Chem. Phys. Lett. 225 (1994) 1.
[20] Y.B. Band, O. Magnes, J. Chem. Phys. 101 (1994) 7528.
[21] B. Kohler, J.L. Krause, F. Raski, K.R. Wilson, V.V. Yakovlev, R.M. Whitnell, Y. Yan, Acct. Chem. Res. 28 (1995) 133;
J.W. Che, J.L. Krause, M. Messina, K.R. Wilson, Y.J. Yan, J. Phys. Chem. 99 (1995) 14949.
[22] M. Kaluza, J.T. Muckerman, J. Chem. Phys. 102 (1995) 3897;
M. Kaluza, J.T. Muckerman, Phys. Rev. A 51 (1995) 1694.
[23] M.V. Korolkov, J. Manz, G.K. Paramonov, Chem. Phys. 217 (1997) 341.
[24] M. Demiralp, H. Rabitz, Phys. Rev. A 57 (1998) 2420.
[25] R.X. Xu, J.X. Cheng, Y.J. Yan, J. Phys. Chem. A 103 (1999) 10611.
[26] M. Oppel, G.K. Paramonov, Appl. Phys. B 71 (2000) 319.
[27] M. Shapiro, P. Brumer, J. Phys. Chem. A 105 (2001) 2897.
[28] P. Brumer, M. Shapiro, Chem. Phys. Lett. 126 (1986) 541.
[29] M. Shapiro, P. Brumer, Faraday Disc. Chem. Soc. 82 (1987) 177.
[30] J. Gong, P. Brumer, Phys. Rev. Lett. 88 (2002) 203001.
[31] B. McQuarrie, D.G. Abrashkevich, P. Brumer, J. Chem. Phys. 119 (2003) 3606.
[32] I. Levy, M. Shapiro, P. Brumer, J. Chem. Phys. 93 (1990) 2493.
[33] C.K. Chan, P. Brumer, M. Shapiro, J. Chem. Phys. 94 (1991) 2688.
[34] S. Chelkowski, A.D. Bandrauk, Chem. Phys. Lett. 186 (1991) 284.
[35] A.D. Bandrauk, J.-M. Gauthier, J.F. McCann, Chem. Phys. Lett. 200 (1992) 399.
[36] P. Brumer, M. Shapiro, Ann. Rev. Phys. Chem. 43 (1992) 257.
[37] M. Shapiro, P. Brumer, Chem. Phys. Lett. 208 (1993) 193.
[38] N.E. Henriksen, B. Amstrup, Chem. Phys. Lett. 213 (1993) 65.

[39] M.Yu. Ivanov, P.B. Corkum, P. Dietrich, Laser Phys. 3 (1993) 375.
[40] H.G. Muller, P.H. Bucksbaum, D.W. Schumacher, A. Zavriyev, J. Phys. B 23 (1990) 2761.
[41] R.M. Potvliege, P.H.G. Smith, J. Phys. B 25 (1992) 2501.
[42] K.J. Schafer, K.C. Kulander, Phys. Rev. A 45 (1992) 8026.
[43] E. Charron, A. Guisti-Suzor, F.H. Mies, Phys. Rev. Lett. 71 (1993) 692.
[44] D. Holmes, M. Shapiro, P. Brumer, J. Chem. Phys. 105 (1996) 9162.
[45] M. Shapiro, P. Brumer, Trans. Farad. Soc. 93 (1997) 1263.
[46] M.J.J. Vrakking, S. Stolte, Chem. Phys. Lett. 271 (1997) 209.
[47] A. Abrashkevich, M. Shapiro, P. Brumer, Phys. Rev. Lett. 81 (1998) 3789.
[48] P. Brumer, A. Abrashkevich, M. Shapiro, Faraday Disc. Chem. Soc. 113 (1999) 291.
[49] R.J. Gordon, L.C. Zhu, T. Seideman, Acc. Chem. Res. 32 (1999) 1007.
[50] R. van Leeuwen, M.L. Bajema, R.R. Jones, Phys. Rev. Lett. 82 (1999) 2852.
[51] E. Luc-Koenig, M. Aymar, M. Millet, J.M. Lecomte, A. Lyras, Eur. Phys. D 10 (2000) 205.
[52] M. Shapiro, P. Brumer, Coherent control of atomic molecular, and electronic processes, Adv. Atom. Mol. Opt. Phys. 42 (2000) 287.
[53] J.B. Gong, P. Brumer, Phys. Rev. Lett. 86 (2001) 1741.
[54] J. Gong, P. Brumer, Ann. Rev. Phys. Chem. 56 (2005) 1.
[55] D. Gammon, N.H. Bonadeo, G. Chen, J. Erland, D.G. Steel, Physica E 9 (2001) 99.
[56] Q.H. Park, R.W. Boyd, Phys. Rev. Lett. 86 (2001) 2774.
[57] V.S. Batista, P. Brumer, J. Phys. Chem. A 105 (2001) 2591.
[58] M. Shapiro, J. Chem. Phys. 101 (1994) 3844.
[59] J.M. Papanikolas, R.M. Williams, P.D. Kleiber, J.L. Hart, C. Brink, S.D. Price, S.R. Leone, J. Chem. Phys. 103 (1995) 7269.
[60] R.G. Unanyan, M. Fleischhauer, K. Bergmann, B.W. Shore, Opt. Commun. 155 (1998) 144.
[61] R. Uberna, Z. Amitay, C.X.W. Qian, S.R. Leone, J. Chem. Phys. 114 (2001) 10311.
[62] E. Frishman, M. Shapiro, Phys. Rev. A 54 (1996) 3310.
[63] M. Shapiro, P. Brumer, J. Chem. Phys. 103 (1995) 487.
[64] F.E. Hohn, Elementary Matrix Algebra, MacMillan, New York, 1964.
[65] In the case of $M_2 < M_0$ dynamics directed solely into $\mathsf{A}_0 \oplus \mathsf{A}_1$ *may* is possible if the set of solutions c_{n_i} obtained is normalizable, i.e. $\sum_{n_i=1}^{M_0} |c_{n_i}|^2 = 1$. Otherwise the solutions which exist are nonphysical.
[66] G. Kurizki, M. Shapiro, P. Brumer, Phys. Rev. B 39 (1989) 3435.
[67] J. Gong, P. Brumer, Phys. Rev. E 70 (2004) 016202.
[68] E. Dupont, P.B. Corkum, H.C. Liu, M. Buchanan, Z.R. Wasilewski, Phys. Rev. Lett. 74 (1995) 3596.
[69] F.F. Crim, Annu. Rev. Phys. Chem. 35 (1984) 657.
[70] B.J. Orr, J.G. Haub, R. Haines, Chem. Phys. Lett. 107 (1984) 168.
[71] W. Meier, G. Ahlers, H. Zacharias, J. Chem. Phys. 85 (1986) 2599.
[72] C. Kittrel, E. Abramson, J.L. Kinsey, S.A. McDonald, D.E. Reisner, R.W. Field, D.H. Katayama, J. Chem. Phys. 7975 (1981) 2056.
[73] D.G. Grischkowski, M.M.T. Loy, P.F. Liao, Phys. Rev. A 12 (1975) 2514.
[74] J. Oreg, F.T. Hioe, J.H. Eberly, Phys. Rev. A 29 (1984) 690.
[75] U. Gaubatz, P. Rudecki, M. Becker, S. Schiemann, M. Külz, K. Bergmann, Chem. Phys. Lett. 149 (1988) 463.
[76] U. Gaubatz, P. Rudecki, S. Schiemann, K. Bergmann, J. Chem. Phys. 92 (1990) 5363.
[77] G.W. Coulston, K. Bergmann, J. Chem. Phys. 96 (1992) 3467.
[78] A. Kuhn, G.W. Coulson, G.Z. He, S. Schiemann, K. Bergmann, W.S. Warren, J. Chem. Phys. 96 (1992) 4215.
[79] J.R. Kuklinski, U. Gaubatz, F.T. Hioe, K. Bergmann, Phys. Rev. A 40 (1989) 6741.
[80] B.W. Shore, Contemp. Phys. 36 (1995) 15.
[81] N.V. Vitanov, M. Fleischauer, B.W. Shore, K. Bergmann, Adv. Atom. Mol. Opt. Phys. 46 (2001) 55.
[82] K. Bergmann, H. Theuer, B.W. Shore, Rev. Mod. Phys. 70 (1998) 1003.
[83] N.V. Vitanov, S. Stenholm, Opt. Commun. 135 (1997) 394.
[84] Y.B. Band, P.S. Julienne, J. Chem. Phys. 94 (1991) 5291.
[85] Y.B. Band, P.S. Julienne, J. Chem. Phys. 96 (1992) 3339.
[86] B. Glushko, B. Kryzhanovsky, Phys. Rev. A 46 (1992) 2823.
[87] M. Fleischhauer, A.S. Manka, Phys. Rev. A 54 (1996) 794.
[88] N.V. Vitanov, S. Stenholm, Phys. Rev. A 56 (1997) 1463.
[89] N.V. Vitanov, S. Stenholm, Phys. Rev. A 60 (1999) 3820.
[90] S. Guérin, H.R. Jauslin, Eur. Phys. J. D 2 (1998) 99.
[91] L.P. Yatsenko, S. Guerin, T. Halfmann, K. Boehmer, B.W. Shore, K. Bergmann, Phys. Rev. A 58 (1998) 4683.
[92] H. Theuer, K. Bergmann, Eur. Phys. J. D 2 (1998) 279.
[93] A. Kuhn, S. Steuerwald, K. Bergmann, Eur. Phys. J. D 1 (1998) 67.
[94] T. Halfmann, K. Bergmann, J. Chem. Phys. 104 (1996) 7068.
[95] W. Süptitz, B.C. Duncan, P.L. Gould, J. Opt. Soc. Am. B 14 (1997) 1001.
[96] J. Martina, B.W. Shore, K. Bergmann, Phys. Rev. A 54 (1996) 1556.
[97] B.W. Shore, K. Bergmann, J. Oreg, S. Rosenwaks, Phys. Rev. A 44 (1991) 7442.
[98] P. Marte, P. Zoller, J.L. Hall, Phys. Rev. A 44 (1991) 4118.
[99] V.S. Malinovsky, D.J. Tannor, Phys. Rev. A 56 (1997) 4929.

[100] C.K. Law, J.H. Eberly, Opt. Express 2 (1998) 368.
[101] T. Nakajima, Phys. Rev. A 59 (1999) 559.
[102] T. Esslinger, F. Sander, M. Weidemüller, A. Hammerich, T.W. Hänsch, Phys. Rev. Lett. 76 (1996) 2432.
[103] S. Kulin, B. Saubamea, E. Peik, J. Lawall, M. Leduc, C. Cohen-Tannoudji, Phys. Rev. Lett. 78 (1997) 4185.
[104] M.N. Kobrak, S.A. Rice, Phys. Rev. A 57 (1998) 1158.
[105] M.N. Kobrak, S.A. Rice, J. Chem. Phys. 109 (1998) 1.
[106] M.N. Kobrak, S.A. Rice, Phys. Rev. A 57 (1998) 2885.
[107] R.G. Unanyan, N.V. Vitanov, S. Stenholm, Phys. Rev. A 57 (1998) 462.
[108] H. Theuer, R.G. Unanyan, C. Habschied, K. Klein, K. Bergmann, Opt. Express 4 (1999) 77.
[109] E. Paspalakis, M. Protopapas, P.L. Knight, Opt. Commun. 142 (1997) 34.
[110] N.V. Vitanov, S. Stenholm, Phys. Rev. A 56 (1997) 741.
[111] C.E. Carroll, F.T. Hioe, Phys. Lett. A 199 (1995) 145.
[112] L.P. Yatsenko, R.G. Unanyan, T. Halfmann, B.W. Shore, Opt. Commun. 135 (1997) 406.
[113] C.E. Carroll, F.T. Hioe, Phys. Rev. A 54 (1996) 5147.
[114] R. Unanyan, N.V. Vitanov, B.W. Shore, K. Bergmann, Phys. Rev. A 61 (2000) 043408.
[115] P.L. Knight, M.A. Lauder, B.J. Dalton, Phys. Rep. 190 (1990) 1 and references therein.
[116] A. Shnitman, I. Sofer, I. Golub, A. Yogev, M. Shapiro, Z. Chen, P. Brumer, Phys. Rev. Lett. 76 (1996) 2886.
[117] T. Halfmann, L.P. Yatsenko, M. Shapiro, B.W. Shore, K. Bergmann, Phys. Rev. A 58 (1998) R46.
[118] L.P. Yatsenko, T. Halfmann, B.W. Shore, K. Bergmann, Phys. Rev. A 59 (1999) 2926.
[119] N.J. Kylstra, E. Paspalakis, P.L. Knight, J. Phys. B 31 (1998) L719.
[120] S. Guérin, L.P. Yatsenko, T. Halfmann, B.W. Shore, K. Bergmann, Phys. Rev. A 58 (1998) 4691.
[121] L.P. Yatsenko, B.W. Shore, T. Halfmann, K. Bergmann, A. Vardi, Phys. Rev. A 60 (1999) R4237.
[122] T. Rickes, L.P. Yatsenko, S. Steurwald, T. Halfmann, B.W. Shore, N.V. Vitanov, K. Bergmann, J. Chem. Phys. 113 (2001) 534.
[123] B.M. Garraway, K.-A. Suominen, Phys. Rev. Lett. 80 (1998) 932.
[124] S. Kallush, Y.B. Band, Phys. Rev. A 61 (2000) 041401.
[125] I.R. Solá, J. Santamarría, V.S. Malinkovsky, Phys. Rev. A 61 (2000) 043413.
[126] M. Rodriguez, B.M. Garraway, K.-A. Suominen, Phys. Rev. A 62 (2000) 53413.
[127] A. Vardi, D. Abrashkevich, E. Frishman, M. Shapiro, J. Chem. Phys. 107 (1997) 6166.
[128] A. Vardi, M. Shapiro, K. Bergmann, Opt. Express 4 (1999) 91.
[129] J. Javanainen, M. Mackie, Phys. Rev. A 58 (1998) R789.
[130] M. Mackie, R. Kowalski, J. Javanainen, Phys. Rev. Lett. 84 (2000) 3803.
[131] A. Vardi, V.A. Yurovsky, J.R. Anglin, Phys. Rev. A 64 (2001) 063611.
[132] J.G.B. Beumee, H. Rabitz, J. Math. Phys. 31 (1990) 1253.
[133] E.E. Aubanel, A.D. Bandrauk, Can. J. Chem. 107 (1997) 1441.
[134] L.E.E. de Araujo, J. Phys. Chem. A 103 (1999) 10409.
[135] G.M. Huang, T.J. Tarn, J.W. Clark, J. Math. Phys. 24 (1983) 2608.
[136] R. Unanyan, M. Fleischhauer, B.W. Shore, K. Bergmann, Opt. Commun. 155 (1998) 144.
[137] P. Král, J. Fiurásek, M. Shapiro, Phys. Rev. A 64 (2001) 023414.
[138] P. Král, Z. Amitay, M. Shapiro, Phys. Rev. Lett. 89 (2002) 063002.
[139] P. Král, M. Shapiro, Phys. Rev. A 65 (2002) 043413.
[140] P. Král, J. Mod. Opt. 37 (1990) 889.
[141] P. Král, Phys. Rev. A 42 (1990) 4177.
[142] I. Thanopulos, P. Král, M. Shapiro, Phys. Rev. Lett. 92 (2004) 11003.
[143] P.R. Bunker, P. Jensen, Molecular Symmetry and Spectroscopy, NRC Research Press, Ottawa, 1998.
[144] A.I. Boldyrev, P. von R. Schleyer, J. Am. Chem. Soc. 113 (1991) 9045.
[145] R. Mayer, H.H. Günthard, J. Chem. Phys. 49 (1968) 1510.
[146] R. Mayer, H.H. Günthard, J. Chem. Phys. 50 (1970) 353.
[147] M.A. Hartchcock, J. Laane, J. Phys. Chem. 89 (1985) 4231.
[148] M.V. Berry, Proc. R. Soc. London Ser. A 392 (1984) 45.
[149] C.A. Mead, Rev. Mod. Phys. 64 (1992) 51.
[150] D.R. Yarkony, Rev. Mod. Phys. 68 (1996) 985.
[151] D.R. Yarkony, J. Phys. Chem. A 105 (2001) 6277.
[152] S. Chu, J.E. Bjorkholm, A. Ashkin, A. Cable, Phys. Rev. Lett. 57 (1986) 314.
[153] A. Aspect, C. Cohen-Tannoudji, J. Dalibard, A. Heidemann, C. Solomon, Phys. Rev. Lett. 57 (1986) 1688.
[154] J. Lawall, F. Bardou, K. Shimizu, M. Leduc, A. Aspect, C. Cohen-Tannoudji, Phys. Rev. Lett. 73 (1994) 1915.
[155] J.T. Bahns, W.C. Stwalley, P.L. Gould, J. Chem. Phys. 104 (1996) 9689.
[156] A. Bartana, R. Kosloff, D.J. Tannor, J. Chem. Phys. 99 (1993) 196.
[157] H.R. Thorsheim, J. Weiner, P.S. Julienne, Phys. Rev. Lett. 58 (1987) 2420.
[158] Y.B. Band, P.S. Julienne, Phys. Rev. A 51 (1995) R4317.
[159] A. Vardi, D. Abrashkevich, E. Frishman, M. Shapiro, J. Chem. Phys. 107 (1997) 6166.
[160] R. Coté, A. Dalgarno, Chem. Phys. Lett. 279 (1997) 50.
[161] P.S. Julienne, K. Burnett, Y.B. Band, W.C. Stwalley, Phys. Rev. A 58 (1998) R797.

[162] M. Mackie, J. Javanainen, Phys. Rev. A 60 (1999) 3174.
[163] A. Vardi, M. Shapiro, Phys. Rev. A 62 (2000) 025401.
[164] A. Vardi, M. Shapiro, Phys. Rev. A 58 (1998) 1352;
A. Vardi, M. Shapiro, Commun. At. Mol. Phys. 2 (2001) 233.
[165] A. Vardi, M. Shapiro, J.R. Anglin, Phys. Rev. A 65 (2002) 027401.
[166] A. Vardi, M. Shapiro, J. Chem. Phys. 104 (1996) 5490.
[167] U. Marvet, M. Dantus, Chem. Phys. Lett. 245 (1995) 393.
[168] P. Gross, M. Dantus, J. Chem. Phys. 106 (1997) 8013.
[169] A. Fioretti, D. Comparat, A. Crubellier, O. Dulieu, F. Masnou-Seeuws, P. Pillet, Phys. Rev. Lett. 80 (1998) 4402.
[170] A. Fioretti, D. Comparat, C. Drag, C. Amiot, O. Dulieu, F. Masnou-Seeuws, P. Pillet, Eur. Phys. D 5 (1998) 389.
[171] A.N. Nikolov, E.E. Eyler, X.T. Wang, J. Li, H. Wang, W.C. Stwalley, P.L. Gould, Phys. Rev. Lett. 82 (1999) 703.
[172] R. Wynar, R.S. Freeland, D.J. Han, C. Ryu, D.J. Heinzen, Science 287 (2000) 1016.
[173] R. Hulett, in: Cold Molecules 2002: Cold Molecules and Bose–Einstein Condensates, Les Houches, France, 2002.
[174] K. Winkler, G. Thalhammer, M. Theis, H. Ritsch, R. Grimm, J. Hecker Denschlag, Phys. Rev. Lett. 95 (2005) 063202.
[175] B. Misra, J. Math. Phys. 18 (1977) 756.
[176] G.J. Milburn, J. Opt. Soc. Am. B 5 (1988) 1317.
[177] W.M. Itano, D.J. Heinzen, J.J. Bollinger, D.J. Wineland, Phys. Rev. A 41 (1990) 2295.
[178] P. Knight, Nature 344 (1990) 493.
[179] V. Frerichs, A. Schenzle, Phys. Rev. A 44 (1991) 1962.
[180] A.G. Kofman, G. Kurizki, Phys. Rev. A 54 (1996) R3750.
[181] P. Facchi, S. Pascazio, Phys. Lett. A 241 (1998) 139.
[182] A.G. Kofman, G. Kurizki, Nature 405 (2000) 546.
[183] M.B. Plenio, P.L. Knight, R.C. Thompson, Opt. Commun. 123 (1996) 278.
[184] E. Frishman, M. Shapiro, Phys. Rev. Lett. 87 (2001) 253001.
[185] E. Frishman, M. Shapiro, Phys. Rev. A 68 (2003) 032717.
[186] S.H. Autler, C.H. Townes, Phys. Rev. 100 (1955) 703.
[187] K.C. Friedrichs, Comm. Pure Appl. Math. 1 (1948) 361.
[188] H. Feshbach, Ann. Phys. New York 19 (1962) 287;
H. Feshbach, Ann. Phys. New York 43 (1967) 410.
[189] U. Fano, Phys. Rev. 124 (1961) 1866.
[190] R.D. Levine, Quantum Mechanics of Molecular Rate Processes, Clarendon Press, Oxford, 1969.
[191] M. Shapiro, J. Chem. Phys. 56 (1972) 2582.
[192] C. Cohen-Tannoudji, B. Diu, F. Laloë, Quantum Mechanics, Wiley, New York, 1977.
[193] M. Scully, Zubairy, Quantum Optics, Cambridge University Press, Cambridge, 1997.
[194] R. Loudon, The Quantum Theory of Light (Eqs. 4.111, 4.113, 5.140 and pp. 174–179).
[195] S.E. Harris, Phys. Rev. Lett. 62 (1989) 1033.
[196] A. Alonso-Medina, J. Quant. Spect. Rad. Trans. 55 (2) (1996) 151.
[197] W.J. Stevens, M.M. Hessel, P.J. Bertonicini, A.C. Wahl, J. Chem. Phys. 66 (1977) 1477.
[198] The Na–Na potential curves and the relevant electronic dipole moments are from I. Schmidt, Ph.D. Thesis, Kaiserslautern University, 1987.
[199] P.S. Christopher, M. Shapiro, P. Brumer, J. Chem. Phys. 123 (2005) 064313.
[200] C. Woywod, W. Domcke, A.L. Sobolewski, H.J. Werner, J. Chem. Phys. 100 (1994) 1400.
[201] R. Borrelli, A. Peluso, J. Chem. Phys. 119 (2003) 437.
[202] M. Sukharev, T. Seideman, Phys. Rev. Lett. 93 (2004) 093004.
[203] V. Stert, P. Faramanara, W. Randloff, J. Chem. Phys. 112 (2000) 4460.
[204] P. Christopher, M. Shapiro, P. Brumer, to be published.
[205] J. Kupsch, in: D. Giulini, E. Joos, C. Kiefer, J. Kupsch, I.-O. Stamatescu, H.D. Zeh (Eds.), Decoherence and the Appearance of the Classical World, Springer-Verlag, New York, 1996.
[206] K. Blum, Density Matrix Theory and Applications, Plenum Press, New York, 1981.
[207] V. May, O. Kuhn, Charge and Energy Transfer Dynamics in Molecular Systems, Wiley-VCH, Berlin, 2000.
[208] J. Gong, P. Brumer, Phys. Rev. E 60 (1999) 1643.
[209] R. Omnes, The Interpretation of Quantum Mechanics, Princeton University Press, Princeton, 1994;
R. Omnes, Understanding Quantum Mechanics, Princeton University Press, Princeton, 1999.
[210] A.O. Caldeira, A.J. Leggett, Physica (Amsterdam) 121A (1983) 587;
W.G. Unruh, W.H. Zurek, Phys. Rev. D 40 (1989) 1071;
B.L. Hu, J.P. Paz, Y. Zhang, Phys. Rev. D 45 (1992) 2843;
B.L. Hu, J.P. Paz, Y. Zhang, Phys. Rev. D 47 (1993) 1576.
[211] Y. Elran, P. Brumer, J. Chem. Phys. 121 (2004) 2673.
[212] J. Gong, P. Brumer, Phys. Rev. Lett. 90 (2003) 050402;
J. Gong, P. Brumer, Phys. Rev. A 68 (2003) 022101;
H. Han, P. Brumer, Chem. Phys. Lett. 406 (2005) 237;
H. Han, P. Brumer, J. Chem. Phys. 122 (2005) 144316;
V. Batista, P. Brumer, Phys. Rev. Lett. 89 (2002) 143201.

[213] M. Shapiro, P. Brumer, J. Chem. Phys. 90 (1989) 6179.
[214] For the case of $\phi = 0$, and $T_1 = T_2 = \infty$, see L. Allen, C.R. Stroud Jr., Phys. Rep. 91 (1982) 1. Note, however, that there are serious misprints in Eq. (3.6) of this reference.
[215] J.D. Macomber, The Dynamics of Spectroscopic Transitions, Wiley, New York, 1976.
[216] X.-P. Jiang, P. Brumer, Chem. Phys. Lett. 180 (1991) 222.
[217] X.-P. Jiang, P. Brumer, Chem. Phys. Lett. 208 (1993) 179.
[218] J.C. Camparo, P. Lambropoulos, Phys. Rev. A 55 (1997) 552.
[219] N.E. Karapanagioti, D. Xenakis, D. Charalambidis, C. Fotakis, J. Phys. B 29 (1996) 3599.
[220] X. Wang, R. Bersohn, K. Takahashi, M. Kawasaki, H.L. Kim, J. Chem. Phys. 105 (1996) 2992.
[221] A.I. Pegarkov, Chem. Phys. Lett. 409 (2005) 8.
[222] X.-P. Jiang, M. Shapiro, P. Brumer, J. Chem. Phys. 104 (1996) 607.
[223] Z. Chen, M. Shapiro, P. Brumer, J. Chem. Phys. 102 (1995) 5683.
[224] Z. Chen, P. Brumer, M. Shapiro, Phys. Rev. A 52 (1995) 2225;
Z. Chen, P. Brumer, M. Shapiro, Chem. Phys. 217 (1997) 325.
[225] P.W. Shor, in: S. Goldwasser (Ed.), Proceedings of the 35th Annual Symposium on the Foundations of Computer Science, IEEE Computer Society, Los Alamos, CA, 1994, p. 124;
L.K. Grover, Phys. Rev. Lett. 79 (1997) 4709.
[226] M.A. Nielsen, I.L. Chuang, Quantum Computation and Quantum Information, Cambridge University Press, Cambridge, 2000.
[227] G.M. Palma, K.-A. Suominen, A.K. Ekert, Proc. R. Soc. London Sect. A 452 (1996) 567;
L.-M. Duan, G.-C. Guo, Phys. Rev. Lett. 79 (1997) 1953;
L.-M. Duan, G.-C. Guo, Phys. Rev. A 57 (1998) 737;
P. Zanardi, Phys. Rev. A 56 (1997) 4445;
P. Zanardi, M. Rasetti, Phys. Rev. Lett. 79 (1997) 3306.
[228] D.A. Lidar, I.L. Chuang, K.B. Whaley, Phys. Rev. Lett. 81 (1998) 2594;
D. Bacon, J. Kempe, D.A. Lidar, K.B. Whaley, Phys. Rev. Lett. 85 (2000) 1758.
[229] E. Frishman, M. Shapiro, P. Brumer, J. Chem. Phys. 110 (1999) 9.
[230] J.R. Taylor, Scattering Theory, Wiley, New York, 1972.
[231] R.G. Newton, Scattering Theory of Waves and Particles, McGraw Hill, New York, 1966 (Chapter 20).
[232] R.B. Gerber, M. Shapiro, Chem. Phys. 13 (1976) 227.
[233] M. Shapiro, P. Brumer, Phys. Rev. Lett. 77 (1996) 2574;
A. Abrashkevich, M. Shapiro, P. Brumer, Phys. Rev. Lett. 81 (1998) 3789;
A. Abrashkevich, M. Shapiro, P. Brumer, Phys. Rev. Lett. 82 (1999) 3002;
J. Gong, M. Shapiro, P. Brumer, J. Chem. Phys. 118 (2003) 2626;
V. Zeman, M. Shapiro, P. Brumer, Phys. Rev. Lett. 92 (2004) 133204.